Helmholtz-Zentrum Geesthacht
Zentrum für Material- und Küstenforschung

Universität Hamburg
DER FORSCHUNG | DER LEHRE | DER BILDUNG

German Bight Storm Activity over the Last Century

Daniel Krieger

Master's Thesis

supervised by
Dr. Oliver Krüger
Prof. Dr. Felix Ament

Institute of Coastal Research, Helmholtz-Zentrum Geesthacht
Meteorological Institute, Universität Hamburg

March 3, 2020

A Reconstruction of Historical Storm Activity
from Air-Pressure Observations

Contents

List of Acronyms

ACRE	Atmospheric Circulation Reconstructions over the Earth.
BMWi	Bundesministerium für Wirtschaft und Energie.
CFS	Climate Forecast System.
CFSR	Climate Forecast System Reanalysis.
DJF	December-January-February.
DMI	Danmarks Meteorologiske Institut.
DWD	Deutscher Wetterdienst.
ECMWF	European Centre for Medium-Range Weather Forecasts.
ERA	ECMWF Re-Analysis.
FINO	Forschungsplattformen in Nord- und Ostsee.
FSDE	First and Second Derivative Extrema.
GMAO	Global Modeling and Assimilation Office.
ICOADS	International Comprehensive Ocean-Atmosphere Data Set.
ISPD	International Surface Pressure Databank.
JJA	June-July-August.
KNMI	Koninklijk Nederlands Meteorologisch Instituut.
MAM	March-April-May.
MERRA	Modern-Era Retrospective analysis for Research and Applications.
MSLP	Mean Sea Level Pressure.
NAO	North Atlantic Oscillation.
NASA	National Aeronautics and Space Administration.
NCEP	National Centers for Environmental Prediction.
NE	Northeast.
PtJ	Projektträger Jülich.
SCAND	Scandinavia Pattern.
SMHI	Sveriges Meteorologiska och Hydrologiska Institut.
SON	September-October-November.
UTC	Universal Time Coordinated.
WMO	World Meteorological Organization.
Z	Zulu Time Zone, equivalent to Universal Time Coordinated.

Abstract

This thesis investigates the evolution of German Bight (southeastern North Sea) storminess from 1897 to 2018 through analyzing upper quantiles of geostrophic wind speeds, which act as a proxy for past storm activity. Here, geostrophic wind speeds are calculated from triplets of mean sea level pressure observations that form triangles over the German Bight. The data used in the thesis are provided by the International Surface Pressure Databank (ISPD) and the national meteorological services, namely the Deutscher Wetterdienst (DWD), the Danmarks Meteorologiske Institut (DMI), and the Koninklijk Nederlands Meteorologisch Instituut (KNMI).

The derivation of storm activity is achieved by enhancing the established triangle proxy method via combining and merging storminess time series from numerous partially overlapping triangles in an ensemble-like manner. The utilized approach allows for the construction of robust, long-term and subdaily German Bight storminess time series. Further, the method provides insights into the underlying uncertainty of the time series.

The results show that storm activity over the German Bight is subject to multidecadal variability. The latest decades are characterized by an increase in activity from the 1960s to the 1990s, followed by a decline lasting into the 2000s and below-average activity up until present. The results are backed through a comparison with reanalysis products from four datasets, which provide high-resolution wind and pressure data starting in 1979, and offshore wind speed measurements taken from the FINO-WIND project. This study also finds that German Bight storminess positively correlates with storminess in the NE Atlantic in general. In certain years, however, notably different levels of storm activity in the two regions can be found, which can be attributed to variabilities in the occurrence frequency of large-scale circulation patterns. An investigation of the underlying uncertainty reveals that uncertainty is inversely related to data availability and generally reduced compared to previous studies for the Northeast Atlantic, owing to the increased number of triangles and the more robust method.

Zusammenfassung

Diese Arbeit befasst sich mit der Entwicklung der Sturmaktivität über der Deutschen Bucht (südöstliche Nordsee) zwischen 1897 und 2018. Die Sturmaktivität wird durch einen Proxy quantifiziert, welcher aus oberen Quantilen der geostrophischen Windgeschwindigkeit abgeleitet wird. Die Berechnung des geostrophischen Windes erfolgt aus Dreierkombinationen von Messungen des auf Meereshöhe reduzierten Luftdrucks, welche so gewählt werden, dass sie Dreiecke über der Deutschen Bucht bilden. Als Datengrundlage dienen Datensätze der International Surface Pressure Databank (ISPD), sowie die Datenarchive nationaler Wetterdienste, wie dem Deutschen Wetterdienst (DWD), dem Danmarks Meteorologiske Institut (DMI) und dem Koninklijk Nederlands Meteorologisch Instituut (KNMI).

Die bereits etablierte Dreiecksmethode zur Ableitung der Sturmaktivität wird in dieser Arbeit durch die Verwendung eines Ensembles von Zeitserien 18 verschiedener, teils überlappender Dreiecke verbessert, was die Erstellung einer robusteren Zeitreihe der Sturmaktivität über der Deutschen Bucht ermöglicht. Zusätzlich können durch die Methode Aussagen über die Unsicherheit der Zeitreihe getroffen werden.

Die Ergebnisse zeigen, dass die Sturmaktivität über der Deutschen Bucht einer multidekadischen Variabilität unterliegt. Die 1960er bis 1990er sind hierbei durch einen Anstieg der Sturmaktivität gekennzeichnet, während die 2000er einen Rückgang aufweisen, welcher sich in unterdurchschnittlicher Sturmaktivität in der aktuellen Dekade manifestiert. Diese Resultate werden durch einen Vergleich mit vier Reanalyseprodukten belegt, welche hochauflösende Winddaten für den Zeitraum seit 1979 liefern. Zudem stimmen die Ergebnisse dieser Studie auch überwiegend mit Offshore-Messungen des FINO-WIND-Projekts überein. Weiterhin ergibt sich aus dieser Arbeit, dass die Sturmaktivität über der Deutschen Bucht positiv mit der größerskaligen Sturmaktivität über dem Nordostatlantik korreliert ist. Dennoch weichen die Sturmaktivitäten der beiden Regionen in einigen Jahren stark voneinander ab, was durch die Variabilität der Eintrittshäufigkeit großräumiger Zirkulationsmuster erklärt werden kann. Eine Untersuchung der der Zeitserie zugrundeliegende Unsicherheiten zeigt auf, dass die Unsicherheit reziprok an die Datenverfügbarkeit gekoppelt ist und allgemein niedrigere Werte aufweist als in bisherigen Studien für den Nordostatlantik. Verursacht wird dies durch die größere Anzahl an Dreiecken und die Verwendung einer robusteren Methodik.

1 Introduction

1.1 A Background on Storm Activity

In times where mitigating climate change has become one of the biggest global challenges (IPCC, 2014), the energy industry is moving towards renewable energy production, such as wind farms (Breton and Moe, 2009). An increasing demand for land with high wind potential makes energy companies take to the sea to install large offshore wind farms (Bilgili et al., 2011). As for Germany, multiple offshore wind farms have already been constructed in the German Bight, with more being planned or under construction (BSH, 2019). The economic efficiency of wind farms strongly depends on the wind climatology, to which storms contribute a large part. At the same time, wind turbines that are repeatedly being exposed to high wind speeds are vulnerable to mechanical failure. Consequently, storm risk assessments heavily rely on dependable and robust statistics of extreme wind events (Buchana and McSharry, 2019).

From a societal point of view, storms are one of the major extreme events affecting the population in Germany and Europe due to high wind speeds and triggering of other phenomena, such as storm surges, high waves, flooding, and extreme precipitation events. Due to the high damage potential of storms and their inherent large impact on society, the assessment of long-term storm activity provides valuable information to mitigate potential risk factors.

However, acquiring information about long-term trends and temporal variability of storm activity requires the availability of homogeneous wind speed records. Such homogeneous records are usually not available as technological advances or improvements in the measurement techniques can lead to inhomogeneities in the data records over time (Trenberth et al., 2007). For instance, wind observations along the German coastline during the early 20th century relied on visual estimates of the sea state in conjunction with the Beaufort scale (Wagner, 2016). The subjectivity of such estimates and possible changes of the classification scheme with time are a source of inhomogeneities in wind speed records (Thomas et al., 2005). Also, changes in the surroundings of an observation site, such as station relocations, vegetation changes, or the construction of buildings, can disturb the wind measurements and thus cause inhomogeneities (Vose et al., 1992; Heino, 1999; Lindenberg et al., 2012). Similarly, long reanalysis datasets do not pose a suitable alternative as they are affected by an increasing station density and better data quality over time, also from the introduction of satellite data at the end of the 1970s, resulting in artificial trends (Bengtsson et al., 2004; Krueger et al., 2013). Wohland et al. (2019) noted that these trends likely result from assimilated wind speeds and improvements in the wind measurement techniques. Additionally, Wohland et al. (2019) found disagreements in wind speed trends between different 20th century reanalyses. Such inconsistencies between reanalyses were also detected by Bloomfield et al. (2018), who investigated long-term changes in the Arctic Oscillation.

As air pressure is a large-scale variable, measurements of air pressure are usually less affected by the aforementioned factors. Additionally, instruments and techniques used for air pressure observations have undergone only small changes in the past century and therefore produce more consistent data. For that reason, less inhomogeneities are found in time series of air pressure measurements. There are several methods of assessing storminess based on making use of the air pressure. For instance, it is possible to derive statistics of the air pressure at a weather station, which are based on pressure tendencies or low pressure values. However, Krueger and von Storch (2012) showed that the informational value of such statistics is medium at best to describe past storminess. Furthermore, it is also possible to count the number of low-pressure systems with a central pressure below a certain threshold in weather analyses provided by national meteorological services. Yet, Schmidt and von Storch (1993) note that this approach is hampered as improvements in the quality and resolution of atmospheric analyses likely result in artificial trends in the data causing storminess to increase over time. Consequently, one approach to avoid inhomogeneities and uncertainties from station data is to make use of the geostrophic wind speed proxy based on triplets of air pressure measurements. Schmidt and von Storch (1993) used the proxy to describe the long-term behavior of upper quantiles of geostrophic wind speeds under the assumption that the variation of the statistics of this proxy describes the variation of the statistics of wind speed. This assumption was later shown to be valid by Krueger and von Storch (2011), in particular over sea surfaces and flat terrain, where ageostrophic disturbances on atmospheric movements are minor. Other studies adapted the proxy to infer about the long-term storm climate, mostly over the Northeast Atlantic Ocean (e.g. Alexandersson et al., 1998, 2000; Matulla et al., 2008; Wang et al., 2009, 2011; Krueger et al., 2019). Most studies found an increase of storminess from the 1960s to the 1990s, but when viewed over longer time scales, storm activity is mostly stationary with a super-imposed pronounced interdecadal variability (Feser et al., 2015). The proxy of geostrophic wind speed statistics is also used by national meteorological services. For instance, the Swedish national service SMHI makes use of the method to provide analyses of the wind climate all over Sweden (Wern and Bärring, 2009).

For the North Sea region, which is one of the most densely observed regions in the world, there is also the possibility of making use of other records for different variables, such as records of storm surges along the coasts, to make inferences about storm activity (Dangendorf et al., 2014). The surge-based storminess displays interannual to multidecadal variability without any significant trend. However, as the occurrence of surges strongly depends on wind direction or the layout of the coastlines (Ganske et al., 2018), storm surges can only provide complimentary information with regard to the description of long-term storm activity. Cusack (2013) deduced the Dutch storm climate from 101 years of homogenized near-surface wind measurements and insurance losses, showing a prevalent multidecadal cycle in windstorm loss estimates. Furthermore, the recent years are characterized by below-average storm losses, caused by a minimum in the occurrence of damaging windstorms.

As the synoptic atmospheric activity over Europe is influenced by the large-scale circulation, atmospheric modes can contribute to the variability of the storm climate. The dominant mode in the Northeast Atlantic is the NAO described by the NAO index. The NAO index is based on the standardized differences in pressure anomalies between Rejkyavik (Iceland) and either Lisbon (Portugal), Gibraltar, or Ponta Delgada (The Azores) (Hurrell, 1995; Jones et al., 1997). Positive NAO phases coincide with an increase in zonal weather patterns, favoring cyclogenesis and storm tracks over Central Europe (Trigo et al., 2002; Feser et al., 2015). Negative NAO phases are often accompanied by meridional or easterly dominated synoptic patterns, leading to a reduced number of storms over Europe and generally lower wind speeds (Donat et al., 2010). Allan et al. (2009) examined the relationship between NAO phases and winter storm activity over the British Isles and found that, even though a significant positive correlation exists, the connection fluctuates over time. Matulla et al. (2008) concluded that the variations in the NAO can be used to explain the northwestern European storminess variability to some extent, but the link fails for other regions in Europe. Matulla et al. (2008) also emphasized that the connection between the NAO and storminess strongly depends on the time period and region examined, which was later confirmed by Pinto and Raible (2012) and Raible et al. (2014).

1.2 Thesis Outline

Though Schmidt and von Storch (1993) provide a first analysis of the long-term storm climate over the German Bight, and subsequently the German national meteorological service DWD incorporates and updates the time series annually in their reports about the current state of the German storm climate (DWD, 2017b), there is still a need to investigate German Bight storminess in more detail. The analysis of Schmidt and von Storch (1993) is based on three stations forming a triangle covering the German Bight with missing periods of observations being replaced with data from neighboring stations. Even though Krueger and von Storch (2011) show that one triangle provides sufficient information for the description of storminess, the present analysis utilizes data from eight stations to form an ensemble of 18 triangles exploiting the dense observational network along the North Sea coast to estimate German Bight storminess robustly for the period 1897-2018. Additionally, it also allows for the provision of new uncertainty estimates.

With the use of this approach, the thesis aims to answer the following four questions:

- Does German Bight storminess exhibit temporal variability or trends over the last century?
- How do the reconstructed time series compare to wind measurements and reanalysis products in recent decades?
- To which degree is German Bight storminess connected to the large-scale circulation over Europe and the North Atlantic?
- How large is the underlying uncertainty in the ensemble-based reconstruction of storm activity?

In an effort to answer these questions, the thesis is structured as follows: Chapter 2 describes the data used in this study and provides information about the derivation of German Bight storminess. Chapter 3 presents and discusses the derived annual and seasonal time series of German Bight storm activity. Chapter 4 validates the reconstructions through comparison with in-situ measurements and reanalysis products. Chapter 5 puts German Bight storm activity into context by connecting it to the large-scale circulation, synoptic patterns and further analyses of wind directions. Chapter 6 focuses on the estimation of uncertainties associated with the chosen approach and a varying data availability. Concluding remarks are then given in Chapter 7.

2 From Air Pressure to Storminess

The main focus of this thesis lies on the reconstruction of historical storm activity from air pressure observations and its subsequent validation. This process requires a careful selection of available observational data, a thorough quality control scheme and the use of an established approach to ensure high representativeness of the resulting time series. In this chapter, detailed descriptions of datasets, methods and necessary assumptions are given. Section 2.1 focuses on the sources and properties of atmospheric pressure observations and reanalysis data used in the reconstruction and validation processes. Section 2.2 describes the data preparation and quality control schemes that are used to generate high-quality input data. Section 2.3 then provides a step-by-step explanation of the approach used to compute a proxy for storminess from time series of air pressure observations. Lastly, Section 2.4 describes a method of estimating the underlying uncertainty in a nonparametric way.

2.1 Data Sources

This study uses pressure data from the International Surface Pressure Databank (ISPD) version 3 (Cram et al., 2015; Compo et al., 2015), the Deutscher Wetterdienst (DWD) (DWD, 2019), the Danmarks Meteorologiske Institut (DMI) (Cappelen et al., 2019) and the Koninklijk Nederlands Meteorologisch Instituut (KNMI) (KNMI, 2019) to calculate geostrophic wind speeds over the German Bight following Schmidt and von Storch (1993); Alexandersson et al. (1998, 2000) for the period 1897-2018, which is the period, for which the data sources provide sufficient information to reconstruct geostrophic wind speeds. In total, pressure observations from eight stations in Germany, Denmark, and the Netherlands are considered. The coordinates and data availabilities for each station are displayed in Table 2.1.

Furthermore, results are compared with measurement data from the Forschungsplattformen in Nord- und Ostsee (FINO) measurement site 1 (Leiding et al., 2016, marked in Fig. 2.2) and with data from four current reanalysis datasets, namely ERA5 (Hersbach et al., 2018), ERA-Interim (Dee et al., 2011), MERRA-2 (Gelaro et al., 2017), and a combination of CFSR version 1 (Saha et al., 2010) and version 2 (Saha et al., 2014). Note that version 1 of CFSR stops at the end of 2010 and version 2 directly continues afterward, allowing a concatenation of both datasets. Even though longer reanalyses

Table 2.1: List of stations with coordinates and data availabilities. A plus sign indicates that the station was relocated to the respective location.

Station	Country	Latitude	Longitude	Data availability
Vestervig	Denmark	56.76	8.32	1874-1986
+ Thyborøn	Denmark	56.70	8.22	1987-2018
Nordby	Denmark	55.45	8.40	1874-1986
+ Esbjerg	Denmark	55.53	8.56	1987-2018
List	Germany	55.01	8.41	1934-1944, 1948-2018
Hamburg-Fuhlsbüttel	Germany	53.63	9.99	1936-2018
+ Hamburg-Seewarte	Germany	53.55	9.97	1891-1935
Cuxhaven	Germany	53.87	8.71	1946-2018
Norderney	Germany	53.71	7.15	1935-2018, except 1939, 40, 42-46
Groningen	The Netherlands	53.12	6.58	1906-2018, except 1971, 72, 91, 92
De Bilt	The Netherlands	52.10	5.18	1897-2018

covering the entire 20th century are available, they show inconsistencies and disagreements in wind speed trends (Bloomfield et al., 2018; Wohland et al., 2019), rendering them unusable for this study.

Air Pressure Observations

The ISPD is a global database of historical pressure observation data, spanning the period 1722-2016. The ISPD consists of a blend of international pressure datasets with added metadata, such as station altitudes and coordinates. The database also provides quality control flags, which stem from the production of the 20th Century Reanalysis (Appendix B in Compo et al., 2011) up until 2013. Data that are distributed by the DMI contain pressure observations at sea level, including station metadata. While historical data are available for 1874-2018, the temporal resolution is confined to three data points per day (07Z, 13Z, 20Z) until July 1987, as well as three-hourly and hourly observations thereafter. Pressure records from the DWD Climate Data Center comprise data both at sea and station levels. The data availability differs among the stations with Hamburg being the longest continuous time series (1891-2018). The German datasets contain quality bytes that stem from the DWD quality control, additional stations and instrumental metadata. All data were converted into UTC using provided timezone information. Historical pressure observations from the Netherlands used in this thesis are a blend of data obtained through the ISPD, personal communication with the KNMI, and the KNMI data centre (KNMI, 2019). Available Dutch pressure data at sea level are recorded hourly, respectively every 10 minutes for recent periods.

FINO

Forschungsplattformen in Nord- und Ostsee (FINO) is the unified name for three research platforms located in the German parts of the North and Baltic Seas. The platforms – FINO1, FINO2, and FINO3 – were constructed between 2003 and 2009 to investigate the potential of the German maritimes for offshore wind power generation (Leiding et al., 2016). The research project FINO-WIND, led by the DWD and funded by the Federal Ministry for Economic Affairs and Energy (Bundesministerium für Wirtschaft und Energie (BMWi)) through Project Management Jülich (Projektträger Jülich (PtJ)), was conducted to standardize measurements taken at the three platforms and create intercomparable and consistent datasets of wind observations (Leiding et al., 2016).

For comparison of the reconstructed geostrophic wind speeds with in-situ observations, wind data from the FINO1 station, which lies approximately 45 kilometers north of the German island of Borkum, are utilized. Wind speed and direction are measured with a cup anemometer and an associated wind vane at 71 m above sea level. The measurements cover a period from January 2004 to August 2018 with a temporal resolution of 10 minutes. Due to the reconstruction being based on three-hourly data, only measurements every three hours, starting at 00Z, are selected. Also, as observations from the year 2018 are incomplete, only data from 2004-2017 are considered.

ERA-Interim

ECMWF Re-Analysis-Interim (ERA-Interim) is a global atmospheric reanalyis produced by the European Centre for Medium-Range Weather Forecasts (ECMWF) (Dee et al., 2011). Being developed as a successor to the previous reanalysis ERA-40, it aims at improving key aspects of ERA-40, such as the representation of the hydrological cycle, the quality of the stratospheric circulation, and bias handling (Berrisford et al., 2011). ERA-Interim covers a period from January 1979 to August 2019 and provides surface parameters at three-hour intervals, as well as upper-air parameters at six-hour intervals. The reanalysis uses an irregularly spaced reduced Gaussian grid with a T255 horizontal resolution (0.7° x 0.7°), which corresponds to an approximate grid spacing of 79 km. The vertical extent of the model is represented by 60 levels, with the top of the atmosphere being located at 0.1 hPa (Dee et al., 2011). For this study, six-hourly 10 m wind speed data from 1980-2018 are used.

ERA5

ERA5 is the fifth and latest global climate reanalysis by the ECMWF. It is currently being produced in two phases and is set to replace its predecessor ERA-Interim, which was updated until August 2019 (Hersbach et al., 2018). As of now, reanalysis products generated through ERA5 are available from 1979-2019, the same period covered by ERA-Interim. After completion of the second phase, ERA5 will extend back to 1950 (Hersbach et al., 2018). Like ERA-Interim, the reanalysis utilizes an irregularly spaced reduced Gaussian grid. The horizontal resolution is set to T639 (0.28125° x 0.28125°) with a grid spacing of approximately 31 km, resulting in a more than sixfold increase in grid points with respect to ERA-Interim (Hersbach et al., 2018). ERA5 is able to resolve 137 vertical levels up to 0.01 hPa and outputs data with a temporal resolution of one hour (Hersbach et al., 2018). As geostrophic wind data in this study are computed for three-hour intervals, three-hourly 10 m wind speed data from ERA5 are used for reasons of comparability.

MERRA-2

The Modern-Era Retrospective analysis for Research and Applications (MERRA) version 2 is the latest global atmospheric reanalysis by NASA's Global Modeling and Assimilation Office (GMAO) (Gelaro et al., 2017). It acts as the successor to the first version of MERRA and includes numerous improvements to the forecast model, the data assimilation procedure, and the observing system (Gelaro et al., 2017). MERRA-2 output is gridded with a horizontal resolution of 0.5° x 0.625° and 72 vertical levels up to 0.01 hPa. Model output is available at hourly time steps and only covers the period of 1980-2018 (Gelaro et al., 2017). Similar to ERA5, this study uses three-hourly 10 m wind speed data to match the temporal resolution of the geostrophic wind reconstructions.

CFSR

The Climate Forecast System Reanalysis (CFSR) is a global climate reanalysis developed by the National Centers for Environmental Prediction (NCEP). It replaces previous reanalyses from NCEP by improving the model, the resolution, and the introduction of atmosphere-land-ocean-sea ice coupling (Saha et al., 2010). CFSR is best described as a concatenation of two temporally not-overlapping datasets that were produced with different versions of the underlying model. The original reanalysis, based on the first version of the Climate Forecast System (CFS) model, covers a period from 1979-2010 (Saha et al., 2010). Its T382 grid has a spatial resolution of approximately 38 km (0.5° x 0.5°) with 64 vertical levels up to 0.266 hPa (Saha et al., 2010). From 2011 onwards, CFSR was extended with data output from an upgraded version of the CFS model. Both datasets provide meteorological parameters at six-hour intervals. This study treats the combined products of CFSR versions 1 and 2 as one consistent reanalysis and therefore uses six-hourly 10 m wind speed data from 1980-2018.

2.2 Data Preparation and Quality Control

2.2.1 Reduction to Sea Level

The calculation of geostrophic wind speeds requires quality controlled pressure data at sea level. As pressure data from both the ISPD and DWD have not entirely been reduced to sea level, the barometric equation (Eq. 1) for an atmosphere with a constant vertical temperature gradient and with modified standard atmospheric values is applied to correct for small station altitudes due to the lack of knowledge about the state of atmospheric conditions at the time of the measurements. The pressure reduction assumes an air temperature of 10 °C at station height z, which is close to the annual mean temperature in the area being investigated (van der Schrier et al., 2011; DWD, 2017b; Cappelen et al., 2019). The height correction of the pressure p at height z_{station} to the mean sea level ($z = 0$) reads

$$p\,(z=0) = p\,(z_{\text{station}}) \cdot \left(1 - \frac{0.0065\frac{\mathrm{K}}{\mathrm{m}} \cdot z_{\text{station}}}{283.15\,\mathrm{K}}\right)^{-5.255}, \qquad (1)$$

for which -0.0065 $\frac{\mathrm{K}}{\mathrm{m}}$ is the assumed lapse rate $\frac{\partial T}{\partial z}$ and 5.255 the ratio $\frac{\kappa}{\kappa-1}$ for κ=1.235 being the assumed isentropic coefficient.

2.2.2 Quality Control

After the pressure data have been reduced to sea level, they are subjected to a quality control scheme, which consists of multiple steps. The first level of quality control makes use of the quality control flags provided by the ISPD through a removal of flagged data (where available). Then, manual quality checks are performed based on the idea that erroneous values become detectable when they are either unrealistically high or low, or when absolute differences of pressure tendencies between consecutive time steps exceed certain thresholds. First, unrealistically high or low pressure values are removed. The removal thresholds for low and high values of pressure readings are set to 940 and 1065 hPa based on observed extremes of atmospheric pressure records in Germany, the Netherlands, and Denmark (de Haij, 2009; Würtz, 2017; Cappelen et al., 2019). Second, pressure changes between measurements are examined to filter out pressure spikes that would be physically implausible, following the FSDE approach of Paraskevopoulou et al. (2013). The FSDE approach introduces discrete first and second order differences of pressure in time. The first order difference FD_n at the time t_n is defined by the difference between two consecutive pressure measurements p_n and p_{n-1} at t_n and t_{n-1} (Eq. 2). The second order difference SD_n is then based on the change of first order differences between t_{n+1} and t_n (Eq. 3).

$$FD_n = \frac{p_n - p_{n-1}}{t_n - t_{n-1}} \tag{2}$$

$$SD_n = FD_{n+1} - FD_n = \frac{p_{n+1} - p_n}{t_{n+1} - t_n} - \frac{p_n - p_{n-1}}{t_n - t_{n-1}} \tag{3}$$

If the pressure time series shows a spike at t_n, the absolute second order difference SD_n will exhibit a local maximum. Thus, a threshold for the absolute second order differences is empirically set (Eq. 4), so that pressure data which do not meet the requirement are removed from the dataset. The threshold has been empirically determined through an analysis of pressure tendencies during notable historic storms (not shown).

$$|SD_n| \leq 15\,\frac{\mathrm{hPa}}{\mathrm{h}} \tag{4}$$

Finally, pressure observations are compared to data from adjacent stations to identify spatial outliers (Dey and Morone, 1985). For every station, the median pressure of all stations located within a radius of 250 km is calculated if there are at least two other stations available. An index I_n based on the difference Δp between the pressure of the tested station p and the surrounding reference median pressure p_{median} at the times t_n, t_{n+1} and t_{n-1} is calculated. As shown in Equation 5, the index consists of the two terms A and B.

$$I_n = \underbrace{|\Delta p_n|}_{\mathrm{A}} + \underbrace{\left| \left(\frac{\Delta p_{n+1} - \Delta p_n}{t_{n+1} - t_n} - \frac{\Delta p_n - \Delta p_{n-1}}{t_n - t_{n-1}} \right) \cdot 1\,\mathrm{h} \right|}_{\mathrm{B}} \tag{5}$$

Term A describes the absolute difference Δp between the station pressure p and the median of the surrounding stations p_{median} at the time t_n. Term B takes into account the difference between the rate of change of term A before and after t_n. Term B is comparable to the second order difference from Equation 3 but instead calculated for the pressure difference Δp.

The index I_n is then tested against a threshold, which is modified by the reference median pressure p_{median} at t_n. The modification factors in stronger pressure gradients and fluctuations near areas of lower pressures. Again, the threshold has been empirically determined through an analysis of strong storm events (not shown). Valid observations conform to the conditions given in Equation 6, which reads

$$I_n < 13\,\text{hPa} + \left(\frac{1013\,\text{hPa} - p_{\text{median}}}{10}\right). \tag{6}$$

2.2.3 Data Synchronization

In order to calculate geostrophic wind speeds from pressure gradients, pressure data need to be available at simultaneous time steps (as in Krueger et al., 2019). Due to different time zones, measurement techniques, and guidelines, observations have not always been recorded at the same time during the day. To overcome these inconsistencies, synchronized pressure data have to be obtained every three hours starting at 00Z. As changes in air pressure occur on synoptic time scales, a linear approximation of the variable is considered to be sufficient for the temporal resolution of the available data. Therefore, the pressure data is linearly interpolated to three-hourly values. Gaps in the dataset that are longer than 13 hours are discarded because the interpolation would remove too much of the natural synoptic-scale pressure variability. More sophisticated interpolation techniques such as cubic or spline interpolation would probably not add additional value to the dataset.

2.3 Geostrophic Storminess

To derive geostrophic winds from pressure values, this study adapts the approach of Schmidt and von Storch (1993). First, the $\binom{8}{3} = 56$ possible distinct triangles that can be formed by combining eight stations into triplets are evaluated for geometric features. Investigations have shown that strongly obtuse triangles exhibit a larger error propagation of pressure uncertainties resulting in a shift of the average wind direction towards the orientation axis of the triangle and a significant increase in overall wind speeds (Fig. 2.1). For that reason, triangles with an interior angle smaller than 15° are discarded. Also, triangles that only cover coastlines or land areas are manually

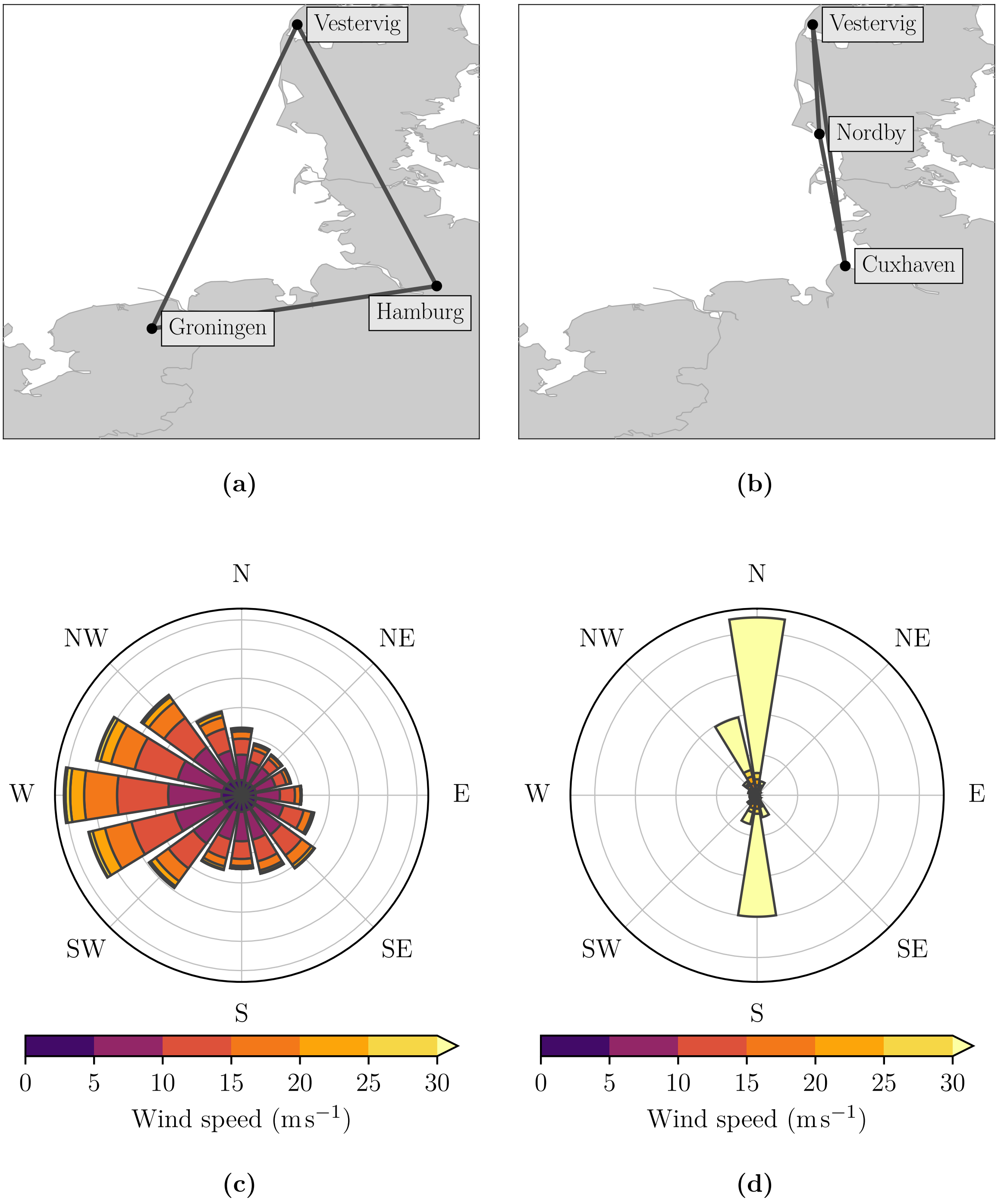

Figure 2.1: Example of a triangle fulfilling the geometric criteria **(a)** and an obtuse triangle **(b)** with their associated wind roses **(c, d)**.

removed. These geometric and physical criteria are chosen to ensure that the selected triangles cover a sufficiently large part of the German Bight. An overview over all 56 theoretically possible triangles and their geometric criteria is given in Table A.1.

Following the approach of Alexandersson et al. (1998), it is assumed that, for each of

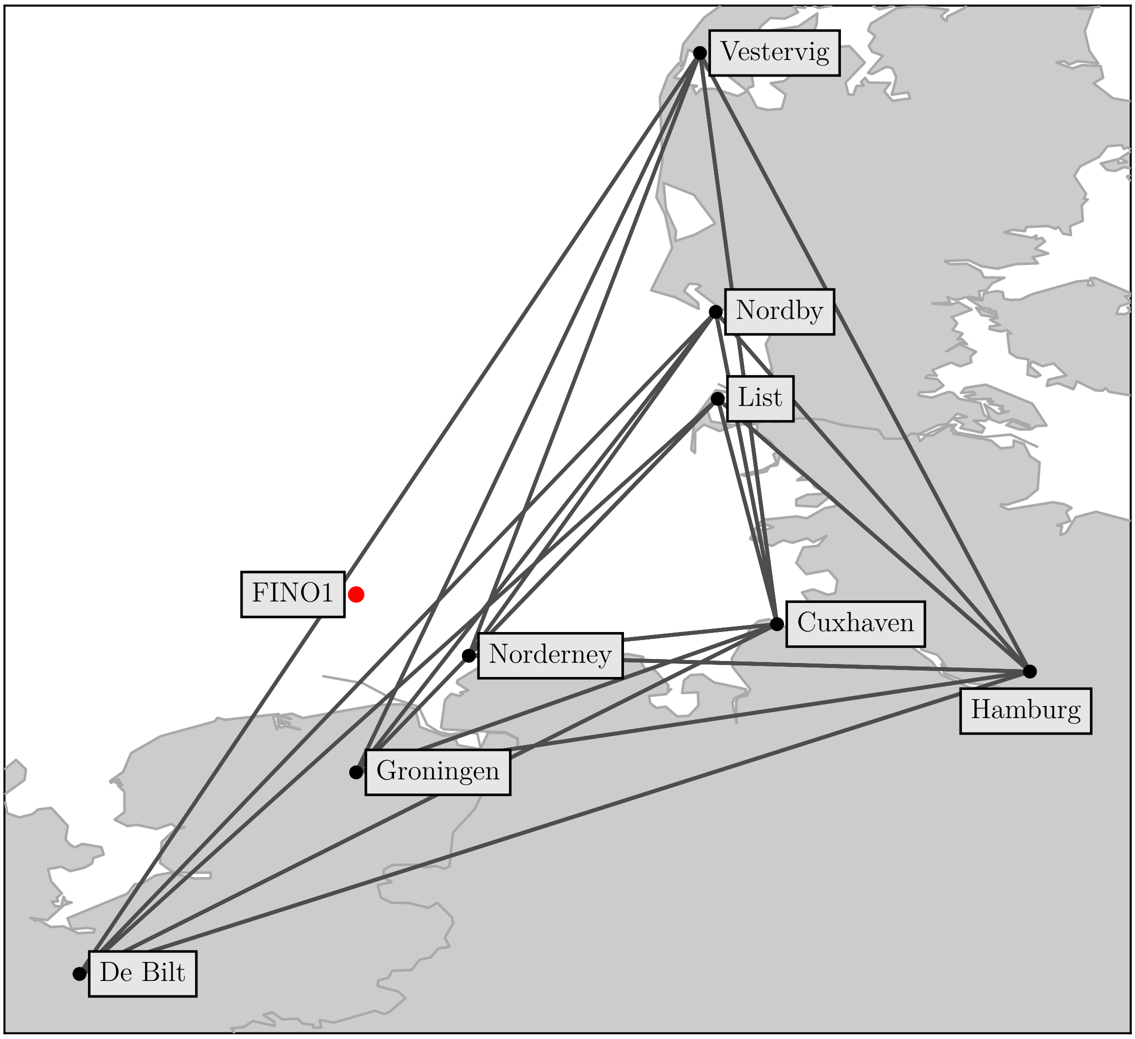

Figure 2.2: Map of eight stations from which pressure observations are used to calculate geostrophic winds and 18 triangles that are constructed based on geometric criteria. The location of the FINO1 research platform is marked in red.

the remaining 18 triangles (Fig. 2.2 and Tab. 2.2), the air pressure field can be approximated by a two-dimensional linear function, so that the pressure p at the coordinates (x, y) within one triangle can be described by the equation

$$p = ax + by + c, \tag{7}$$

with x and y being defined in a local cartesian coordinate system:

$$x = R_\mathrm{e}\lambda \cos(\phi), \tag{8}$$

$$y = R_\mathrm{e}\phi. \tag{9}$$

Here, R_e denotes the Earth radius, λ the longitude, and ϕ the latitude. The coefficients a, b, and c in Equation 7 can be derived through solving the set of equations 10, for which the pressure p_i at the station location $(x_i,\, y_i)$ with $i = 1, 2, 3$ is made use of.

$$\begin{aligned} p_1 &= ax_1 + by_1 + c \\ p_2 &= ax_2 + by_2 + c \\ p_3 &= ax_3 + by_3 + c \end{aligned} \tag{10}$$

The geostrophic wind speed is then calculated as

$$U_\mathrm{g} = (u_\mathrm{g}^2 + v_\mathrm{g}^2)^{1/2}, \tag{11}$$

with

$$u_\mathrm{g} = -\frac{1}{\rho f}\frac{\partial p}{\partial y} = -\frac{b}{\rho f} \qquad \text{and} \qquad v_\mathrm{g} = \frac{1}{\rho f}\frac{\partial p}{\partial x} = \frac{a}{\rho f}, \tag{12}$$

where ρ is the density of air (set at 1.25 kg m^{-3}) and f the Coriolis parameter, which is the average of the Coriolis parameters from the three measurement sites. The coefficients a and b denote the meridional and zonal pressure gradients, which were determined by solving Equation 10.

Besides the geostrophic wind speed, the wind direction d_g can also be derived from the zonal and meridional components of the geostrophic wind u_g and v_g (Eq. 13).

$$d_\mathrm{g} = \left(270^\circ - \operatorname{arctan2}(v_\mathrm{g},\, u_\mathrm{g}) \cdot \frac{180^\circ}{\pi}\right) \mod 360^\circ \tag{13}$$

The arctan2 function, which is a modification of the inverse tangent function, is defined as

$$\operatorname{arctan2}(v,\, u) = \begin{cases} \arctan(\frac{v}{u}) & \text{for } u > 0, \\ \arctan(\frac{v}{u}) + \pi & \text{for } u > 0,\ v \geq 0, \\ \arctan(\frac{v}{u}) - \pi & \text{for } u > 0,\ v < 0, \\ \frac{\pi}{2} & \text{for } u = 0,\ v > 0, \\ -\frac{\pi}{2} & \text{for } u = 0,\ v < 0, \\ 0 & \text{for } u = 0,\ v = 0. \end{cases} \tag{14}$$

After the derivation of U_g at each time step, the 95th and 99th seasonal and annual percentiles of geostrophic wind speeds U_{95} and U_{99} for each triangle are determined. To reduce errors resulting from years in which geostrophic wind data is too sparse to be considered representative for the entire year, years with a data availability of less than 80.0 % (79.8 % in a leap year) are removed. The threshold of 80.0 % is based on a sensitivity analysis by Krueger et al. (2019), who found that uncertainty estimates are almost stable for data availabilities of above 80.0 %. The removal of years with low data availability introduces an additional constraint compared to previous studies (e.g. Wang et al., 2009, 2011), which did not restrict the use of sparsely populated datasets. The requirements for seasonal values follow similar criteria.

In a last step, the resulting time series of the 18 triangles are treated as an ensemble of realizations of storminess time series covering the German Bight. This ensemble treatment is needed, as the ensemble mean is defined as a proxy for storminess, and a statistical analysis of the ensemble allows for the estimation of underlying uncertainties (see Sec. 6). First, the individual storminess time series $U_{q,t}$ are standardized and then averaged over the entire ensemble (as in Alexandersson et al. (1998) and subsequent studies). Following Equation 15, the standardization is achieved by the subtraction of the long-term average $\overline{U_{q,t}}$ and division by the standard deviation $\sigma(U_{q,t})$, both calculated for the period 1961-2010.

$$S_{q,t} = \frac{U_{q,t} - \overline{U_{q,t}}}{\sigma(U_{q,t})} \tag{15}$$

Standardizing the time series brings individual storminess values into the same range and makes them comparable. The resulting values of the time series $S_{q,t}$ are dimensionless; however, they can be understood as multiples of one standard deviation, with 0 denoting the 1961-2010 long-term average. The indices q and t indicate the percentiles and triangles, respectively.

The individual standardization, which is performed before the ensemble averaging, is necessary to avoid in- or deflation of annual percentiles of geostrophic wind speeds. Long-term averages of upper percentiles of wind speeds are generally lower in larger triangles and vice versa, as the assumption that the pressure field within the triangle can be described as a two-dimensional linear function smoothes out small-scale variability, which would cause higher wind speed peaks. Accordingly, certain triangles exhibit higher or lower 95th and 99th percentiles of geostrophic wind speeds than others, even though they are in the same vicinity and overlap (compare Tab. 2.2 and A.1). Should, for instance, data from a very large triangle (i.e. a triangle with lower wind speeds) be unavailable for a certain year, the ensemble average would increase artificially during that year, leading to a false assumption of increased storminess. Therefore, the ensemble average should only be performed on individually standardized dimensionless indices. These averages of the resulting 18 time series for the 95th and the 99th percentiles of geostrophic wind speeds, S_{95} and S_{99}, are then considered as proxies for German Bight storminess (Eq. 16). Despite not explicitly shown in Equation 16, missing values are excluded from the calculations of the averages. Additionally, the resulting annual and seasonal time series are smoothed using a Gaussian low-pass filter with $\sigma = 3$. The low-pass filtering removes variability on an annual or seasonal scale and is therefore better suited to point out long-term variability.

$$\begin{aligned} S_{95} &= \frac{1}{18} \sum_{t=1}^{18} S_{95,t} \\ S_{99} &= \frac{1}{18} \sum_{t=1}^{18} S_{99,t} \end{aligned} \tag{16}$$

It should be noted that, for the actual comparison with measurements and data from reanalyses, non-standardized geostrophic wind speeds at shorter and annual time scales are used as seen fit (see Chap. 4).

Table 2.2: List of triangles with 1961-2010 means and standard deviations of annual 95th and 99th percentiles of geostrophic wind speeds in $\mathrm{m\,s^{-1}}$.

Triangle	$\overline{U_{95}}$	$\overline{U_{99}}$	$\sigma(U_{95})$	$\sigma(U_{99})$
De Bilt-Vestervig-Cuxhaven	22.03	28.63	1.12	1.95
De Bilt-Vestervig-Hamburg	20.84	26.73	1.02	1.52
De Bilt-Nordby-Cuxhaven	22.21	29.31	1.36	2.28
De Bilt-Nordby-Hamburg	20.70	26.80	1.15	1.73
De Bilt-List-Cuxhaven	23.28	30.89	1.65	2.26
De Bilt-List-Hamburg	21.65	28.60	1.36	2.02
Groningen-Vestervig-Cuxhaven	22.47	29.31	1.26	2.10
Groningen-Vestervig-Hamburg	21.47	27.50	1.04	1.60
Groningen-Nordby-Cuxhaven	22.66	29.89	1.43	2.33
Groningen-Nordby-Hamburg	21.30	27.51	1.10	1.77
Groningen-List-Cuxhaven	23.97	31.91	1.60	2.41
Groningen-List-Hamburg	22.58	29.87	1.29	2.10
Vestervig-Norderney-Cuxhaven	22.26	28.59	1.38	1.99
Vestervig-Norderney-Hamburg	21.78	27.86	1.04	1.61
Nordby-Norderney-Cuxhaven	22.01	28.67	1.51	2.25
Nordby-Norderney-Hamburg	21.34	27.49	1.10	1.73
List-Norderney-Cuxhaven	23.84	31.53	1.75	2.36
List-Norderney-Hamburg	22.97	30.16	1.30	2.04
Ensemble mean	22.19	28.96	1.30	2.00

2.3.1 Trend Detection

This thesis aims at uncovering long-term changes in the reconstructed time series of German Bight storm activity, which makes it necessary to investigate possible trends in the data. Therefore, linear regressions are performed on the annual and seasonal time series based on the Theil-Sen estimator (Sen, 1968). The Theil-Sen estimator is considered more robust than other regression methods, such as the least squares approach, as it is less sensitive to outliers (Wilcox, 2001), and has been used to detect trends in wind speeds before (Romanić et al., 2015). To evaluate the significance of the resulting regressions, the individual slopes m are tested against the null hypothesis $m_0 = 0\,\mathrm{year}^{-1}$. The 95 % confidence intervals are then computed for the slope of each linear regression, following Sen (1968). Should the confidence interval for a certain slope include the null hypothesis, the associated trend is deemed insignificant.

As previous studies have shown, storm activity is often subject to temporal variability (see Sec. 1.1), which brings up an issue with linear regressions. Consider two identical time series with an underlying long-term variability, only shifted in phase by one half of a period. If, for instance, the first time series starts in a below-average phase and ends in an above-average phase, a linear regression will result in a positive trend. The second time series, which covers the same time span but starts in an above-average and ends in a below-average phase, will be estimated to exhibit a negative trend. Thus, simple estimations of linear trends can be misleading due to the dependency of the trend parameters on the choice of starting and ending points. To evaluate the effects of this dependency, linear trends are fitted for every combination of starting and end points between 1897 and 2018. A required span of 3 years is set as a lower boundary, so that year-to-year trends are excluded from the calculations. This method is based on the approach of Liebmann et al. (2010) who found that the choice of the time period has notable effects on global temperature trend estimates.

2.4 A Nonparametric Approach to Uncertainty Estimation

Even though it is assumed that inferring storminess from pressure observations provides a more robust and homogeneous time series compared to the direct use of wind speed measurements (Weisse and von Storch, 2009), unavoidable uncertainties and errors induced by limited instrument accuracy, measurement routines, and the sampling process described in Section 2.3 have to be accounted for. As there are no extensive metadata available that would consistently describe such errors, this study makes use of a bootstrapping approach (Efron and Tibshirani, 1986; DiCiccio and Efron, 1996) to mimic and quantify the uncertainty of the time series. Bootstrapping is a nonparametric and established method of estimating sample frequency distributions of a variable or statistic through the repeated use of subsampling with replacement. The approach presented in this thesis aims at estimating the range of possible realizations of German Bight storminess, which acts as an approximation of the uncertainty.

Therefore, the applied bootstrapping method first selects random values from the three-hourly geostrophic wind database for a specific year, month and triangle until the size of the selected subset reaches the number of three-hourly time steps in one month. Missing observations that stem from low data availability or result out of the quality control procedures are included in the sample and inflate the uncertainty estimates. This process is repeated for every month within one year, whereby the monthly subsets are assigned to their respective seasons. Afterward, 95th and 99th percentiles are determined for the four seasons and the entire year, on the condition that the data availability of the original dataset for the respective season or year and triangle is at least 80.0 % (compare Sec. 2.3). Note that, for the calculation of winter storminess, data from the December of the previous year have to be used. The entire sampling procedure is then iterated over every year in the 122-year period and subsequently repeated for each of the 18 triangles. Eventually, the 18 resulting time series are standardized and averaged, following the methods described in Section 2.3.

By repeatedly performing this sampling routine for 10000 times, an empirical distribution of possible realizations of German Bight storminess is obtained, which can be used to quantify the uncertainty. To illustrate the uncertainty, the 95 % confidence interval of German Bight storminess is calculated as the difference of the 2.5 % and 97.5 % quantiles of bootstrapped values. A flowchart visualization of the uncertainty estimations is given in Figure 2.3.

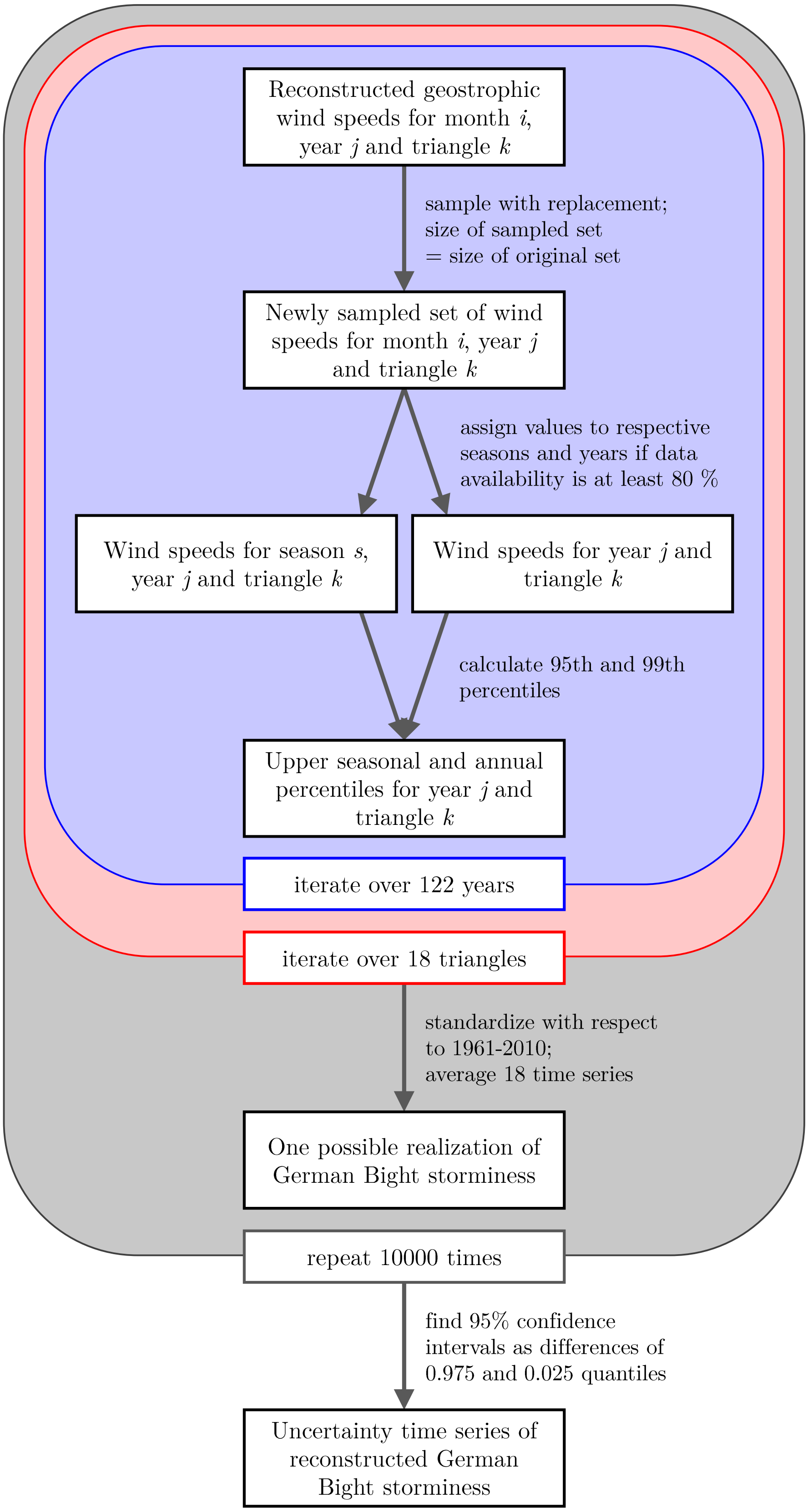

Figure 2.3: Flowchart visualization of the applied bootstrapping scheme.

3 A Historical Record of German Bight Storminess

As described in Section 2.3, three-hourly geostrophic wind speeds are calculated over 18 triangles (shown in Fig. 2.2), which are then used to build annual and seasonal frequency distributions to derive the 95th and 99th percentiles of geostrophic wind speeds. These percentiles are standardized and averaged to form dimensionless indices, all of which are considered proxies for German Bight storminess.

This chapter aims at the evaluation of temporal characteristics of these indices, as well as a contextualization with regard to notable storm events. Therefore, a detailed description of the time series of the indices is given in Section 3.1, focusing on both the multiannual variability and long-term trends of annual and seasonal storminess. Section 3.2 then relates historic storm events in the German Bight to the storminess indices of the respective years and seasons to further show the connection between the reconstructions of storm activity and actual storms.

3.1 Long-Term Storminess

Figure 3.1 depicts the time series of the standardized annual 95th and 99th percentiles of geostrophic winds over the German Bight from 1897-2018, averaged over all 18 triangles. A low-pass filter (Gaussian with σ=3) has been applied to highlight interdecadal variability. The German Bight storminess time series are subject to multidecadal variability for both the 95th and 99th percentiles. Storm activity is characterized by a period of near-average activity around 1900, followed by an increase in the years thereafter. Afterward, the 1930s and 1940s show below-average storm activity in the German Bight. Storminess subsequently increases again to shortly reach above-average levels around 1950. This phase features a peak in 1949, when annual 95th and 99th percentiles increase to 3.30 and 2.35, coinciding with historical records of observed storm events (Lamb, 1991). Throughout the 1960s and 1970s, storminess shows slightly below-average activity levels followed by an increase during the 1980s and early 1990s to above-average activity levels. In the late 1990s, German Bight storminess decreases again to below-average levels. Until the end of the examined period, storm activity remains below the long-term average. During this period, the lowest values of storminess

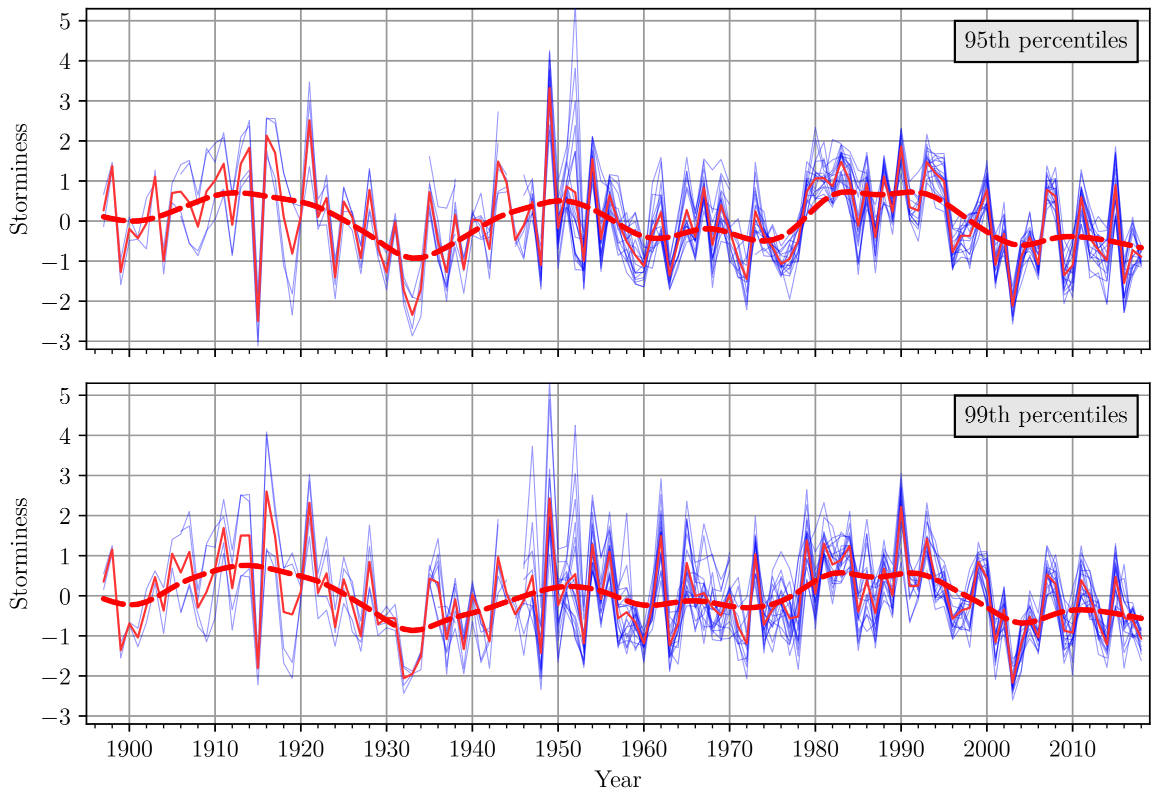

Figure 3.1: Standardized annual 95th (top) and 99th (bottom) percentiles of geostrophic winds over the German Bight, 1897-2018. Solid red lines denote values averaged over 18 triangles, dashed red lines indicate Gaussian low-pass filtered data (with parameter σ=3). Thin blue lines show values for single triangles.

are found in 2003, with a minimum value of -2.09 (-2.14) for the 95th (99th) percentiles. The corresponding absolute geostrophic wind speeds for annual 95th (99th) percentiles range between 18.4 and 26.5 $\mathrm{m\,s^{-1}}$ (23.8 and 33.9 $\mathrm{m\,s^{-1}}$), whereas the absolute annual medians lie within 8.2 and 10.9 $\mathrm{m\,s^{-1}}$ (Fig. 3.2).

To evaluate possible trends in the storminess time series, linear regressions are performed on the data for all possible time periods that cover at least three years. The slopes of the linear regressions are displayed in Figure 3.3. Trends that are considered significant at the 0.05 level are shown in Figure 3.4. Figure 3.3 illustrates that, for both percentiles, the sign of the trend of annual German Bight storminess strongly depends on the selection of starting and ending years. Extremes can be found for time periods of one to two decades, approximately half of the period duration of the dominant multidecadal variability. These extremes mark the transitions between phases of high and low storm activity and are therefore not representative of a long-term

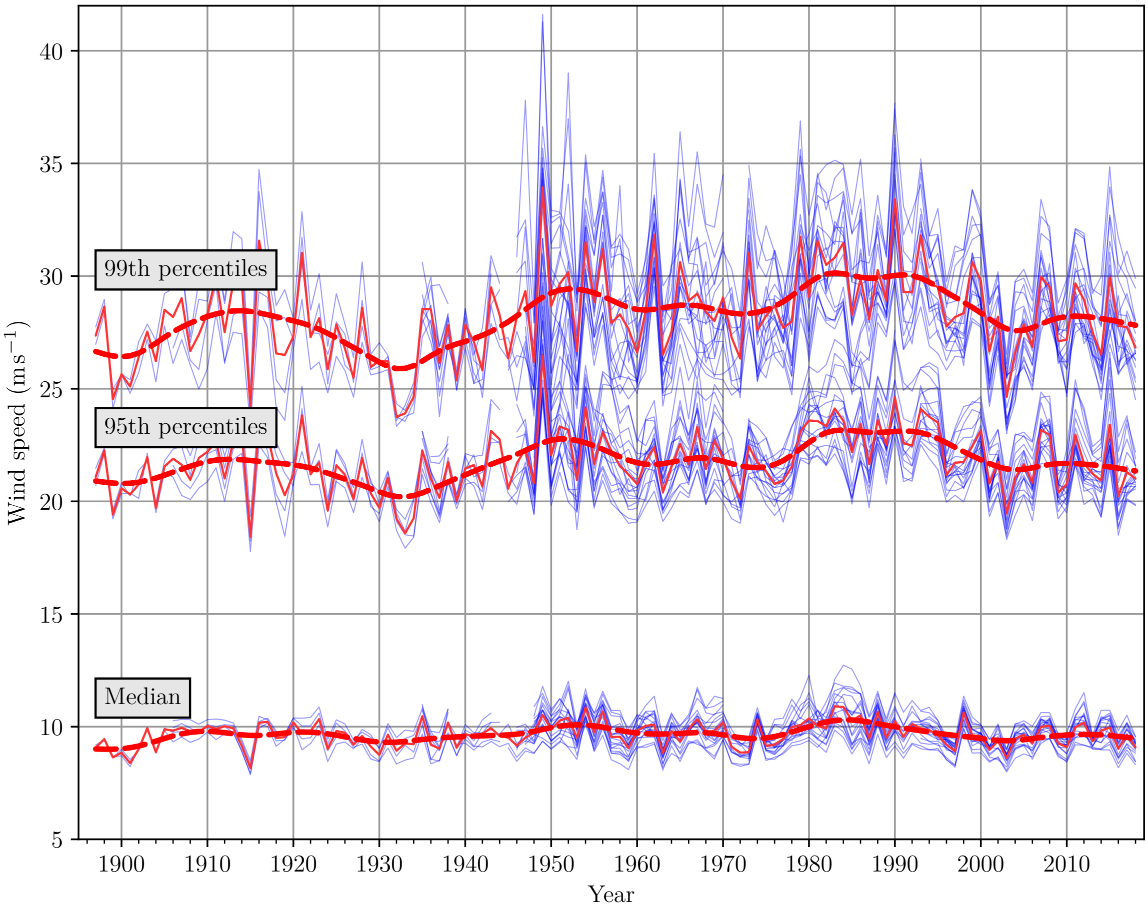

Figure 3.2: Like Figure 3.1, but non-standardized percentiles of geostrophic wind speeds are shown.

trend. Taking the entire time series into account, annual storminess exhibits a slight downward trend. However, Figure 3.4 demonstrates that the slopes of these long-term trends are not significant at the 0.05 level for periods of more than 84 years (83 years for 99th percentiles). Hence, this investigation concludes that no significant long-term is detectable in the annual German Bight storminess time series.

On the seasonal time scale, the behavior is similar (Fig. 3.5). For DJF, pronounced periods of high activity around 1910, 1950 and 1990 alternate with phases of lower activity around 1940, 1970 and the early 2000s. The recent years are characterized by a slight increase in activity. The remaining three seasons do not exhibit such a dominant variability. The activity maximum around 1950 is also visible in the spring (MAM) time series, although occurring a few years earlier than for DJF. The MAM maximum in 1906 coincides with strong storm events in March 1906 that led to storm surges at the North Sea coast (Lamb, 1991). Other phases of high storminess levels are far less pronounced in spring. Contrary to the increase in winter storminess over the past

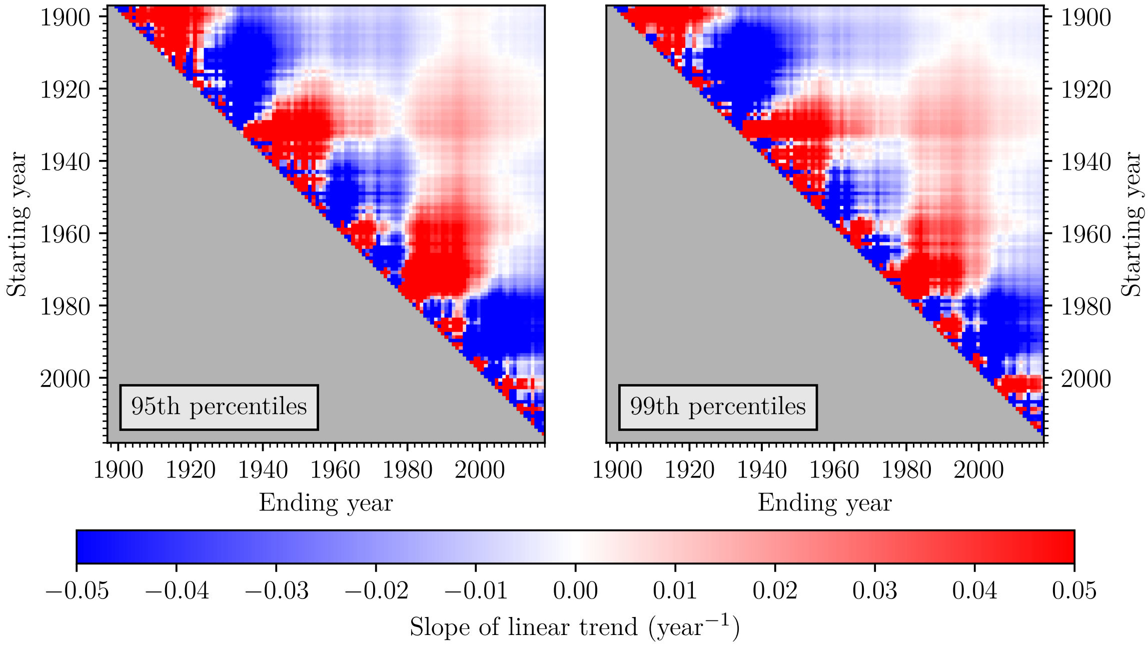

Figure 3.3: Trends of 95th and 99th percentile-based annual German Bight storminess as a function of starting and ending years. The shortest periods are found near the diagonal, while the period length increases towards the top and right.

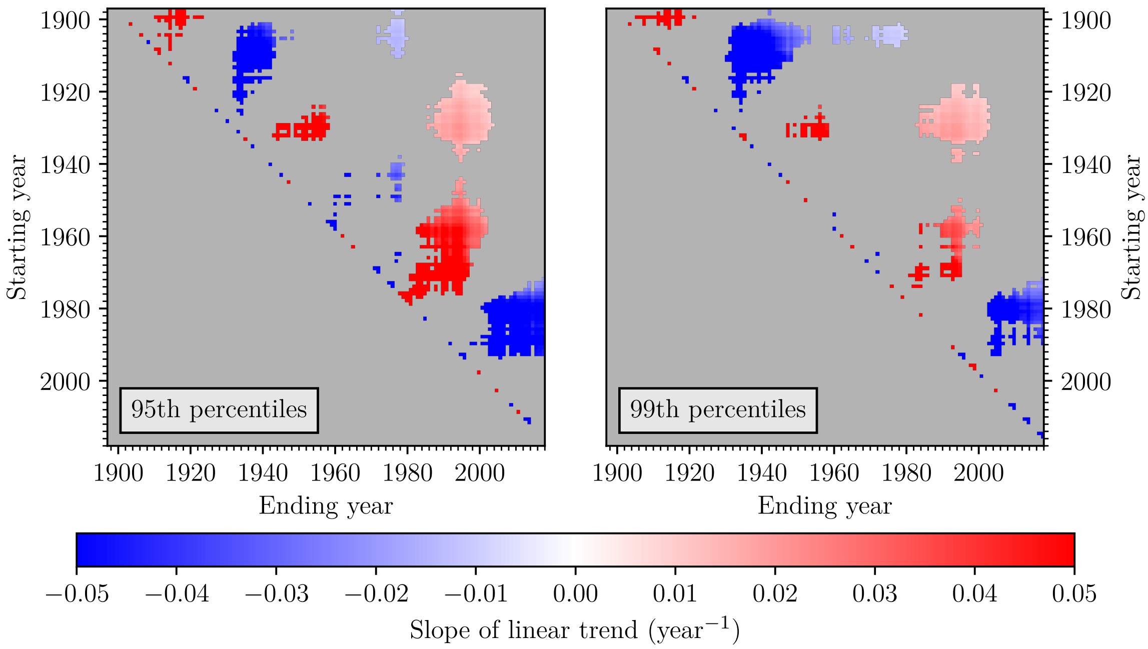

Figure 3.4: Like Figure 3.3, but only trends that reject the null hypothesis at the 0.05 significance level are shown.

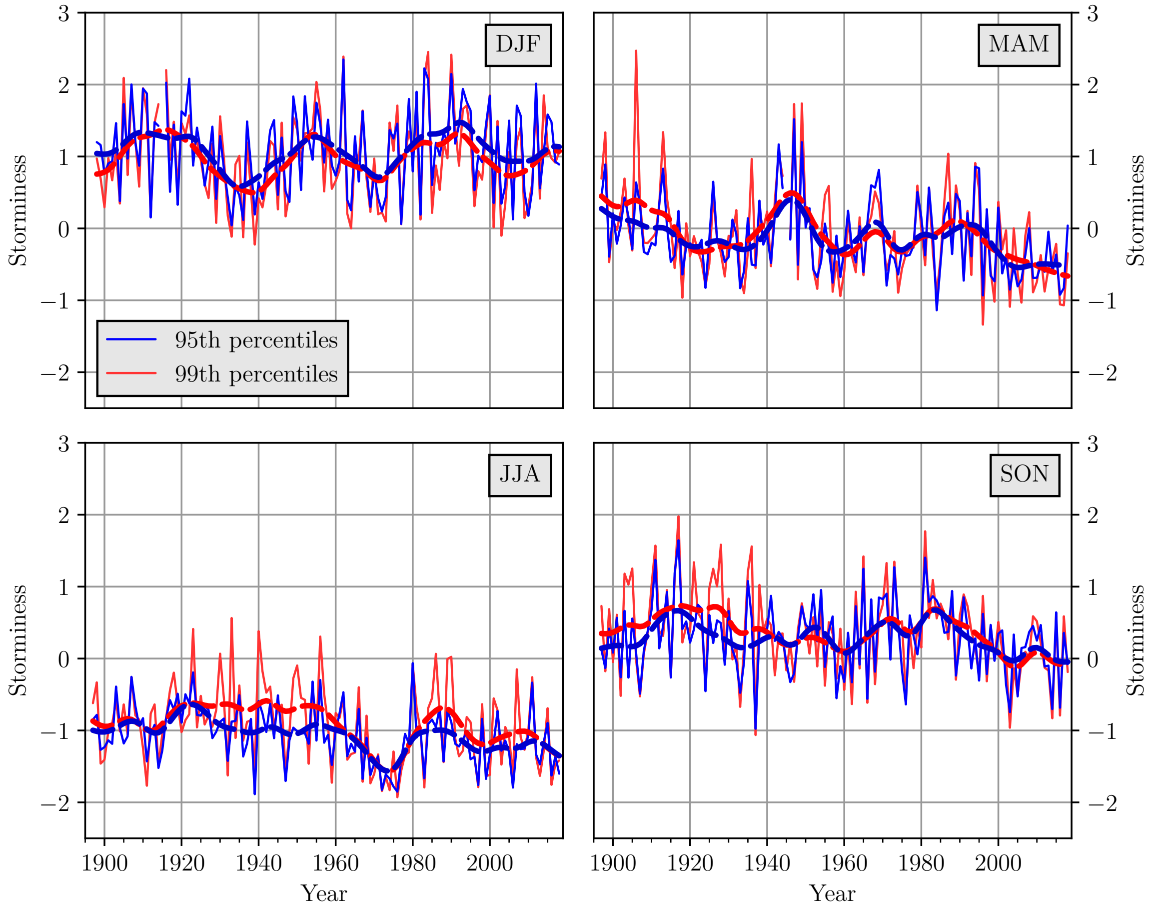

Figure 3.5: Standardized seasonal 95th (blue) and 99th (red) percentiles of geostrophic wind speeds over the German Bight, 1897-2018. Thin solid lines denote annual values, thick dashed lines show low-pass filtered data.

couple of years, spring storminess is on a downward trend starting in 1990. Summer (JJA) and fall (SON) storminess share even less features with both the winter and the annual time series. JJA storminess remains unchanged between the 1890s and 1960, but decreases below its long-term average during the 1970s. After that, storminess returns to near-normal values around 1980, followed by two slight increases around 1990 and 2010. Similarly, SON storminess increases slightly during the 1910s, then starts to slowly decline until 1960. After another increase until 1980, SON storminess decreases for two decades and remains steady throughout the 2000s. Long-term trends of fall storm activity are strongly superimposed by year-to-year fluctuations.

The derivation of seasonal statistics of geostrophic winds is based on the annual mean and standard deviation of 1961-2010 in order to explain the seasonal contribution of storm activity with regards to the annual time series. The winter (DJF) time series shows the closest resemblance to the annual time series (Fig. 3.1). As the magnitude of DJF storminess is highest compared with the other seasons with long-term means of 1.07 and 0.97 for the 95th and the 99th percentiles, DJF storminess contributes most to German Bight storm activity. In contrast, JJA shows the weakest activity levels (-1.07 and -0.93). Spring (-0.14 and -0.10) and fall (0.29 and 0.36) can be described as transitioning periods between high-activity winters and low-activity summers. Depending on the temporal extent of the winter storm season, the number of windstorm events and eventually the storminess level during this transitioning period is subject to fluctuations. Therefore, the contribution of MAM and SON storminess varies from year to year, but can be described as generally higher than JJA and lower than DJF.

Analogous to the annual time series, linear regressions are performed to investigate possible trends. The slopes of the linear regressions for 95th and 99th percentiles are displayed in Figures A.1 and A.2, respectively. Trends that are considered significant at the 0.05 level are shown in Figures A.3 and A.4. Again, trends in storminess assume positive and negative values depending on the time period used. The dominant pattern of positive and negative extremes for periods between one and two decades is best visible in DJF storminess. Above a time span of 88 years (79 years for 99th percentiles) however, the absolute slopes of linear regressions of DJF storminess become too small to be considered significantly different from 0. Therefore, DJF storminess is presumed to not exhibit a trend over the last century. MAM and SON storminess reveal slightly more pronounced downward trends on long time scales. Even though these trends show statistical significance for several combinations of starting and ending years, the fraction of insignificant trends over long periods is still much higher. On the contrary, JJA storminess displays a downward trend which is significant at the 0.05 level not only for the entire time series, but for the majority of periods above 90 years. Thus, the regressions indicate that JJA storminess is showing a slow but significant decline over the last century. As previously described, annual storminess consists of data from all four seasons, with winter storminess being the main contributor. Hence, the downward trend in summer storminess is not enough to cause the annual trend to become significantly negative, as it is counteracted by the small, insignificant trends that spring, summer, and, to the largest extent, winter contribute.

The time series of German Bight storm activity generally resemble the reconstruction of Dutch storminess from homogenized windstorm insurance losses by Cusack (2013). Here, the time series follows a multidecadal oscillation with maxima in the 1910s, 1940s and 1980s, close to the maxima in German Bight storminess. Periods of lower storm activity levels are found during the 1930s, 1960s, and since the late 1990s, largely coinciding with phases of reduced storminess over the nearby German Bight. Similarly, the

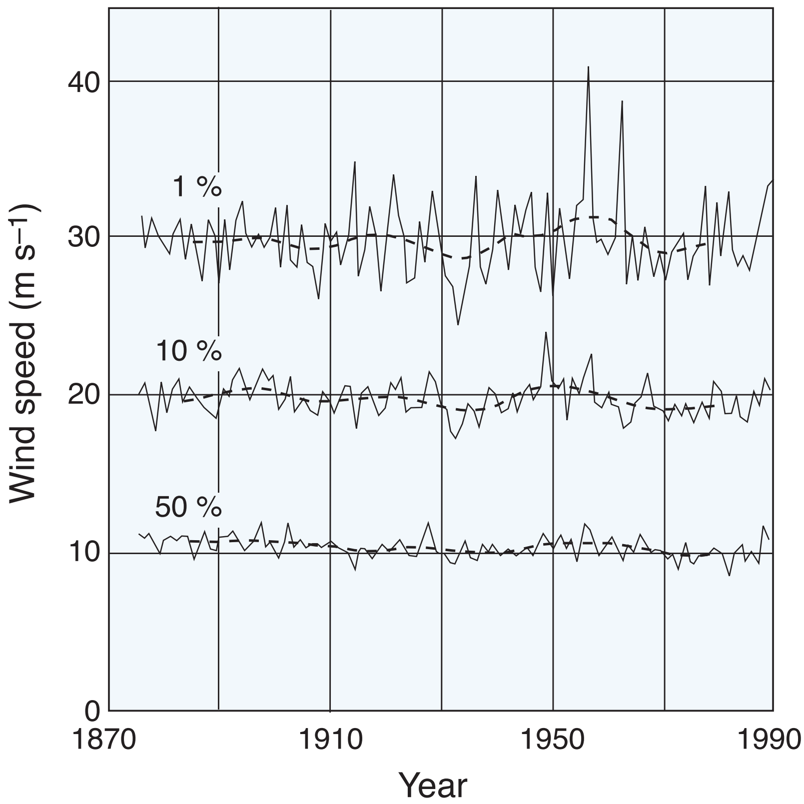

Figure 3.6: Annual 50th, 90th and 99th percentiles (labeled as 50 %, 10 % and 1 %) of geostrophic wind speeds over the German Bight, 1876-1989. Solid lines denote annual values, dashed lines show 30-year low pass filtered data. Figure taken from Schmidt and von Storch (1993).

comparison with Schmidt and von Storch (1993) (Fig. 3.6) shows an agreement in the order of magnitude for the median and the 99th percentiles of geostrophic wind speeds, even though the details in Schmidt and von Storch (1993) are rather unclear.

The results after the 1960s also agree with the storm surge reconstructions of Dangendorf et al. (2014) (Fig. 3.7). The increase in upper annual quantiles of storm surge levels from the 1960s to the 1980s and a decline thereafter is similar to the behavior of German Bight storminess. However, the earlier reconstructions of surge levels do not correspond with our results. Contrary to storm activity, storm surge levels vary little between 1900 and 1940, and recede to below-average values during the 1940s and 1950s, a period characterized by higher than normal storm activity. However, Dangendorf et al. (2014) reconstructed the surge record for the tide gauge at Cuxhaven, which is located in the Elbe estuary and therefore especially prone to surges caused by northwesterly winds. As later investigations will show (Sec. 5.3.2), the frequency

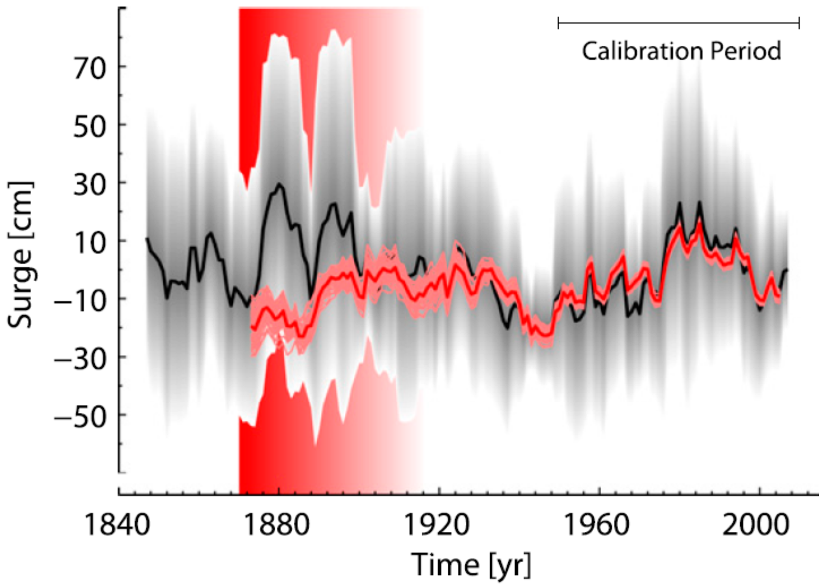

Figure 3.7: Reconstructed (red) and observational (black) record of surges for the tide gauge at Cuxhaven. The red shaded area shows the period where reconstructions and observations differ significantly. Figure taken from Dangendorf et al. (2014). © American Meteorological Society. Used with permission.

of northwesterly winds stays below average during the fall and winter seasons in the 1950s, despite above-average German Bight storminess in the same time frame. Thus, the discrepancy between storminess and surge reconstructions indicates that the surge record can only provide complementary information for the reconstruction of storm activity as the surges strongly depend on the wind direction and the layout of coastlines (Ganske et al., 2018).

3.2 A Link to Notable Storm Events

The previous section contained an overview of the temporal behavior of 95th and 99th percentile-based German Bight storminess between 1897 and 2018 on an annual and seasonal scale. As a follow-up, notable historic storm events, such as powerful extratropical cyclones or storm surges that affected the German Bight, are compared against the respective storminess values of the year and season they occurred in. This comparison contextualizes historical events through checking if they are represented by peaks in annual or seasonal statistics. Lamb (1991) compiled a vast record of notable past storm events and periods of enhanced storm activity over the North Sea, which serves as the main data foundation for subsequent comparisons. Hence, unless otherwise noted, data and information about storms before 1990 in this section are taken from Lamb (1991). Table 3.1 lists notable historical storm and storm surge events that affected the German Bight and its surrounding coastlines between 1897 and 2018. The table also shows the corresponding seasonal and annual storminess index values for each event, a selection of which will be discussed below.

In March 1906, a deepening cyclone moved across Ireland, the North Sea, northern Denmark, and eventually into southern Sweden. The low reached a minimum central pressure of 960 hPa and maintained a steep pressure gradient on its western side throughout the passage across the North Sea, leading to a prolonged period of northerly winds over the German Bight and adjacent waters. This setup caused water levels along the German and Dutch coastlines to rise considerably, exceeding the previous record level set at the Emden tide gauge in 1825. The storm event of 1906 can be found in the time series of 99th percentile-based MAM storminess, which reaches its absolute maximum during that year.

In February 1916, a low-pressure system, that had previously formed over Iceland, tracked across Scotland and the North Sea into Sweden and continued moving across the Baltic Sea. The low attained a minimum core pressure of 959 hPa over northern Denmark and placed the German Bight under a tight meridional pressure gradient. The resulting westerly winds caused a significant storm surge on the coast of Schleswig-Holstein, comparable to the surge events of 1825 and 1906. Additionally, the entire winter of 1915/16 was dominated by a zonal flow regime and generally westerly winds. This pattern reflects in the annual and seasonal storminess indices, both of which are more than two standard deviations above average. The 99th percentile-based annual index of 2.60 is the highest in the entire time series.

The highest storminess index for 95th percentiles (second highest for 99th percentiles) can be found in the year 1949. While the year did not produce a historic storm, such as the cyclones of 1962 or 1976, its unusually high storminess index is rather caused by above-average storm activity in winter, spring and fall and a number of smaller storm events, as, for instance, in February and October of 1949.

One of the most famous storms to affect the German Bight and adjacent coastlines is the cyclone of February 1962, colloquially known as *Vincinette*. The storm originated in the NE Atlantic (Fig. 3.8a) and moved southeastward across Norway into the Baltic Sea, placing the German Bight in an area of persistent and strong northwesterly flow (Fig. 3.8b). Geostrophic winds over the German Bight stayed near or above $35\,\mathrm{m\,s^{-1}}$

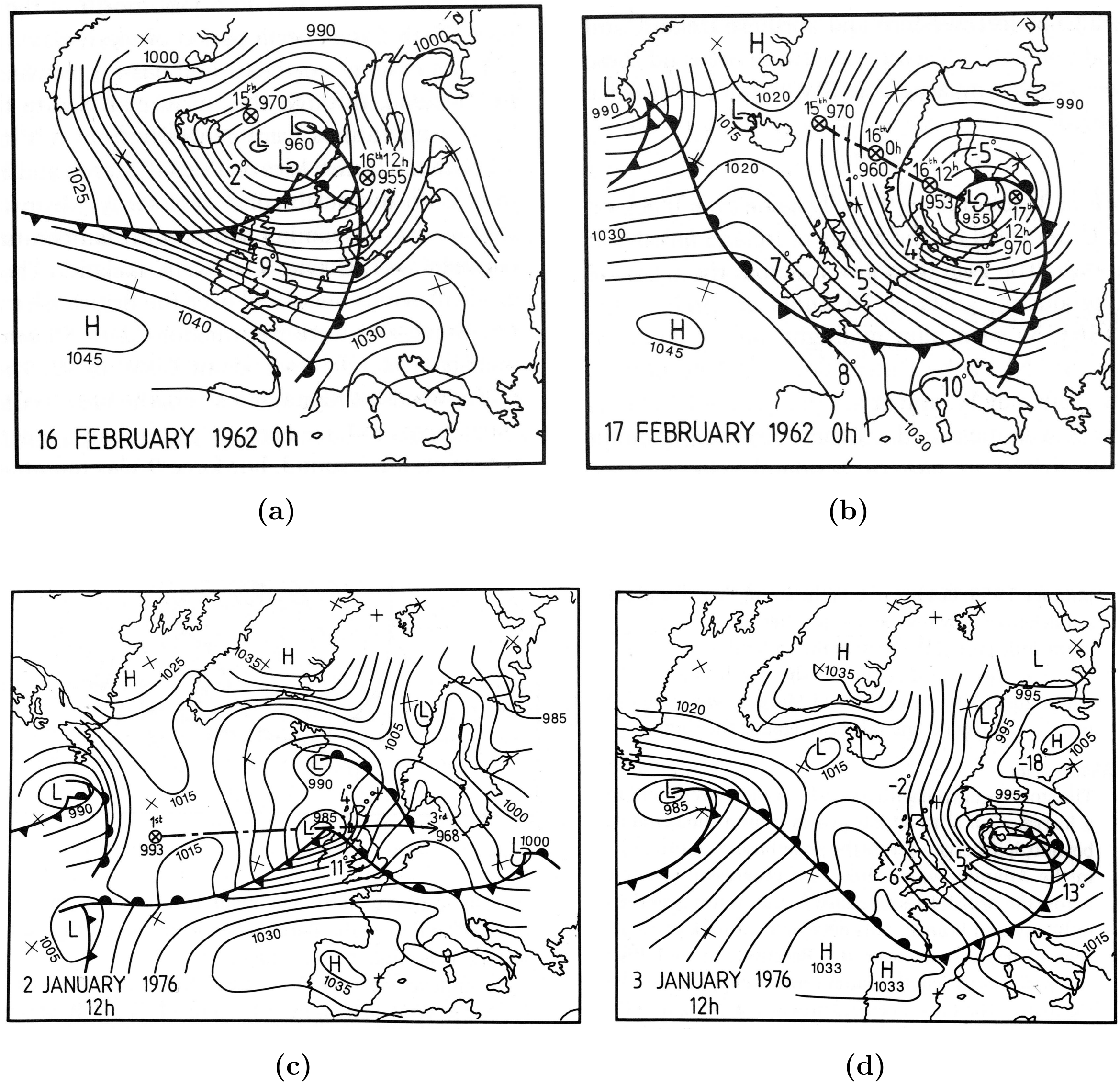

Figure 3.8: Exemplary surface analysis charts for Feb 16, 1962 00Z **(a)** and Feb 17, 1962 00Z **(b)**, during the cyclone *Vincinette*, and for Jan 2, 1976 12Z **(c)** and Jan 3, 1976 12Z **(d)**, during *Capella.* The charts are scans of images printed in Lamb (1991).

for two days (Fig. 3.9). With a minimum central pressure of 953 hPa and a northward displaced Azores high with a pressure of more than 1045 hPa, the strong winds resulting from the pressure gradient induced a severe storm surge along the German coast. Multiple long stretches of dikes were breached and destroyed, causing a devastating flood that killed 340 people in Hamburg and Oldenburg. This event is strongly visible in the seasonal storminess index for DJF 1961/62, which reaches its highest overall value for 95th percentiles (third highest for 99th percentiles).

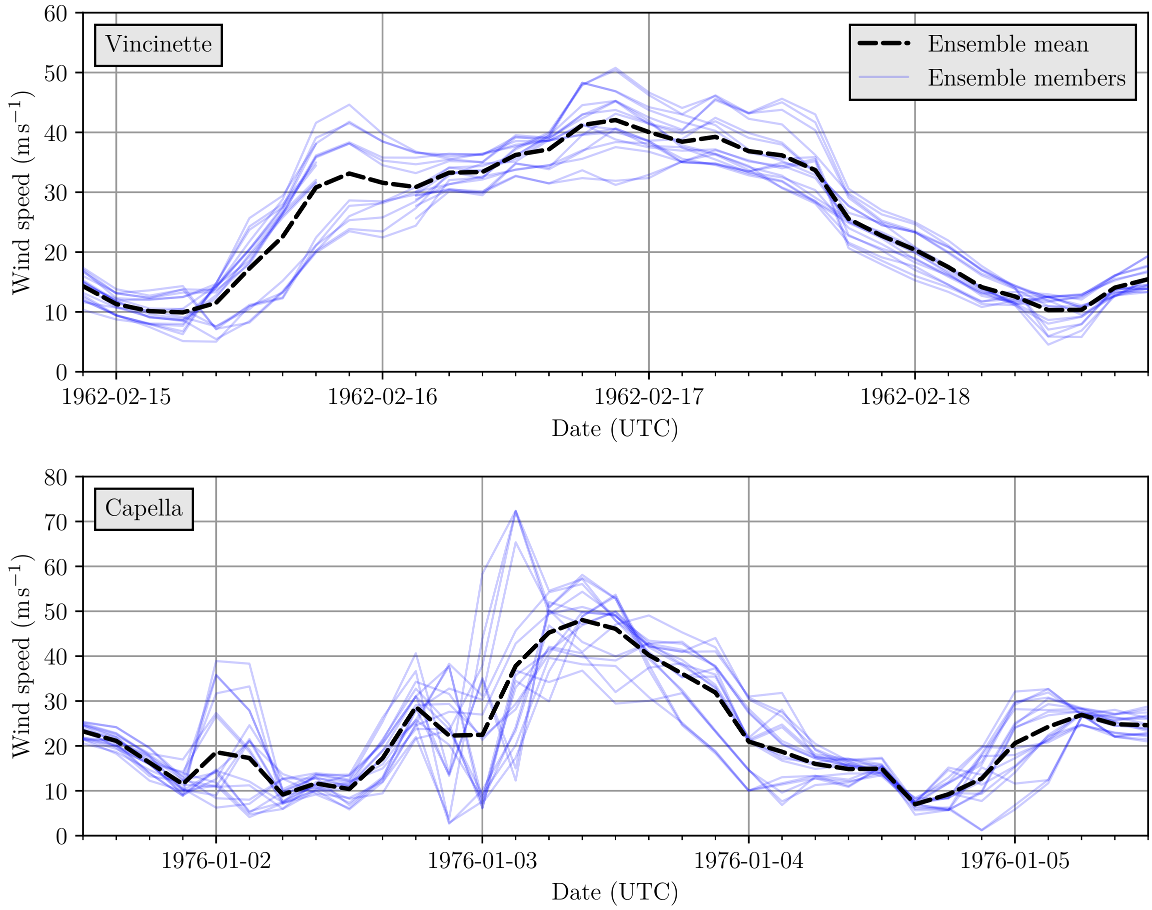

Figure 3.9: Exemplary reconstructed geostrophic wind speeds over the German Bight during the cyclones *Vincinette*, Feb 14-18, 1962, and *Capella*, Jan 1-5, 1976. Thin blue lines denote values for individual triangles, whereas the thick dashed line indicates the mean over all 18 triangles.

Another notable example of a historic storm event over the German Bight is the cyclone of January 1976, which is also called *Capella-Orkan*. The low formed over the open Atlantic and moved quickly eastward across Scotland and the southeastern North Sea (Fig. 3.8c). While crossing Denmark, the cyclone reached its lowest pressure at 968 hPa, shortly before emerging into the Baltic Sea. The storm's southwestern quadrant had a very steep pressure gradient (Fig. 3.8d) and hence very intense winds, with an ensemble mean geostrophic wind speed around $50\,\mathrm{m\,s^{-1}}$ and individual triangles peaking near $70\,\mathrm{m\,s^{-1}}$ (Fig. 3.9). The intensity of the wind allowed for an unusually high storm surge to build up along the German and Danish coasts. At multiple tide gauges, water levels exceeded the previous record marks set just 14 years prior. However, reinforced dikes and additional efforts in coastal protection after the 1962 storm prevented another disastrous flood. The 1976 storm occurred in a year of below-average storm activity.

Even though the 99th percentile-based seasonal index is ranked in the upper quartile, the annual index is negative, indicating that this single event was not large enough to compensate for the inactivity during the remainder of the year.

Seven years after cyclone *Capella*, the winter of 1982/83 showed one of the highest frequencies of severe cyclones over Europe in recorded history. Between December 1982 and February 1983, multiple strong low-pressure systems with central pressures of as low as 930 hPa tracked across the North Atlantic. The sustained zonal flow with embedded storm systems led to above-average temperatures in large parts of the northern hemisphere and is reflected in high storminess indices on both the annual and seasonal scale.

In the winter of 1989/90, the German Bight was affected by multiple hurricane-force storms, with *Daria*, *Vivian* and *Wiebke* being the strongest cyclones in January and February 1990 (DWD, 2002). The storms caused gusts of up to 265 $\mathrm{km\,h^{-1}}$, consecutive severe storm surges and high insurance losses (DWD, 2002). This streak of high storm activity is visible in both the annual and seasonal storminess indices, both of which rank in the upper quartile, with the 99th percentile-based winter storminess reaching its second highest value. Note that the entire winter was unusually warm (DWD, 2002), which is an indicator for enhanced zonal flow and above-average storm activity.

A comparable winter with multiple strong storm systems occurred ten years later. In early December 1999, *Anatol* affected the northern parts of Germany, Denmark and adjacent areas, including the German Bight (DWD, 2002). Later that season in January 2000, two storms named *Kerstin* and *Liane* again caused hurricane-force gusts over North Germany (DWD, 2002). As the series of storms took place over a span of two distinct years, the annual storminess values for 1999 and 2000 are lower than in other years with similarly active winters, whereas winter storminess values are well above the 75 % quantile. This winter was also marked by another historic storm, *Lothar*, which moved across northern France and central Germany and resulted in heavy forest damage (DWD, 2002). However, as the center of the cyclone track moved well south of the German Bight, the effects on German Bight storminess are negligible.

In recent years, two notable examples of strong storm events over the German Bight are the cyclones *Kyrill* and *Xaver*, which impacted the area in January 2007 and December 2013, respectively (DWD, 2017a). *Kyrill* caused 13 casualties in Germany, regional power outages and heavy tree damage (DWD, 2017a). *Xaver* mainly affected North Germany, where the persistent northwesterly flow forced water up the Elbe estuary, which resulted in a storm tide of almost 4 m above mean high water in Hamburg (BSH, 2013), the highest level since 1976. For both events, high storminess values can be seen in the respective seasons. In 2007, annual storminess is also well above average, whereas 2013 exhibits generally lower annual storminess. The low annual index in 2013 can be explained by multiple cold periods during the late winter and spring (DWD, 2017a), which indicate an anticyclonic pattern and reduced storm activity during the beginning of the year.

Table 3.1: List of notable storm or storm surge events in the German Bight with storminess indices for the respective years and seasons. $S_{\mathrm{ann},95}$ and $S_{\mathrm{ann},99}$ mark annual storminess values based on the 95th and 99th percentiles, whereas corresponding seasonal values are denoted by $S_{\mathrm{seas},95}$ and $S_{\mathrm{seas},99}$. Index values are colored red or blue when they are ranked in the upper or lower quartile of all years or seasons, respectively. Unless otherwise noted, data for the storm events are taken from Lamb (1991).

	Annual		Seasonal	
Storm Event(s)	$S_{\mathrm{ann},95}$	$S_{\mathrm{ann},99}$	$S_{\mathrm{seas},95}$	$S_{\mathrm{seas},99}$
28-29 Nov 1897	0.27	0.35	0.12	0.73
25-26 Dec 1902	-0.05	-0.25	1.46	1.09
26-27 Feb 1903	1.11	0.46	1.46	1.09
12-13 Mar 1906	0.74	0.58	0.64	2.47[a]
3 Dec 1909	0.75	0.10	1.20	1.24
16 Feb 1916	2.14	2.60[a]	2.03	2.20
6-7 Jan 1928	0.78	0.85	1.41	1.18
16-17, 23-25 Nov 1928	0.78	0.85	0.49	1.58
5-7 Dec 1929	-0.67	-0.71	1.28	1.56
17-19, 26-27 Oct 1936	-0.51	0.33	0.56	1.56
10-13 Feb 1938	0.15	-0.09	0.87	0.53
23-24 Nov 1938	0.15	-0.09	0.39	1.02
9-10 Feb 1949	3.32[a]	2.42	1.84	1.54
23-26 Oct 1949	3.32[a]	2.42	0.72	0.77
21-23 Dec 1954	1.55	1.28	1.75	2.04
16-17 Feb 1962	0.22	1.49	2.35[a]	2.39
23 Feb 1967	0.84	0.06	1.63	1.64
12-13 Nov 1972	-1.44	-1.19	-0.01	0.03
2-3 Apr 1973	0.25	1.04	-0.42	-0.04
6-30 Nov 1973[b]	0.25	1.04	1.27	1.35
1-17 Dec 1973[b]	0.25	1.04	1.37	1.47

	Annual		Seasonal	
Storm Event(s)	$S_{ann,95}$	$S_{ann,99}$	$S_{seas,95}$	$S_{seas,99}$
2-3 Jan 1976	-1.07	-0.09	1.46	1.71
11-12 Jan, 13-14 Feb 1979	0.74	1.38	1.80	1.35
23-25 Nov 1981	1.07	1.30	1.40	1.77
18 Jan, 1 Feb 1983	1.48	0.89	2.23	2.10
9-10 Feb 1988	1.12	0.67	1.33	1.21
25-26 Jan, 26 Feb-1 Mar 1990[c,d]	1.86	2.21	2.15	2.42
13 Jan 1993[d]	1.48	1.42	1.94	1.66
3-4 Dec 1999[d]	0.19	0.85	1.84	1.85
29-31 Jan 2000[d]	0.78	0.45	1.84	1.85
18 Jan 2007[e]	0.78	0.53	1.71	1.20
5-6 Dec 2013[e]	-0.72	-0.68	1.06	1.85

[a] highest value in the entire time series

[b] listed as one continuous sequence of storms in Lamb (1991), but split into two parts to account for the respective seasons

[c] 1 Mar 1990 is not separately listed, as the majority of the events occurred in winter

[d] from DWD (2002)

[e] from DWD (2017a)

4 Validating German Bight Storminess

Despite the fact that the time series exhibit uncertainty (see Chap. 6), the method of calculating geostrophic wind speeds and their statistics is a valuable tool to make inferences about storm activity. To demonstrate the validity of the geostrophic storminess time series, it is necessary to compare the reconstructions with available reference data. Although the temporal coverage of such reference data makes up only a small part of the last century, it can still give insight into certain characteristics of the reconstucted geostrophic wind speeds that are derived through the methods and assumptions used (see Chap. 2). For this reason, the three-hourly reconstructed geostrophic wind speeds are first compared with measurements of wind speed taken at the FINO1 site in the North Sea at a height of 71 m above sea level. The use of data from 71 m above sea level is motivated by data availability, which is higher than for instruments closer to the surface. Afterward, annual statistics of German Bight storminess are compared with statistics from reanalysis datasets.

Both time series exhibit a very dominant annual cycle, with the highest wind speeds typically occurring in winter (Fig. 4.1). The geostrophic wind speeds are notably higher, peaking above $40\,\mathrm{m\,s^{-1}}$ at multiple times, whereas the highest wind speed measured at FINO1 is $32.75\,\mathrm{m\,s^{-1}}$ (Fig. 4.2). Note that sampling 10-minute mean data at three-hourly intervals can hide the extent of wind speed variability at smaller time scales.

Overall, the measured wind speed at FINO1 is slightly lower than the calculated geostrophic wind over the German Bight during the same period (Fig. 4.1 and 4.2). This is understandable as the geostrophic wind is more or less an approximation of upper atmospheric movements devoid of ageostrophic effects like friction or turbulence (e.g. Hasse, 1974). The absence of friction in the reconstruction can also be detected through wind direction analysis (Fig. 4.3). The windroses, which essentially show polar histograms of wind directions, indicate a discrepancy in both speed and the prevailing wind direction. The aforementioned overestimation of wind speeds by the reconstruction is visible, as well as a directional bias towards the right. The measured winds are predominantly southwesterly instead of westerly as a result of surface friction. The same effect is visible in the seasonal windroses (Fig. A.5 and A.6).

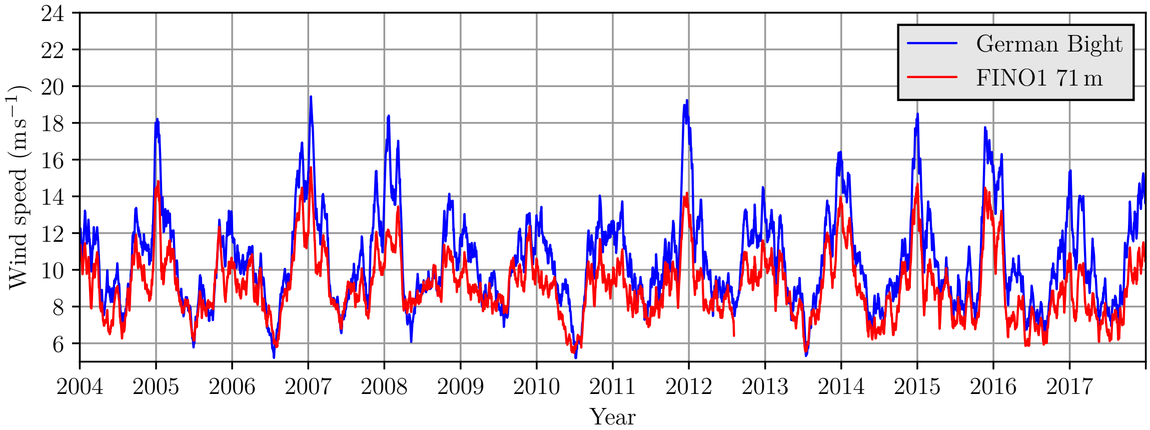

Figure 4.1: 30-day running means of reconstructed geostrophic wind speeds over the German Bight (blue) and wind speed observations from the 71 m cup anemometer at the FINO1 site (red), 2004-2017.

Furthermore, the reconstruction of geostrophic wind speeds via the triangle method assumes a linear two-dimensional pressure field without any curvature (see Sec. 2.3). In cyclones, where the steepest pressure gradients usually occur, strong curvatures are frequent. The additional centrifugal force needed to keep a moving air parcel on a curved track has to be balanced by the Coriolis and pressure gradient forces, resulting in the so called gradient wind. The gradient wind is sub-geostrophic in cyclonic flow, meaning that actual wind speeds around cyclones are lower than the geostrophic wind relation would suggest. This effect becomes more apparent with increasing curvature and wind speed. Figure 4.4 indicates that the discrepancy between measurements and the reconstruction is most evident in high-wind environments. Figure 4.2 confirms the wind speed dependent discrepancy as, for high wind speeds, the maximum of the two-dimensional kernel density function moves towards the reconstructed geostrophic wind. For speeds below $10\,\mathrm{m\,s^{-1}}$, the density function is maximized near the angle bisector, symbolizing that reconstructed and measured wind speeds agree.

Despite the disagreement in the upper range of wind speeds, both time series show good correlation skills. The correlation between the two time series is 0.81 for three-hourly data. On longer time scales, when high frequency variability is smoothed out, the correlation increases to 0.93 for 30-day low-pass filtered data. This increase indicates an agreement in the variabilities of the seasonal and annual cycles. Additionally, it should be considered that wind measurements at the FINO1 platform have increasingly been affected by the ongoing construction of wind power plants upstream over the past years. As these wind turbines take out kinetic energy from the mean flow, they induce a re-

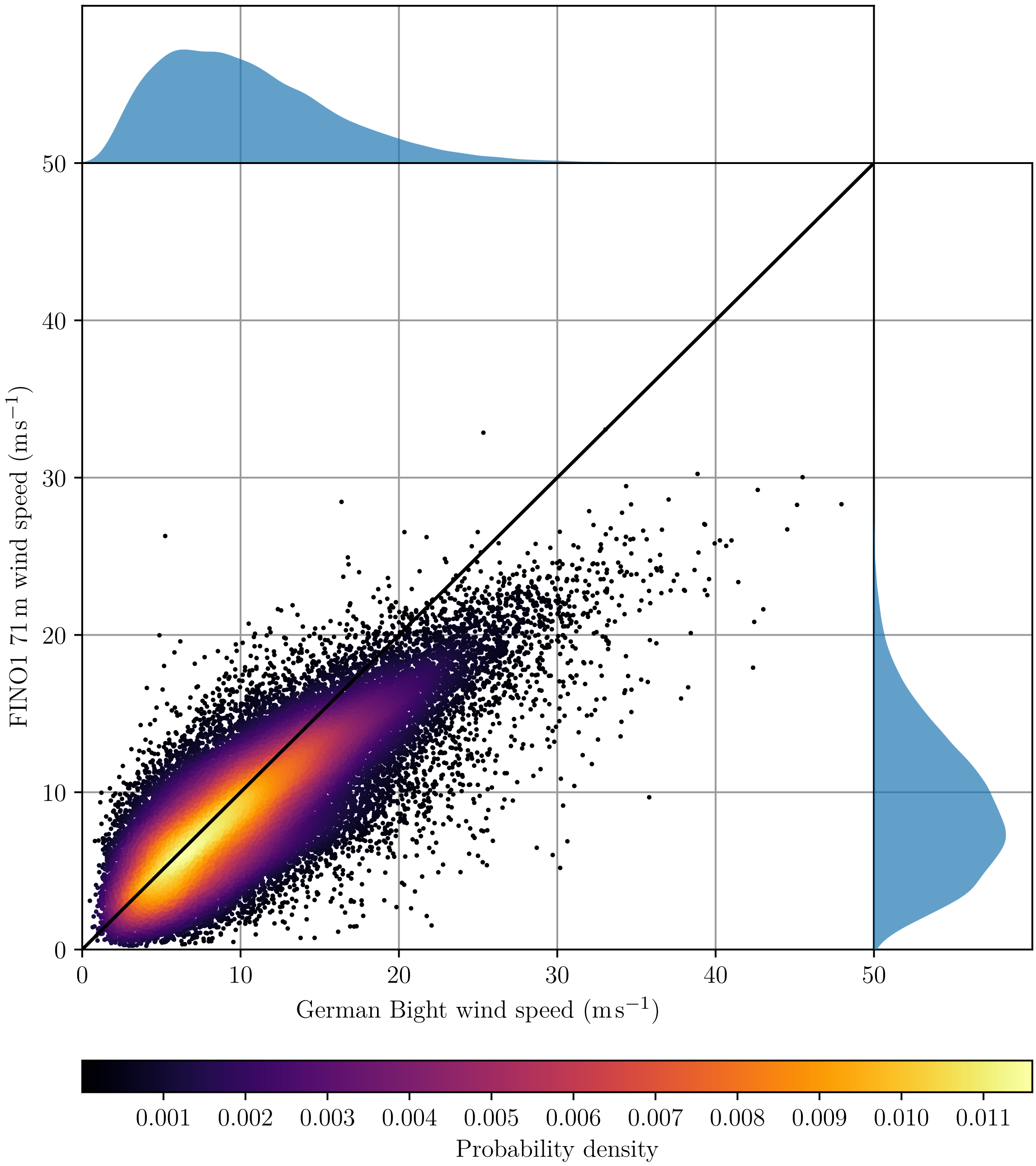

Figure 4.2: Three-hourly reconstructed geostrophic wind speeds over the German Bight vs. three-hourly 10-minute mean wind speed observations from the 71 m cup anemometer at the FINO1 site, 2004-2017. Data points are color-coded based on a bivariate Gaussian kernel density estimation, where brighter colors indicate higher probability densities. The one-dimensional histograms show probability densities of the individual time series.

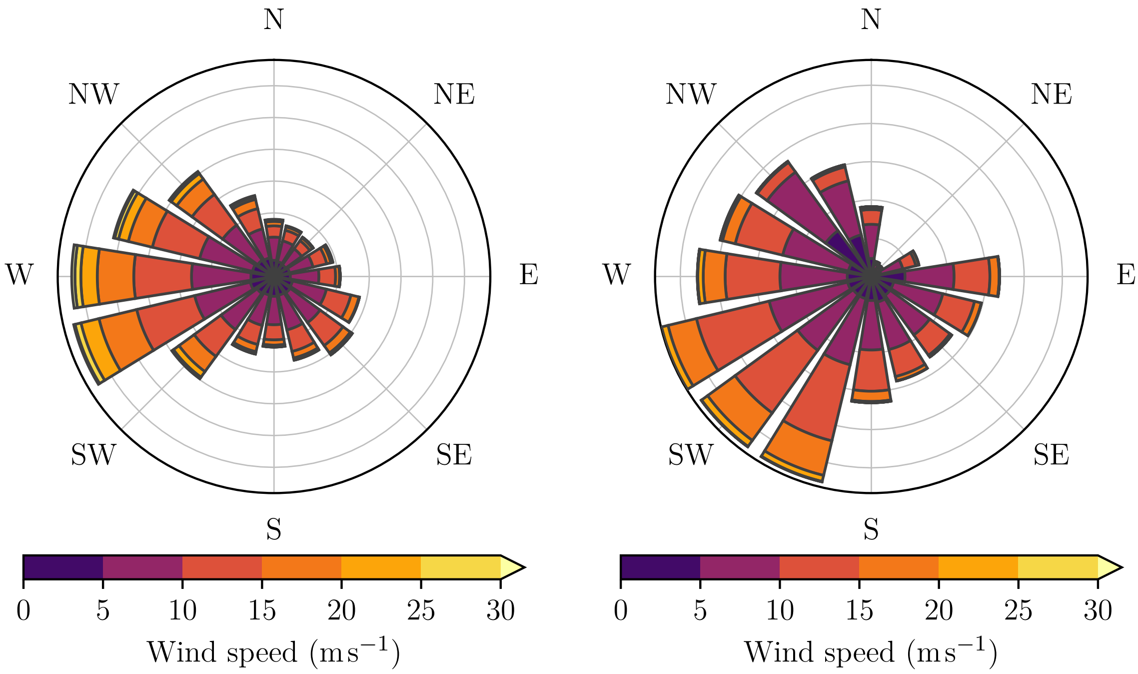

(a) German Bight **(b)** FINO1 71 m

Figure 4.3: Wind roses showing the distribution of wind directions and speeds, based on the reconstructed three-hourly geostrophic wind over the German Bight **(a)**, and on three-hourly 10-minute mean in-situ measurements from the FINO1 research platform **(b)**, 2004-2017.

duction of the overall wind speed at the measurement site (Baidya Roy et al., 2004), which is neither resolved by the reanalysis products nor considered in reconstructions. Thus, it can be argued that, without this anthropogenically caused decrease in wind speeds, the correlation between the reconstructed geostrophic wind and the in-situ measurements would be higher. Unfortunately, it is impossible to investigate longer time scales for interannual variability or examine periods of unobstructed flow with FINO1 measurements as they are too short and recent to make reliable assumptions.

To demonstrate a good agreement on longer time scales, current atmospheric reanalysis datasets, namely ERA5, ERA-Interim, MERRA-2, and a combination of CFSR version 1 and version 2 for the period 1980-2018 are made use of. These datasets contain records of analyses of atmospheric fields, obtained through the assimilation of observational data for meteorological variables (e.g. Kalnay et al., 1996). All gridpoints encompassed by the respective triangles are selected and sampled at the same time steps, i. e. three-hourly for MERRA-2 and ERA5, six-hourly for ERA-Interim and CFSR. Upper quantiles of area-weighted means of 10 m near-surface wind in the

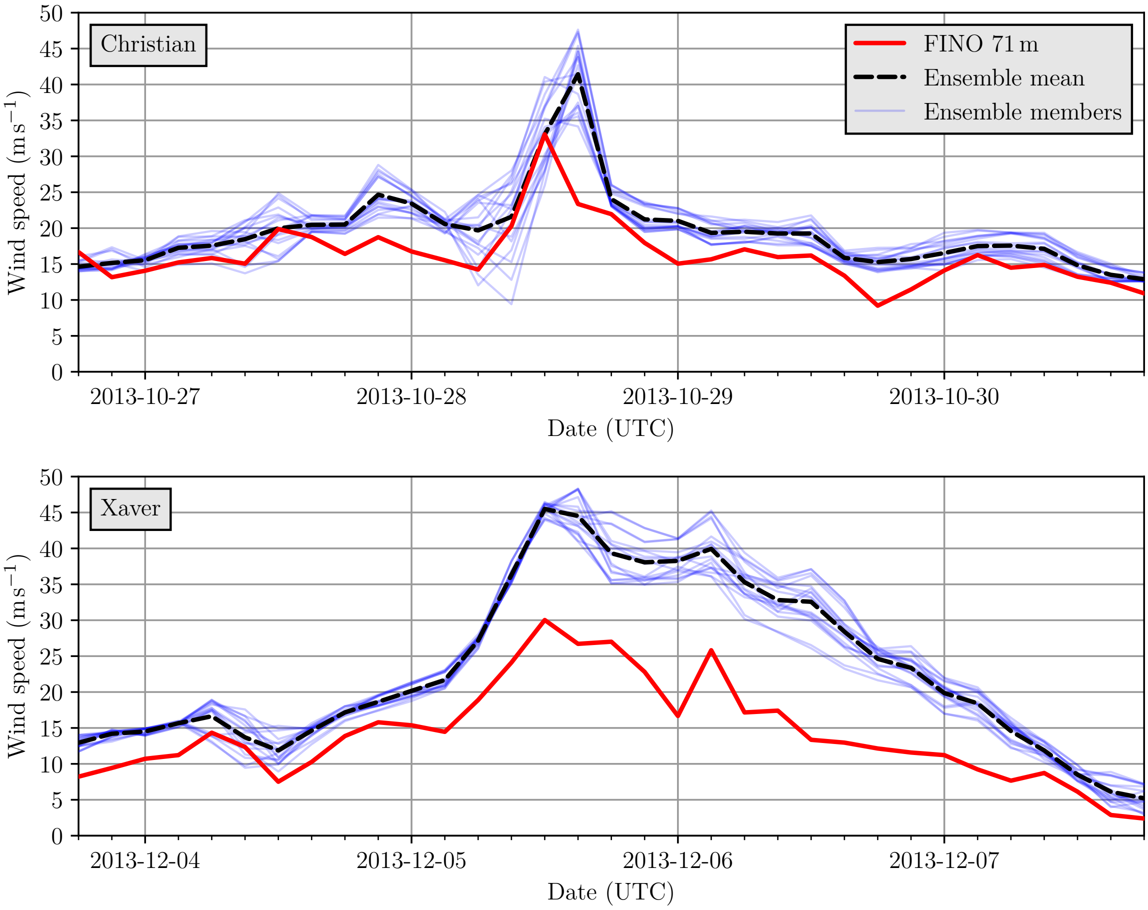

Figure 4.4: Reconstructed geostrophic wind speeds over the German Bight (blue) and wind speed observations from the 71 m cup anemometer at the FINO1 site (red) for the windstorms *Christian* and *Xaver* in 2013. Thin solid lines indicate wind speeds of the 18 individual triangles, whereas the thick dashed line represents the ensemble mean.

reanalyses are calculated and compared with the results from Section 3.1.

The best correlation between observation-based storminess and wind speed reanalysis data is found in ERA-Interim (0.74 and 0.84 for 95th and 99th percentiles), followed by MERRA-2 (0.74 and 0.80), ERA5 (0.70 and 0.79) and CFSR (0.66 and 0.79) (Fig. 4.5 and Tab. 4.1). Even though the comparison stretches among different datasets with different temporal and spatial resolutions, the high correlation coefficients between observation-based and modelled statistics indicate a good agreement between the variability of near-surface wind and geostrophic wind on longer time scales. This agreement confirms that, on longer time scales, statistics of geostrophic wind speeds are valuable to represent storminess conditions over the German Bight, furthermore confirming Krueger and von Storch (2011).

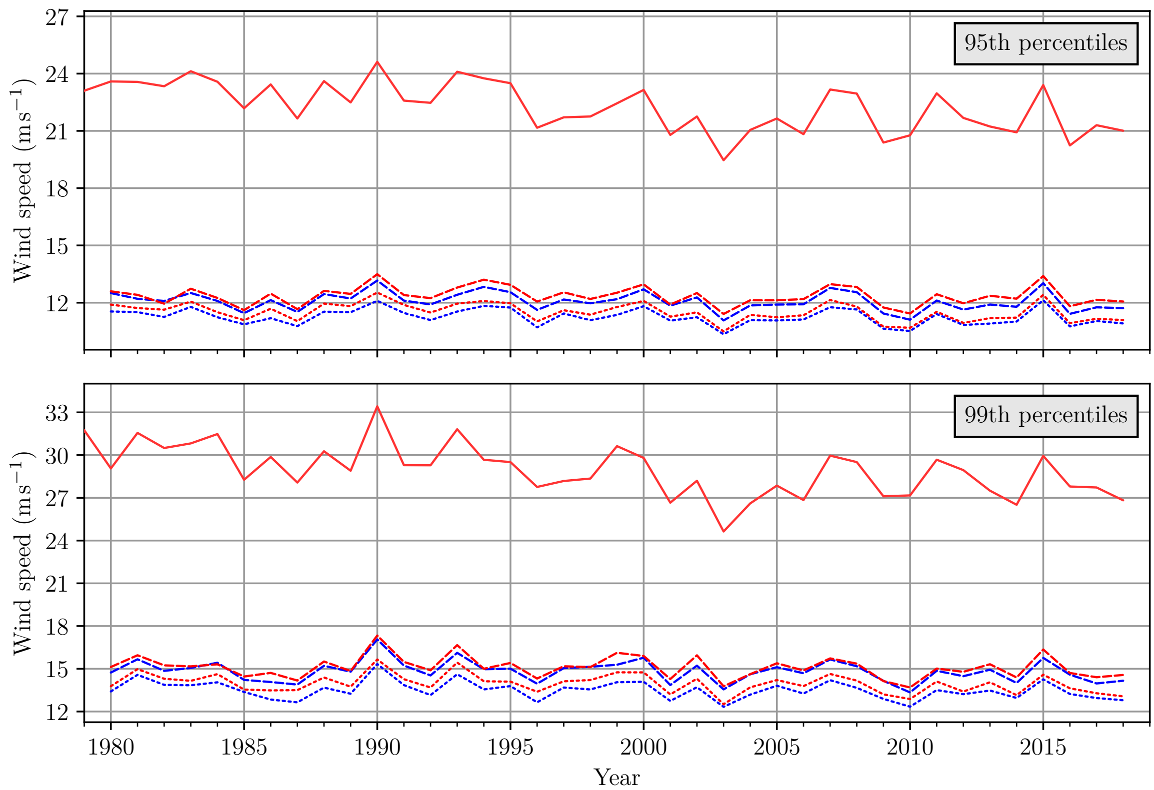

Figure 4.5: Time series of annual upper percentiles of geostrophic wind speeds from pressure observations (red, solid) and reanalysis datasets (CFSR (red, dashed), MERRA-2 (blue, dashed), ERA-Interim (red, dotted), and ERA5 (blue, dotted)), 1980-2018.

Table 4.1: Correlations between observation-based geostrophic storminess and storminess derived from wind speed reanalysis data. 1980-2018 was chosen as the reference period for both storminess calculations and correlation analysis due to limited data availability.

Reanalyis Dataset	95th percentiles	99th percentiles
ERA5	0.70	0.79
ERA-Interim	0.74	0.84
MERRA-2	0.74	0.80
CFSR v1+v2	0.66	0.79

5 The Large-Scale Circulation

As the German Bight is located in the eastern sector of the NE Atlantic storm track (Feser et al., 2015), its storm climate is influenced by the large-scale circulation, whose properties can be quantified by time series of NE Atlantic storminess. These time series, which had originally been reconstructed by Alexandersson et al. (1998) and subsequently extended by Krueger et al. (2019), serve as a reference for comparisons between German Bight storm activity and the large-scale circulation. Furthermore, the North Atlantic Oscillation (NAO) represents the dominant mode of large-scale atmospheric variability in the Atlantic sector that drives the westerlies in the Atlantic midlatitudes (Stendel et al., 2016). Although NE Atlantic storminess correlates relatively well with the NAO within the last decades (Krueger et al., 2019), there are periods over time, for which other modes of atmospheric variability dominate the storm climate. In order to better understand the influence of the large-scale atmospheric circulation on German Bight storminess, Sections 5.1 and 5.2 draw comparisons with the NE Atlantic storminess time series reproduced after Krueger et al. (2019) and the station-based NAO index (NCAR, 2019) to illustrate similarities and differences to the large-scale wind climate. In Section 5.3, phases of above- and below-average activity in German Bight storminess are then related to the variability of the synoptic setup over Europe.

5.1 Northeast Atlantic Storm Activity

A comparison between German Bight and NE Atlantic storminess reveals that both the annual and low-pass filtered time series of German Bight storminess are significantly positively correlated at the 0.05 significance level with the corresponding time series of NE Atlantic storminess (0.58 and 0.65 for annual and low-pass filtered 95th percentiles, 0.52 and 0.48 for 99th percentiles) (Fig. 5.1). The low-pass filtered curves generally agree with each other and show the underlying multidecadal variability. As the German Bight is essentially a part of the NE Atlantic, the underlying multidecadal variability in storm activity can be found in both low-pass filtered time series. In some decades however, storminess levels in the two regions prove to be remarkably different from one another. In the 1910s, German Bight storminess is above average, whereas NE Atlantic storminess recedes to near-average values, leaving a gap of roughly one standard deviation between the two curves. While both regions show a reduction in

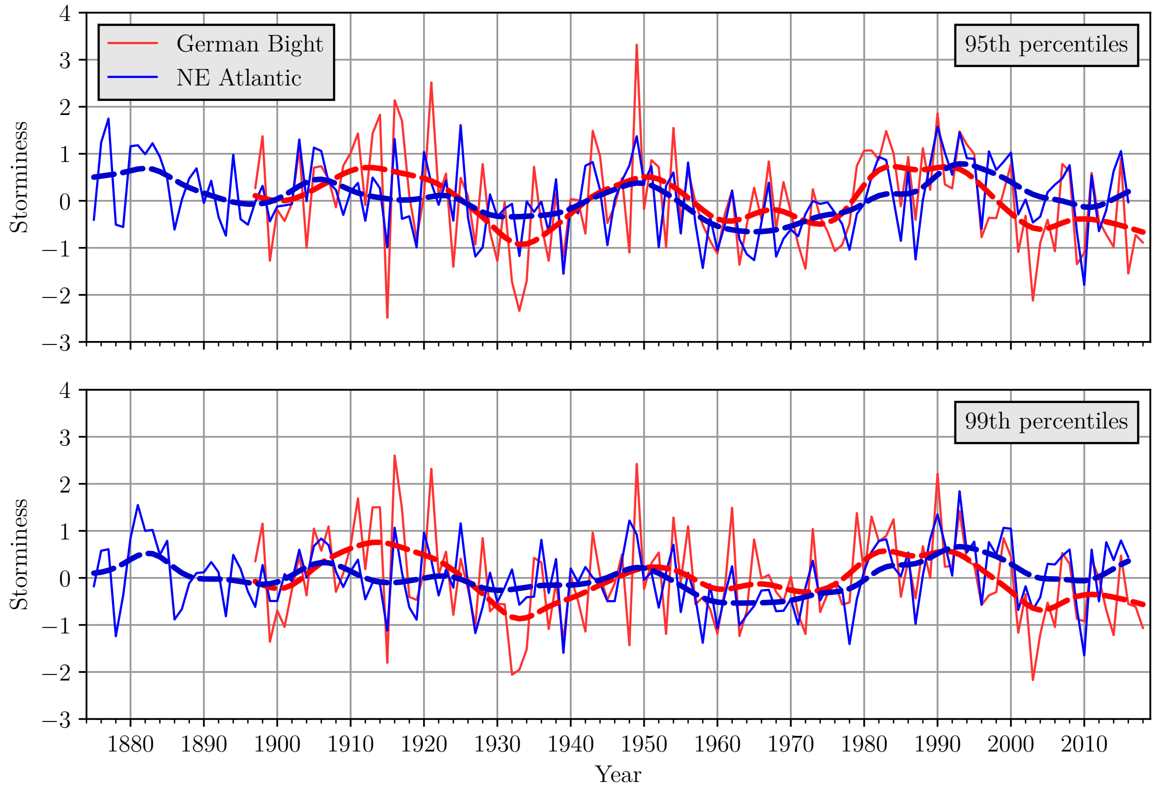

Figure 5.1: Standardized annual 95th (top) and 99th (bottom) percentiles of geostrophic wind speeds over the German Bight (red, 1897-2018), and the NE Atlantic (blue, 1875-2016). Thin solid lines denote annual values, thick dashed lines show low-pass filtered data.

storminess during the late 1920s, the low activity during the 1930s is much more pronounced over the German Bight. In the 1940s, both low-pass filtered curves show an increase in activity with a return to sub-average levels in the 1960s. The subsequent increase in German Bight storm activity leads to a storminess maximum in the 1980s, when NE Atlantic storminess is still near the long-term average. The NE Atlantic time series reaches its maximum in the early 1990s, nearly a decade after the German Bight. In recent years, the two curves show an increase in disagreement, both for the 95th and 99th percentiles. Especially during the 2010s, a period with recurring anticyclonic circulation patterns over the German Bight during the storm seasons (DWD, 2015, 2017a), German Bight storminess exhibits a downward trend to below-average levels, while NE Atlantic storminess rises to above-average levels.

The significant positive correlation with NE Atlantic storminess implies that storm activity over the German Bight covaries with the larger-scale storm activity over the NE Atlantic. Still, there are notable differences between the annual and low-pass filtered storminess curves for the German Bight and the NE Atlantic, such as in the years 1949 or 2003. One explanation for the differences can be given by the extent of the examined domain. Variability on a smaller spatial scale is more likely to be disregarded when the triangle method is applied to a larger area, as the geostrophic wind acts as a proxy for the area mean of the true wind. Because the German Bight comprises a smaller area than the entire NE Atlantic, the storminess proxy allows for consideration of smaller-scale features, increasing the annual variability compared to the NE Atlantic.

5.2 The North Atlantic Oscillation

A correlation analysis between annual 95th (99th) percentile-based German Bight storminess and the NAO index finds a correlation coefficient of 0.36 (0.34), which is weak, but significant at the 0.05 significance level (Fig. 5.2). The correlation indicates that the variability of German Bight storminess is only weakly connected to that of the NAO, visible as strong disagreeing periods between the time series in Figure 5.2. Moreover, these correlation coefficients are lower than values found for the correlation between the NAO and the NE Atlantic (Krueger et al., 2019).

Additionally, the pronounced multidecadal variability in the low-pass filtered curves for both the German Bight and the NE Atlantic does not agree with the underlying variability of the NAO index indicated by a low correlation of about 0.32 (0.31). However, the correlation between German Bight storminess and the NAO index increases to 0.52 (0.47) for 95th (99th) percentiles if only the winter season (DJF) is considered. This increase suggests that, for winter months only, the NAO is a larger contributor to the variability of German Bight storminess than in other seasons. The increased contribution in winter months stems from the NAO acting as one of the major drivers of European winter climate (Hurrell et al., 2013). A positive NAO phase is characterized by a large-scale westerly flow inducing strong winds over both the NE Atlantic and the German Bight, whereas a negative NAO phase is accompanied by high pressures and calm winds over Europe. Still, the natural variability in storm tracks and the positions of low- and high-pressure systems result in differing wind fields over the German Bight and the NE Atlantic, which in turn manifest in fluctuating correlations between climate indices over time.

The connection between the NAO and storminess over the NE Atlantic has been shown to vary with time (Matulla et al., 2008; Hanna et al., 2008; Pinto and Raible, 2012).

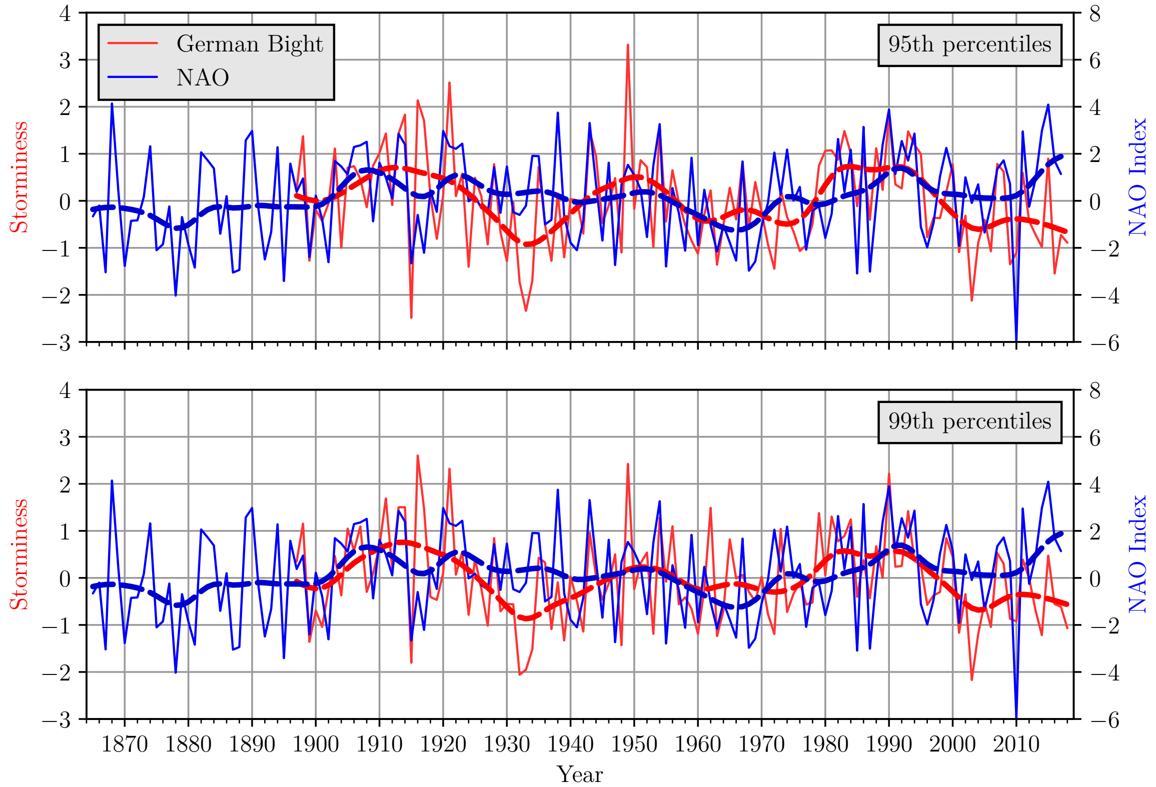

Figure 5.2: Standardized annual 95th (top) and 99th (bottom) percentiles of geostrophic wind speeds over the German Bight (red, 1897-2018) and annual North Atlantic Oscillation (NAO) index values (blue, 1865-2017). Thin solid lines denote annual values, thick dashed lines show low-pass filtered data. Note that the same NAO time series is used in both subfigures as the NAO index is not defined via upper quantiles.

As the previously calculated correlation coefficients only take the entire 122-year time series into account, moving correlations between annual German Bight storminess and the NAO index, as well as NE Atlantic storminess, are computed over centered 31-year windows (Fig. 5.3). The moving correlation between German Bight and NE Atlantic storminess is high during the 1910s and 1920s with a maximum of 0.6 (0.62) for the 95th (99th) percentiles and remains between 0.4 and 0.6 until the mid-1960s. From around 1970 onward, the correlation increases to about 0.7 near the end of the period. The running correlation with the NAO is weaker and finds its minimum in the 1960s at about 0.1. Afterward, the correlation with the NAO index increases to levels above 0.4, with maxima between 0.5 and 0.6. The changes of the correlation between the NAO index and German Bight storminess indicates that the connection between the NAO and German Bight storm climate strongly varies with time, agreeing with the

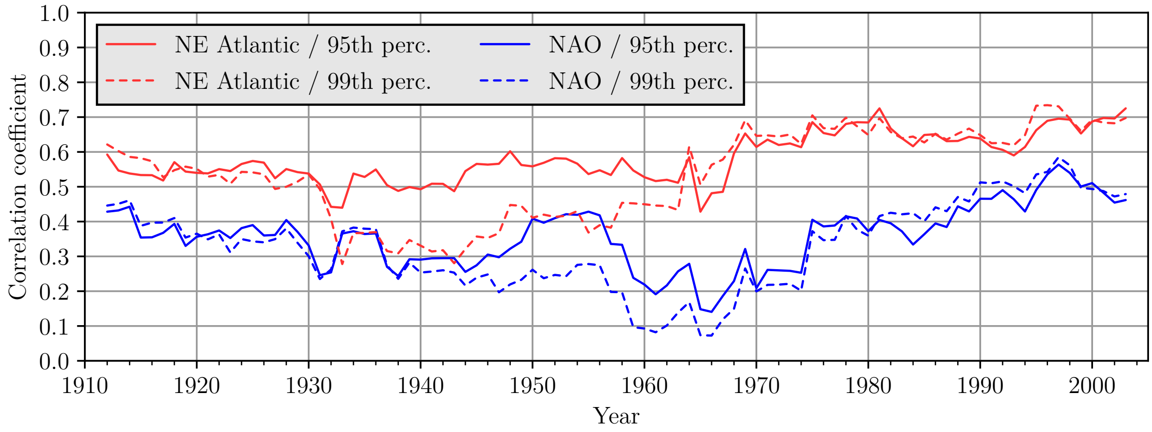

Figure 5.3: Running correlations between German Bight and NE Atlantic storminess (red), as well as the NAO index (blue), 1897-2017. Solid and dashed lines depict 95th and 99th percentiles, respectively. All correlations have been calculated over a centered 31-year moving window.

findings of Matulla et al. (2008), Hanna et al. (2008), Pinto and Raible (2012), and Krueger et al. (2019) for the NE Atlantic.

5.3 Relating Storminess to the Synoptic Setup

5.3.1 Weather Regimes in Europe

To further discuss multidecadal variability in German Bight storminess, storm activity needs to be compared with the occurrence of dominant weather regimes in Europe. Werner and Gerstengarbe (2010) showed that the relative frequency of synoptic circulation patterns over Europe on seasonal and annual scales is subject to interannual variability.

Breaking down the circulation into three categories – zonal, mixed and meridional – Werner and Gerstengarbe (2010) found a peak in the rate of zonal weather regimes around 1990 and a steep subsequent decline (Fig. 5.4), similar to the behavior of German Bight storm activity. The late 1980s also feature absolute minima of meridional weather patterns in the annual, fall, and winter time series, as well as an absolute maximum of zonal patterns in winter (Fig. 5.5). Predominantly meridional periods can be found in the late 1960s and 1970s, which correspond to the phase of low activity in the German Bight. The evolution of the annual prevalence of synoptic weather setups

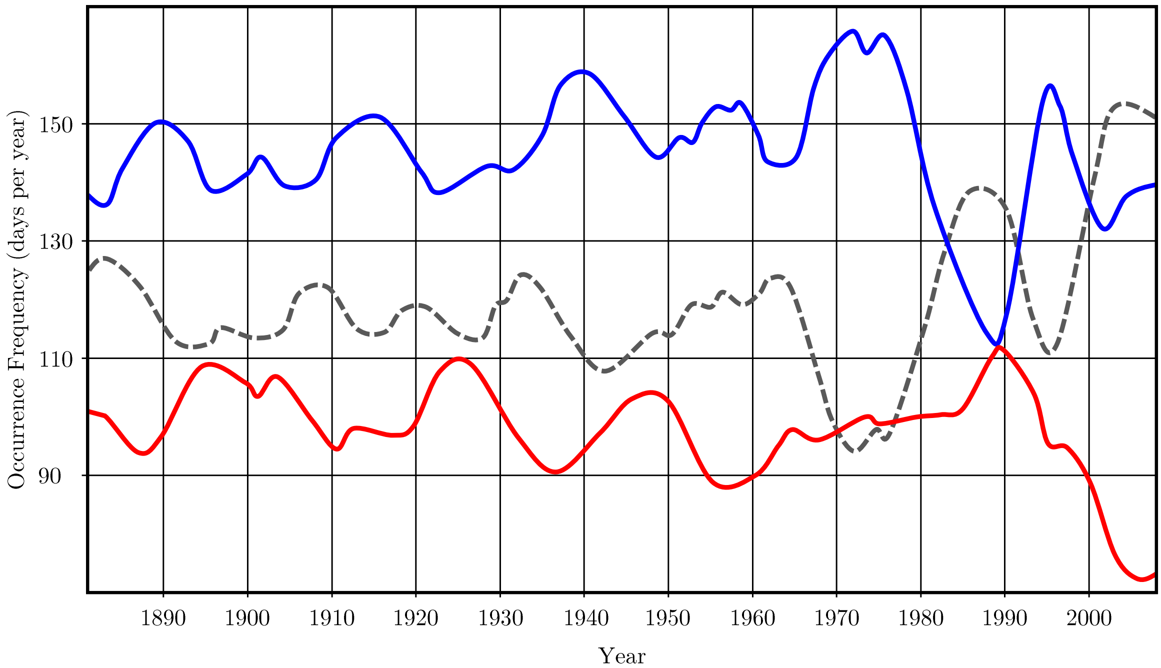

Figure 5.4: 10-year running means of annual occurrence frequencies of zonal (red), meridional (blue), and mixed (grey, dashed) synoptic regimes over Central Europe, 1881-2008. Figure redrawn after Werner and Gerstengarbe (2010).

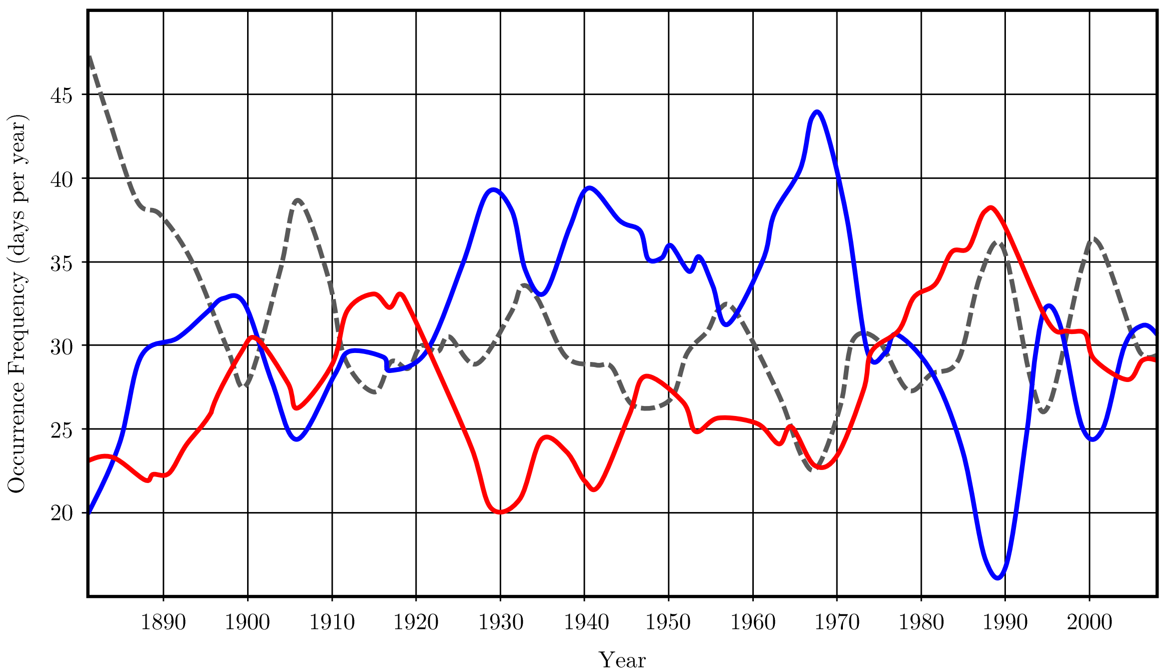

Figure 5.5: Like Figure 5.4, but based on DJF data. Figure redrawn after Werner and Gerstengarbe (2010).

shares many attributes with the time series of German Bight storminess. However, the method used by Werner and Gerstengarbe (2010), which quantifies frequencies by counting the days per year with a specific prevalent pattern, causes an overrepresentation of the summer months in the annual data compared to the method used in this study. Thus, periods with meridionally dominated summers and falls and zonally dominated winters like the 1910s appear as overly meridional in the statistics. Annual German Bight storm activity on the other hand, which is closely coupled to the winter months, reaches above-average values in the same time frame. It is therefore important to focus on the evolution of winter weather regimes. Using winter pattern statistics only, the high storm activity periods around 1910 and 1950 can be explained by an increasing number of zonal circulation patterns, while the decrease in storminess with its negative peak during the early 1930s coincides with a shift towards a meridional regime lasting from the 1920s well into the 1940s (Fig. 5.5). For recent years, disparities between German Bight storminess and indices for the large-scale circulation can be attributed to the repeated occurrence of anticyclonic patterns over Central Europe, which dampen storminess over the German Bight. A dominant example for such a case can be found in fall of 2016, when the Azores high extended across Central Europe into Siberia, steering storms away from the German Bight, while still contributing to a positive NAO index and increased storminess over the entire NE Atlantic (DWD, 2017a).

5.3.2 Wind Directions

The previous sections mainly focused on reconstructed geostrophic wind speeds that result from the the application of the triangle proxy method. Statistical properties of wind speeds and their evolution in time have been examined and compared to proxies and indices covering larger spatial domains. The applied method, however, does not only provide time series of wind speeds, but also wind directions, as initially, the zonal and meridional components of the geostrophic wind are computed separately. This makes it possible to gain insight into the distribution of wind directions and their frequency of occurrence over time. Further investigations into this data are necessary in order to uncover possible changes in the predominant wind direction over the German Bight, which may explain the temporal variability of German Bight storminess.

Hence, this section analyzes the temporal evolution of the occurrence frequencies of the eight main cardinal wind directions over the German Bight (Fig. 5.6). Over the entire period, westerly winds dominate as they make up between 15 and 25 percent of

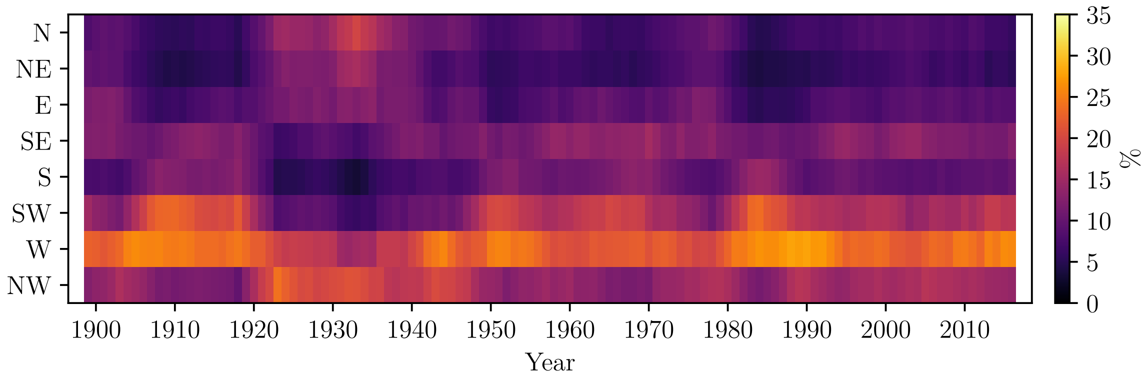

Figure 5.6: Annual occurrence frequencies of cardinal wind directions over the German Bight, based on reconstructed geostrophic wind speed components, 1897-2018. A centered 5-year running mean has been applied to smooth out interannual variability.

all winds during a certain time frame. Northwesterly, southwesterly and southeasterly winds are slightly less common, while the remaining four directions occur even less frequently. Around 1910, 1950, 1990, and in the 2010s, the prevalence of southwesterly and westerly winds is further increased in comparison to the long-term average. The first three of these phases coincide with periods of increased German Bight storminess. This confirms the findings from Section 5.3.1, which attributed storm events to synoptic setups with a dominant zonal flow. The increase in westerly winds during the 2010s cannot be tied to a significant change in annual storminess. This discrepancy between the time series of annual storminess and annual wind direction distributions during the past decade can be traced back to the contributions of the individual seasons to the annual statistics, which are shown in Figure 5.7. An increase in the frequency of westerly winds during the winter season is apparent during the 2010s. Accordingly, DJF storminess follows a positive trend near the end of the investigated period (compare Fig. 3.5) as well. However, while German Bight storminess in spring, summer and fall stays below average during the 2010s, the frequencies of westerly winds are near or above average in the same time frame. Hence, the low values of MAM, JJA and SON storminess compensate the high values of DJF, leading to no notable increase in annual storm activity. Concurrently, the near or above-average frequencies of westerly winds in all four seasons add up to an above-average value in the annual data, which reflects in an increase during the 2010s.

During the 1920s and 1930s, a significant shift in the wind direction distribution is visible. Wind frequencies from the southeast, south, southwest and west decrease,

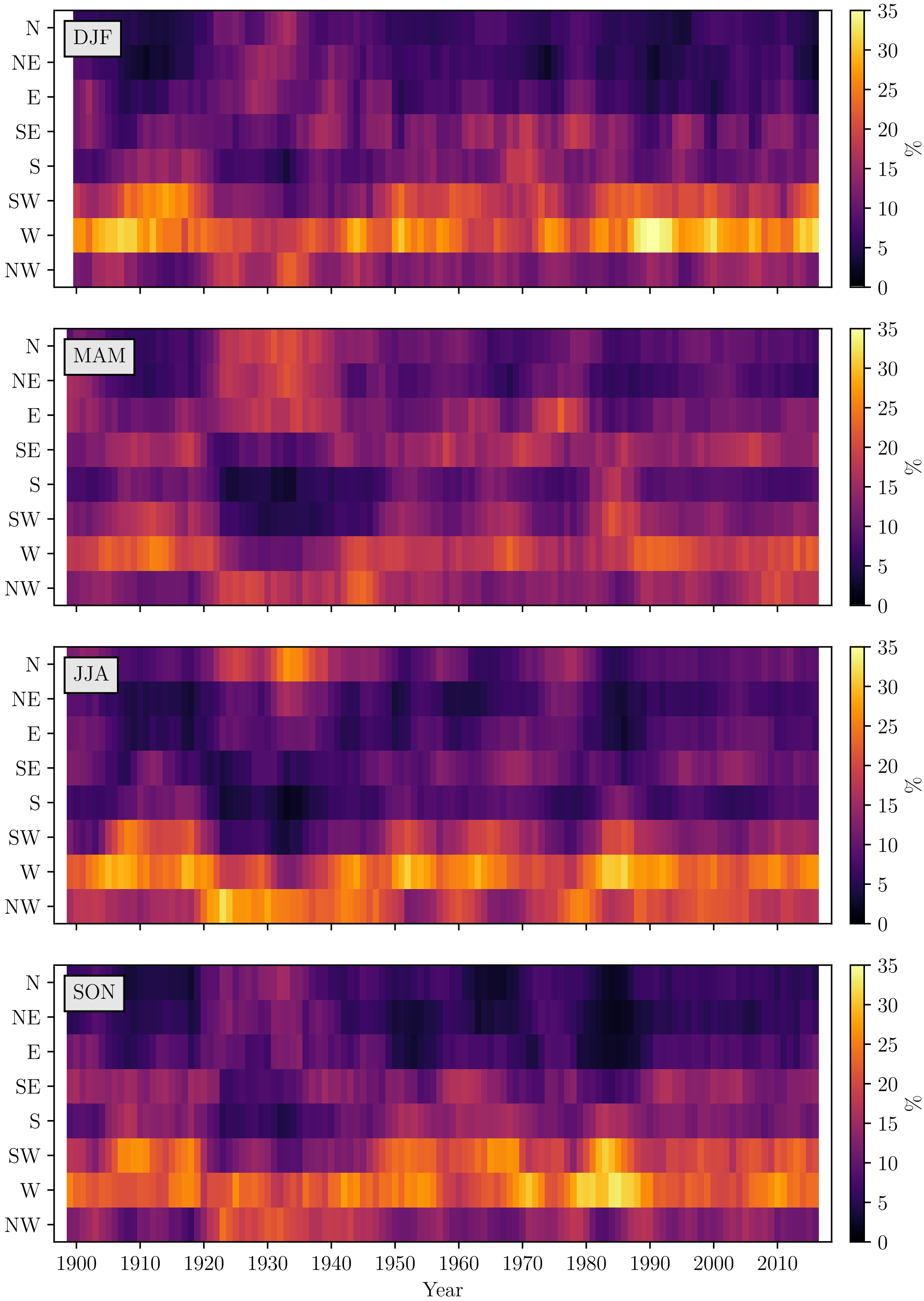

Figure 5.7: Like Figure 5.6, but based on seasonal data.

while the fractions of northwesterly, northerly, northeasterly and easterly winds increase compared to their respective long-term averages. The phase associated with this shift is marked by below-average annual storm activity, including one of the least active years in the entire time series (1933). From a synoptic standpoint, the change in wind directions translates to a transition towards a meridionally dominated flow regime, which is consistent with the analysis of Werner and Gerstengarbe (2010), who also noted an elevated frequency of meridional weather patterns in that period.

5.3.3 Air Pressure Patterns during Storm Events

Another way to gain insight into the atmospheric patterns that are responsible for storminess over the German Bight is to perform a composite analysis of mean sea level pressure (MSLP) data for periods of enhanced geostrophic wind speeds. The composite analysis computes temporal means of an atmospheric variable for every grid point within a certain domain over selected time steps and periods. For the present study, three-hourly MSLP fields are selected from the ERA5 reanalysis within a domain bounded by 30 °N, 85 °N, 65 °W and 39 °E, which covers the North Atlantic and Europe. Only time steps for which the reconstructed geostrophic wind speed over the German Bight exceeds the upper quantiles of the respective year are used. Subsequently, the remaining set of MSLP fields is averaged over a ten- and 40-year period.

During the period of 1979-2018, high geostrophic wind speeds over the German Bight are predominantly associated with a westerly flow regime, induced by a cyclone over western Scandinavia and an anticyclone extending from the Iberian Peninsula into adjacent parts of the Atlantic Ocean (Fig. 5.8). The spatial distribution of these two major pressure systems allows for the formation of a tight meridional pressure gradient over the German Bight, which balances a strong geostrophic wind. The 95th and 99th percentile-based MSLP fields mainly differ in the magnitude of their respective pressure extremes. While the 99th percentile-based high-pressure system is 2.1 hPa stronger than the 95th percentile-based anticyclone (1026.8 and 1024.7 hPa), the Scandinavian low during 99th percentile-based storm events is 5.3 hPa deeper than its 95th percentile-based counterpart (985.3 and 990.6 hPa).

On a decadal scale, the temporal evolution of mean MSLP patterns within the domain can also be represented by the strength of the Scandinavian low. For both the 95th and 99th percentile-based composites, the second and third decade (1989-2008) show a considerably deeper low-pressure system than the decades before and after (Fig. 5.9 and 5.10). As the Iberian high does not change its intensity significantly over time,

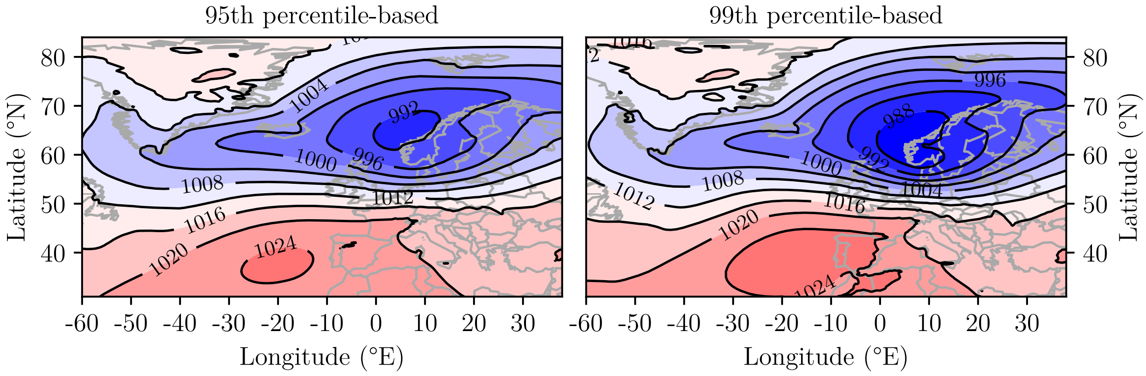

Figure 5.8: 1979-2018 mean MSLP fields of three-hourly time steps at which the reconstructed geostrophic wind speed over the German Bight exceeds upper percentiles of the respective year. MSLP fields are taken from the ERA5 reanalysis.

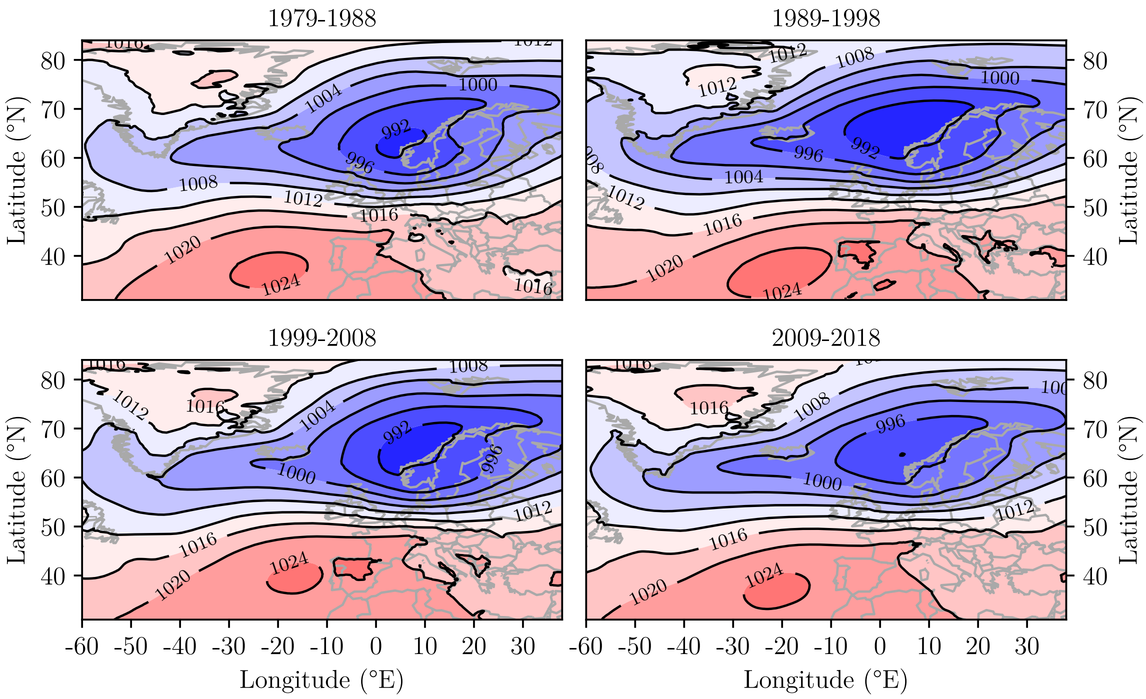

Figure 5.9: Like Figure 5.8, but averaged over four different ten-year periods and based on annual 95th percentiles only.

the pressure gradient and therefore also the geostrophic wind speeds over the German Bight are expected to be higher compared to 1979-1988 and 2009-2018. To some extent, this agrees with German Bight storminess, which also increases during the 1980s and recedes back to below-average levels in the 2000s and 2010s (compare Fig. 3.1).

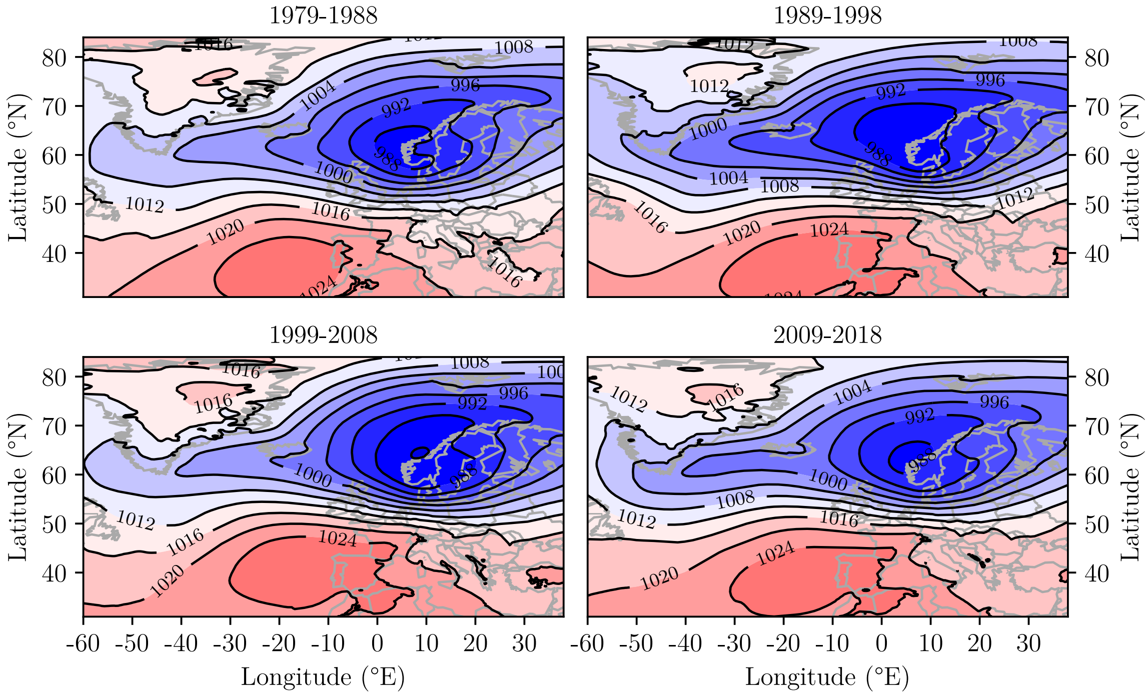

Figure 5.10: Like Figure 5.9, but based on annual 99th percentiles.

The location of the Scandinavian low in these scenarios acts as an indicator for the comparably low correlation between German Bight storm activity and the NAO. As the station-based NAO depends on the difference in MSLP between Iceland and the Azores, it reaches high values when strong cyclones are centered over Iceland. High geostrophic wind speeds over the German Bight, however, occur in the events of deep cyclones over western Scandinavia, which contribute less to a strong positive NAO signal. Nevertheless, the occurrence of strong Scandinavian lows is still tied to a positive NAO phase, as most of these cyclones originate in the North Atlantic and track near or across Iceland before reaching Scandinavia (Blender et al., 1997).

5.3.4 The Scandinavia Pattern

Section 5.3.3 illustrated how strength and position of the Scandinavian low are influential factors for the variability of storm activity over the German Bight during the last four decades. The associated climate pattern, also called Scandinavia Pattern (SCAND), which describes the variability of the Scandinavian low and the Iberian high, was detected by Barnston and Livezey (1987), who referred to it as the Eurasia-1 pattern. The positive phase of the Scandinavia Pattern is characterized by positive height anomalies over Scandinavia, whereas negative height anomalies accompany the

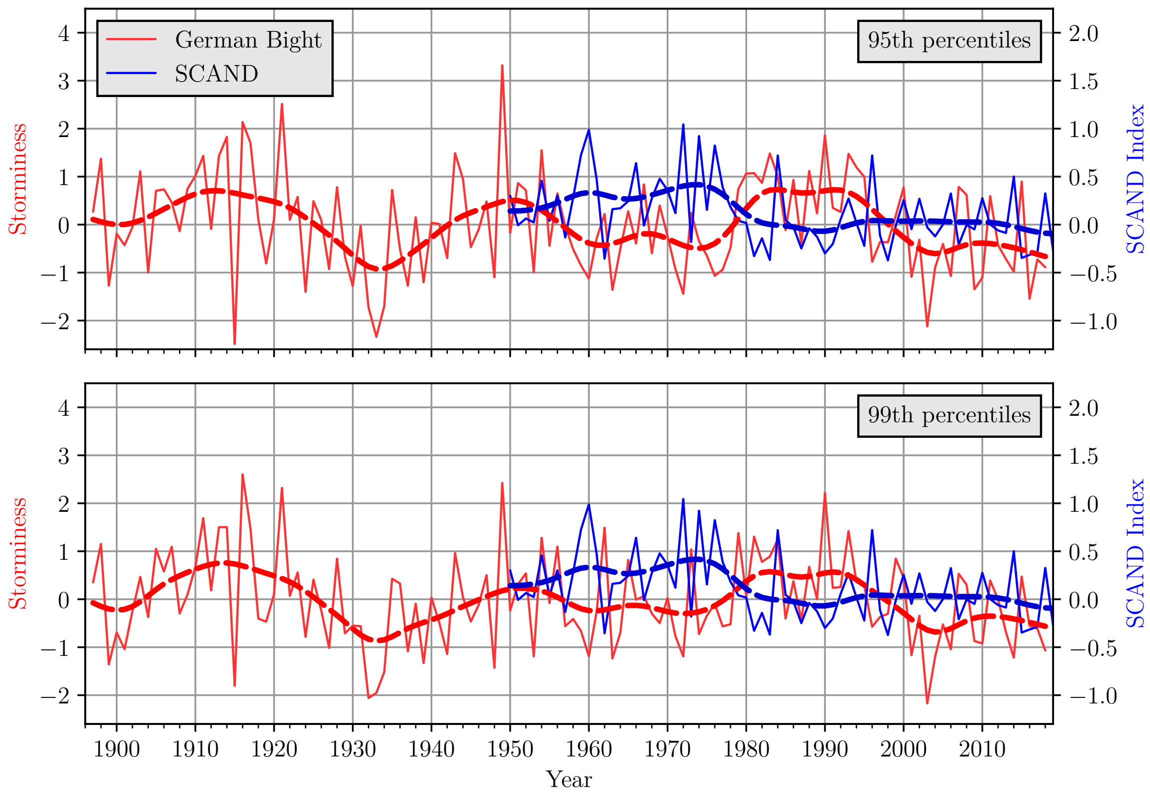

Figure 5.11: Standardized annual 95th (top) and 99th (bottom) percentiles of geostrophic wind speeds over the German Bight (red, 1897-2018) and annual SCAND index values (blue, 1950-2019). Thin solid lines denote annual values, thick dashed lines show low-pass filtered data. Note that the same SCAND time series is used in both subfigures as the SCAND index is not defined via upper quantiles.

negative phase (Barnston and Livezey, 1987). Therefore, the SCAND index, which is computed via an orthogonal rotated principle component analysis of Northern Hemisphere height fields (Barnston and Livezey, 1987), usually shows a different sign than the NAO index.

In order to relate German Bight storminess to the temporal variability of the Scandinavia Pattern, the annual storminess index is compared to annual means of monthly SCAND index data from CPC (2020) (Fig. 5.11). The annual time series show a low correlation of -0.31 (-0.28) for the 95th (99th) percentiles, which is significant at the 0.05 level, but even lower than the correlation between German Bight storminess and the NAO index. Note that the correlation coefficient is expected to be negative as the sign of the SCAND index is inverted compared to previously discussed indices. The low-pass filtered time series are in a similar range with a correlation of -0.35 (-0.20).

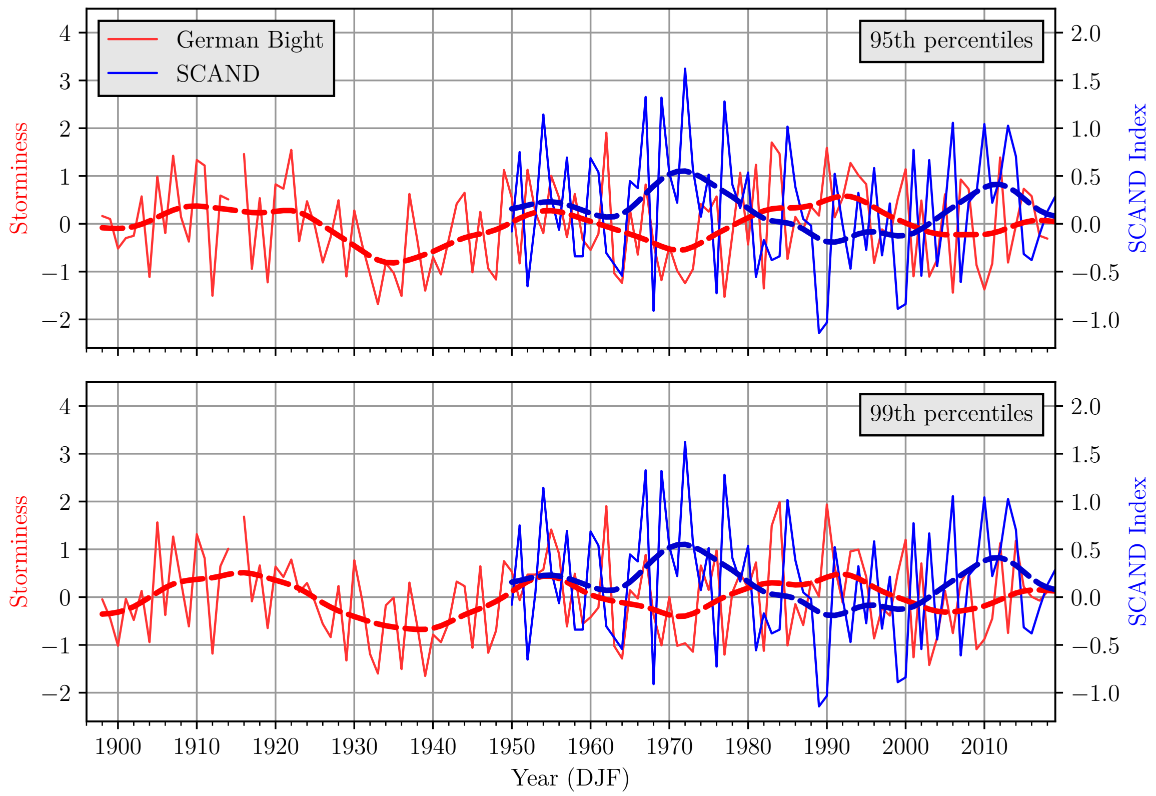

Figure 5.12: Like Figure 5.11, but based on seasonal data from DJF only.

These low correlations indicate that on an annual scale, the variability of the Scandinavia Pattern cannot sufficiently demonstrate a possible influence on German Bight storminess.

However, the composite analysis performed in Section 5.3.3 did not take all time steps into account. Instead, it only used time steps for which the geostrophic wind speed exceeds the upper quantiles of the respective year. In fact, 58.2 % (64.2 %) of the selected time steps for the 95th (99th) percentiles stem from winter months. Hence, the comparison between German Bight storminess and the SCAND index is repeated for winter months only (Fig. 5.12). Using DJF data only, the correlation increases to -0.52 (-0.39) for the 95th (99th) percentiles. The low-pass filtered curves exhibit even higher correlations of -0.78 (-0.58). The coefficients, which for both unfiltered and low-pass filtered data are notably higher compared to the NAO, demonstrate that for the winter season, where most storms occur, the Scandinavia Pattern is a major driver behind German Bight storminess. As the region of the Scandinavia Pattern is geographically closer to the German Bight than the region of the NAO, the Scandinavia Pattern and its variability can contribute to storm activity in the German Bight in a more direct way.

6 Quantifying the Uncertainties

This study uses an ensemble of 18 time series of geostrophic wind speeds to derive a robust time series of German Bight storminess. The ensemble would bring its own estimate of uncertainty, such as the ensemble spread or any other measure of ensemble variability. On the contrary, as the triangles used to derive the proxy time series cover almost identical areas, the differences among the time series are relatively small, and hence would make such an estimate of uncertainty rather small. In order to investigate the effect of various sources of uncertainty on the estimation of geostrophic wind speed statistics, a bootstrapping approach is utilized. Through repeated random sampling, the applied bootstrapping is able to estimate the combined uncertainty caused by different error sources, such as undetected invalid pressure readings, the data selection process, sampling, and assumptions made to calculate geostrophic winds. The approach, however, does not give insight into the contributions of individual error sources to the cumulative uncertainty. Also, errors in the initial data which cannot be found by the quality control routine account for a fraction of the total uncertainty. Such errors result from differences in instrumentation, measurement techniques, rounding errors, and errors during the digitization of handwritten records and are not taken into account by the bootstrapping scheme. For instance, observations are usually rounded to the nearest 0.1 hPa, which can induce an error of up to 0.1 hPa in the pressure difference between two stations, greatly influencing the pressure gradient and thus the reconstructed wind speed as well. To investigate the magnitude of the individual error sources, a detailed sensitivity analysis would be needed. However, the present analysis focuses only on the total uncertainty that underlies the reconstruction of storm activity. Therefore, an assessment of the sensitivity of the uncertainty lies outside the scope of this study and is subject to further research.

Figures 6.1 and 6.2 show that, on both seasonal and annual scales, the uncertainty is generally smaller for the 95th than for the 99th percentiles. The uncertainty for the 95th percentile-based annual time series ranges from 0.19 to 1.00, whereas the 99th percentile counterpart lies between 0.20 and 1.16, excluding the years 1904 and 1905, for which the uncertainties are 2.04 and 1.77, nearly twice as much as before and after. The same effect is apparent in the seasonal time series. Higher quantiles naturally possess a greater variability, which increases the uncertainty. Both the annual and seasonal time series of uncertainties follow a similar pattern. Uncertainties are at a maximum during the early years of the dataset, peaking around and shortly after 1900.

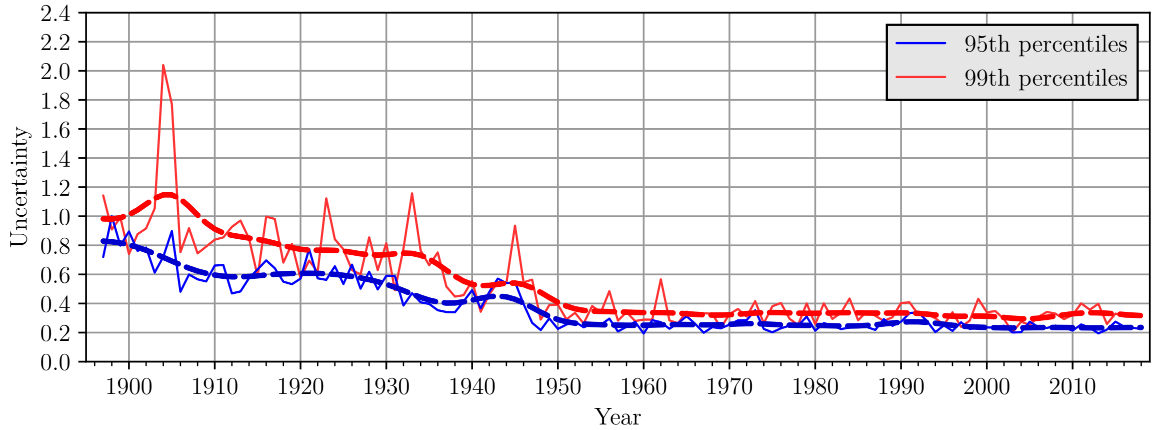

Figure 6.1: Sizes of the 95 % confidence intervals as differences between 0.975 and 0.025 quantiles of standardized annual 95th (blue) and 99th (red) percentiles of geostrophic wind speeds over the German Bight, 1897-2018. Thin solid lines indicate annual values, thick dashed lines show low-pass filtered data.

They steadily decline until the early 1950s, but show a very erratic and highly variable behavior. Uncertainties in fall are characterized by a secondary peak during the late 1920s and another smaller peak in the 1970s, both of which are not that pronounced in other uncertainty time series. Starting in the 1950s, uncertainties remain steady at relatively low levels, indicating that the lowest uncertainties can be found after 1950.

The general trend of annual and seasonal uncertainties can be explained by data availability (Fig. 6.3). As all uncertainties are simulated through the application of a bootstrapping scheme, lower availability rates (derived through the quality control procedures) correspond to higher levels of uncertainty and vice versa. Pressure observations are incomplete or too sparse for various stations before the early 1950s. The unavailability of pressure data results in a reduced number of possible triangles and thus a smaller usable ensemble for storminess calculations. The lowest percentage of data availability is found during the early decades of the 20th century, explaining the highest uncertainties during that time frame. Noteworthy increases in the number of usable triangles in 1935/36 and the late 1940s lead to a stepwise decrease in uncertainty. From the 1950s onwards, with the exception of 1971, 1972, 1991 and 1992, sufficient data is available to ensure that all 18 triangles are represented in the annual storminess calculations. The remaining uncertainty that cannot be attributed to data availability results from the variability caused by the triangles not fully overlapping (see Fig. 2.2

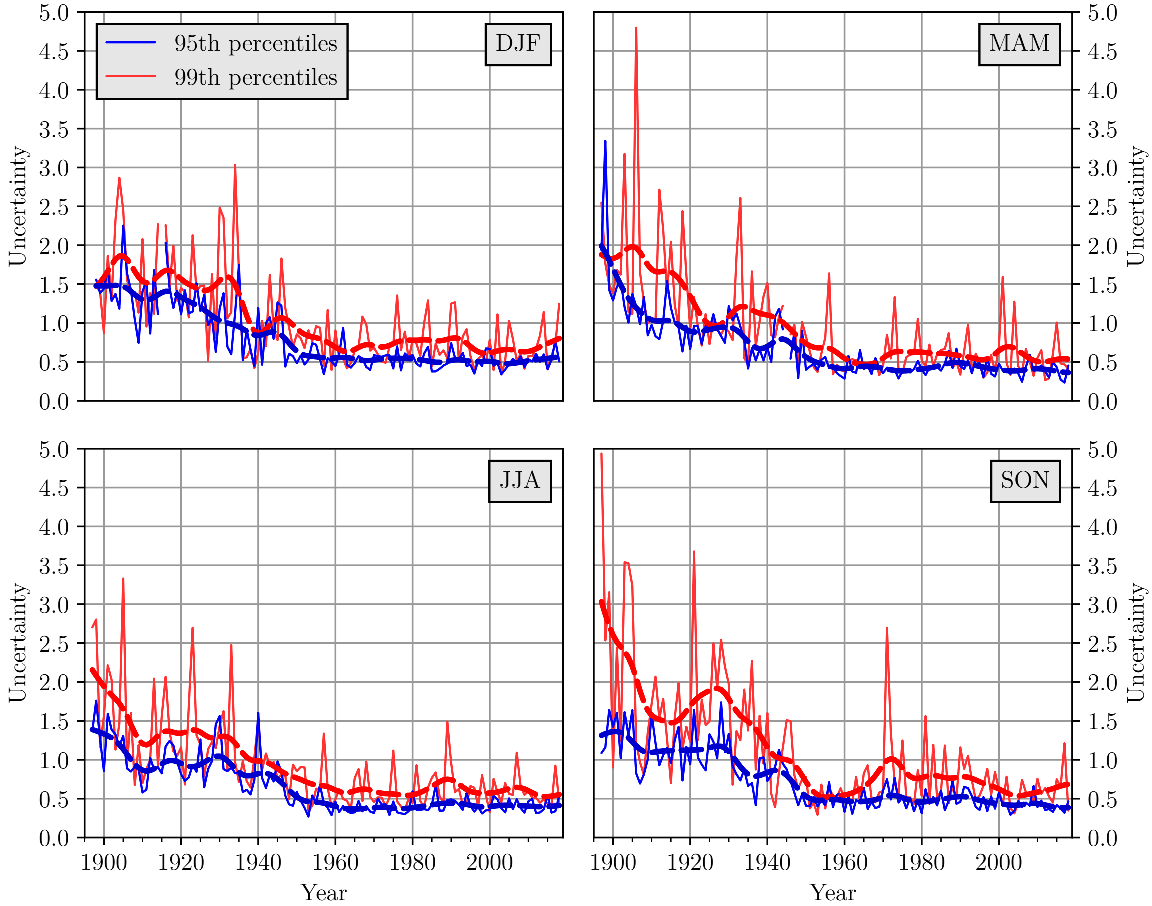

Figure 6.2: Like Figure 6.1, but for seasonal data.

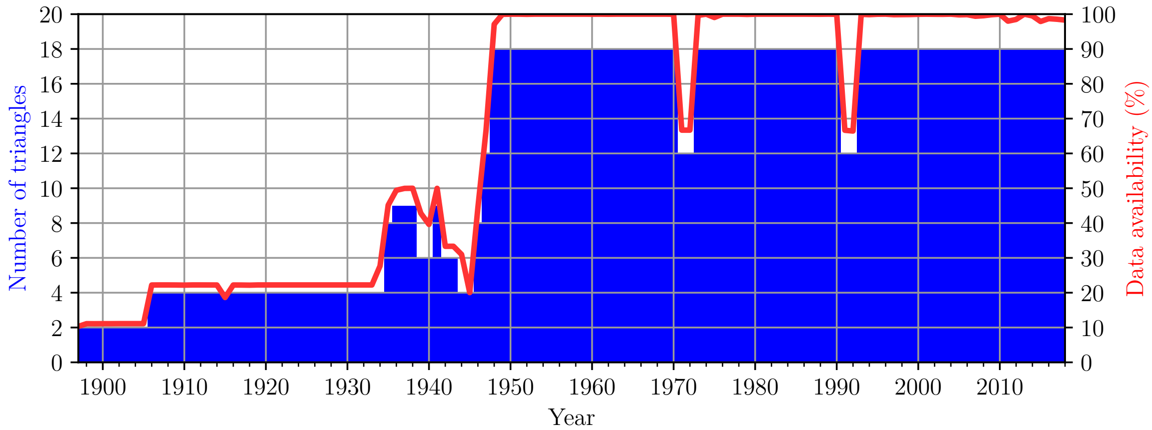

Figure 6.3: Annual data availability rates (red) and resulting number of useable triangles (blue), 1897-2018.

and 3.2). These uncertainty estimates can be used to explain some of the disagreements between the time series of German Bight storminess and other reconstructions

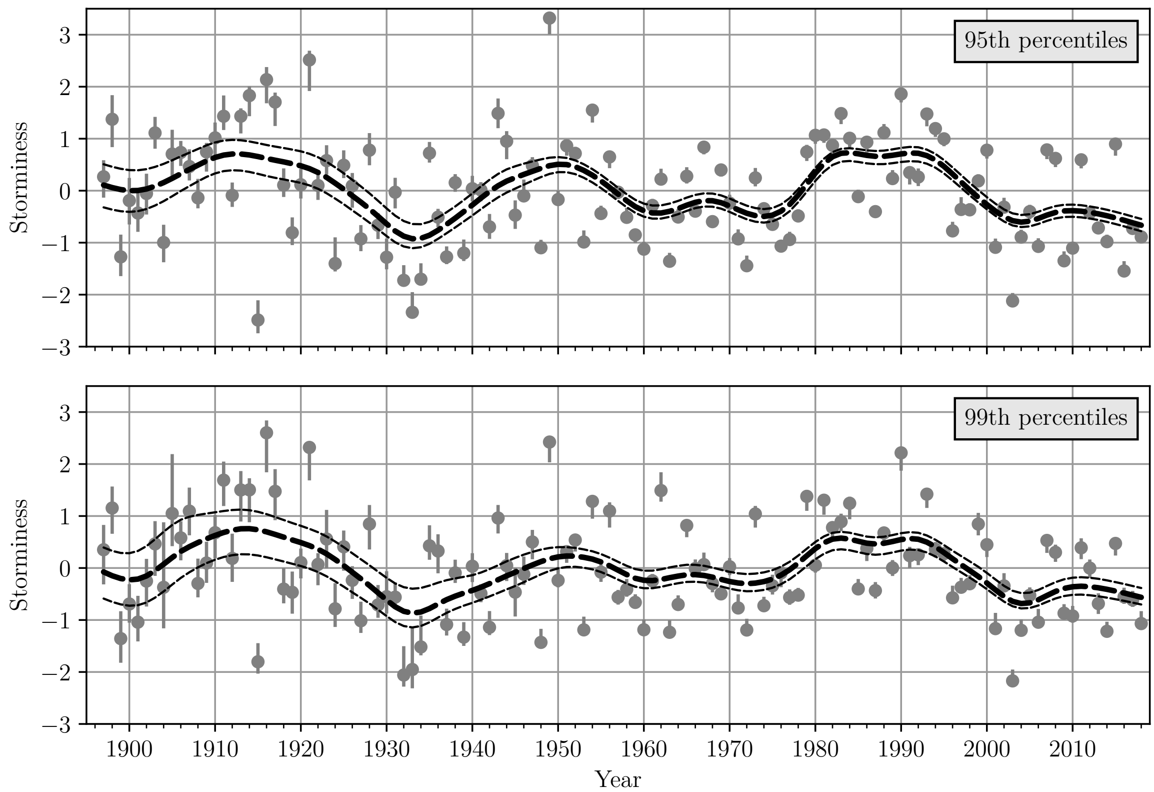

Figure 6.4: Standardized annual 95th (top) and 99th (bottom) percentiles of geostrophic wind speeds over the German Bight, 1897-2018. Dots indicate annual values, thick dashed lines show low-pass filtered data. Error bars indicate annual 95 % confidence intervals, whereas thin dashed lines show the low-pass 95 % confidence interval envelope.

mentioned in Section 3.1, especially for periods before 1950.

Figure 6.4 shows that the 95 % confidence intervals of uncertainties are not symmetrically distributed around the storminess index values. To rule out that the asymmetry is an artifact of a too small number of repetitions during the bootstrapping, uncertainties and their confidence intervals are recalculated according to Section 2.4, except that only 1000 iterations instead of 10000 are used. After 1000 iterations, the confidence intervals only show negligible deviations from the results after 10000 iterations (not shown). An asymmetrical distribution of confidence intervals in storminess reconstructions has also been noted by Krueger et al. (2019), who suggested that the true storminess levels might be shifted. Given that some of the aforementioned error sources, such as rounding errors, cannot be considered by the bootstrapping approach, the initial uncertainties in the data used in this study could explain why upper quantiles of storminess do not follow an expected normal distribution.

From the 1950s onward, uncertainty estimates in this study are generally smaller than comparable uncertainties for the entire NE Atlantic by Krueger et al. (2019), which were estimated through a similar bootstrapping approach. While low-pass filtered uncertainties after 1950 are around 0.3 (0.4) for the annual 95th (99th) percentile-based German Bight storminess time series, Krueger et al. (2019) found values of 0.35 (0.5) for the larger NE Atlantic. The discrepancy is also present in the seasonal time series. Here, the approach used in this study results in uncertainties in the range of 0.3-0.5 (0.6-0.8) after 1950, while the uncertainties for the NE Atlantic are higher at 0.5-0.7 (0.7-1.0) for 95th (99th) percentiles. As the NE Atlantic covers a larger area, and the respective storminess index is based on non-overlapping triangles, high spatial variability is more likely to be incorporated into the index than with the ensemble-based method, thus increasing the uncertainty. Similar to the uncertainty time series in this chapter, limited data availability during the beginning of the period also results in increased uncertainties in the estimates by Krueger et al. (2019), followed by a subsequent decrease as soon as more data becomes available.

7 Conclusion and Outlook

In this thesis, the evolution of storminess over the German Bight from 1897 to 2018 was reconstructed from surface pressure observations. A novel way of building robust storminess time series by enhancing the established proxy method of utilizing triangles of pressure observations was presented. Here, the approach takes advantage of an ensemble of 18 partially overlapping triangles to derive upper annual and seasonal quantiles of geostrophic wind speeds. The results provide an update of existing indices of storm activity for more recent times, so that assessments of the variability of storm activity are more comprehensive and improved.

In order to summarize the findings of this study, the following chapter gives concluding remarks and aims to answer the guiding questions which were introduced in the thesis outline.

- Does German Bight storminess exhibit temporal variability or trends over the last century?

It is made evident that annual German Bight storminess is characterized by a dominant multidecadal variability with periods of high activity around 1910, 1950, and 1990, and low activity in the 1930s, 1970s, and the 2000s. During the last century, there is a slight downward trend in the data, which, however, is not significant at the 0.05 level. On a seasonal scale, DJF storminess closely resembles its annual counterpart and displays the highest storm activity levels of all four seasons. This results in the winter season being the main contributor to annual storm activity, as most storms and the highest geostrophic wind speed generally occur in winter. The remaining three seasons do not exhibit a comparably pronounced oscillation and show lower overall storminess values. Thus, they contribute less to the annual storminess index. Apart from JJA storminess, which exhibits a slight downward trend over the past century, German Bight storminess during the other seasons is not characterized by significant trends at the 0.05 level.

- How do the reconstructed time series compare to wind measurements and reanalysis products in recent decades?

A test of the reconstruction against a 14-year record of in-situ measurements from the FINO1 research platform and data from four different reanalysis products confirms the validity of the approach, as the time series are in good agreement. The correlation coefficients between reconstructed wind speeds and reanalysis data range from 0.66 to 0.84, while the reconstruction and FINO1 measurements are even better correlated, with values of 0.81 for three-hourly and 0.93 for monthly low-pass filtered data. Even though the absolute wind speeds, to which the geostrophic wind data are compared, are generally lower due to ageostrophic effects and the negligence of the gradient wind, the temporal behavior of reconstructed German Bight storminess itself shows a very good correlation with the reference data.

- To which degree is German Bight storminess connected to the large-scale circulation over Europe and the North Atlantic?

A comparison with NE Atlantic storminess, the NAO index, and the Scandinavia Pattern shows that storm activity over the German Bight is connected to the large-scale circulation over the NE Atlantic. This connection is largest during the winter season, in which most storms and the highest wind speeds usually occur. Nonetheless, intermittent periods of disagreement between the reconstructed time series and the other indices also indicate that there are more driving factors behind German Bight storminess, such as local changes in the flow regime. Relating German Bight storminess to synoptic setups over Europe confirms such a dependence, as storm activity levels are closely linked to the occurrence frequency of meridionally and zonally dominated weather patterns, which also shows a pronounced multiannual variability itself. This connection manifests in phases with altered dominant wind directions, which coincide with periods of above- or below-average storminess.

- How large is the underlying uncertainty in the ensemble-based reconstruction of storm activity?

By giving an estimation of uncertainty via the bootstrapping approach, this study finds that annual uncertainty is inversely related to data availability. Low data availability decreases the sample size and therefore inflates the uncertainty in the first decades of this reconstruction, a phenomenon also visible in previous studies for a larger spatial domain. As data availability increases up until the 1950s, uncertainty decreases during the same time frame. After that point, due to the constant high number of usable triangles, the estimated uncertainties are nearly constant as well with values around 0.3 (0.4) for annual and 0.3-0.5 (0.6-0.8) for seasonal statistics. These uncertainties are generally reduced compared to previous studies for the NE Atlantic, owing to the smaller area, a higher number of triangles and the more robust method.

While the bootstrapping approach is suitable to estimate the combined uncertainties stemming from data availability, the data selection, the quality control processes, and the assumptions made during the calculations of geostrophic wind speeds, it does not take into account inhomogeneities in the initial pressure time series. Such inhomogeneities can result from differences in instrumentation, measurement techniques, rounding errors, and errors during the digitization of handwritten records. Moreover, the applied bootstrapping cannot quantify the proportional contributions of individual error sources to the total uncertainty. Investigations into the composition of storminess uncertainty would require a detailed sensitivity analysis, which would go beyond the scope of this study and should be the subject of further research.

The approach to reconstruct German Bight storminess from air pressure observations made use of the dense observation network around the German Bight and demonstrates that reliable and homogeneous reconstructions of the wind climate require a good coverage and availability of historical records. Other nearby areas, for instance the Baltic Sea, are less covered and hence not yet suitable for comparable investigations. In the future, more historical records will become available through digitizing handwritten historical records of pressure observations. These ongoing efforts of the national meteorological services are coordinated by the WMO or by international collaborations, such as the Atmospheric Circulation Reconstructions over the Earth (ACRE) (Allan et al., 2011), the International Comprehensive Ocean-Atmosphere Data Set (ICOADS) (Freeman et al., 2017), and will provide complimentary information for reliable reconstructions of the past storm climate. For German coasts, first analyses of such pressure reconstructions from handwritten records have been shown to provide useful information for the assessment of past storm activity (Wagner, 2016) and with additional records becoming available in the future, more detailed reconstructions of storminess in other areas become possible. Also, as more high-resolution reanalyses are being extended backwards in time, such as ERA5, validations of storminess reconstructions over longer and therefore more significant periods will eventually be achievable.

References

Alexandersson, H., T. Schmith, K. Iden, and H. Tuomenvirta, 1998: Long-term variations of the storm climate over NW Europe. *The Global Atmosphere and Ocean System*, **6 (2)**, 97–120, doi:10.1029/2005GL022371.

Alexandersson, H., H. Tuomenvirta, T. Schmith, and K. Iden, 2000: Trends of storms in NW Europe derived from an updated pressure data set. *Climate Research*, **14 (1)**, 71–73, doi:10.3354/cr014071.

Allan, R., P. Brohan, G. P. Compo, R. Stone, J. Luterbacher, and S. Brönnimann, 2011: The international atmospheric circulation reconstructions over the Earth (ACRE) initiative. *Bulletin of the American Meteorological Society*, **92 (11)**, 1421–1425, doi:10.1175/2011BAMS3218.1.

Allan, R., S. Tett, and L. Alexander, 2009: Fluctuations in autumn–winter severe storms over the British Isles: 1920 to present. *International Journal of Climatology*, **29 (3)**, 357–371, doi:10.1002/joc.1765.

Baidya Roy, S., S. W. Pacala, and R. L. Walko, 2004: Can large wind farms affect local meteorology? *Journal of Geophysical Research: Atmospheres*, **109 (D19)**, doi:10.1029/2004JD004763.

Barnston, A. G., and R. E. Livezey, 1987: Classification, Seasonality and Persistence of Low-Frequency Atmospheric Circulation Patterns. *Monthly Weather Review*, **115 (6)**, 1083–1126, doi:10.1175/1520-0493(1987)115<1083:CSAPOL>2.0.CO;2.

Bengtsson, L., S. Hagemann, and K. I. Hodges, 2004: Can climate trends be calculated from reanalysis data. *Journal of Geophysical Research*, **109**, D11 111, doi:10.1029/2004JD004536.

Berrisford, P., and Coauthors, 2011: The ERA-Interim archive Version 2.0. **(1)**, 23.

Bilgili, M., A. Yasar, and E. Simsek, 2011: Offshore wind power development in Europe and its comparison with onshore counterpart. *Renewable and Sustainable Energy Reviews*, **15 (2)**, 905 – 915, doi:10.1016/j.rser.2010.11.006.

Blender, R., K. Fraedrich, and F. Lunkeit, 1997: Identification of cyclone-track regimes in the North Atlantic. *Quarterly Journal of the Royal Meteorological Society*, **123 (539)**, 727–741, doi:10.1002/qj.49712353910.

Bloomfield, H. C., L. C. Shaffrey, K. I. Hodges, and P. L. Vidale, 2018: A critical assessment of the long-term changes in the wintertime surface Arctic Oscillation and Northern Hemisphere storminess in the ERA20C reanalysis. *Environmental Research Letters*, **13 (9)**, 094 004, doi:10.1088/1748-9326/aad5c5.

Breton, S.-P., and G. Moe, 2009: Status, plans and technologies for offshore wind turbines in Europe and North America. *Renewable Energy*, **34 (3)**, 646 – 654, doi:10.1016/j.renene.2008.05.040.

BSH, 2013: Die Nordseesturmfluten vom 5. und 6.12.2013. Tech. rep., Bundesamt für Seeschiffahrt und Hydrographie, Hamburg, Germany, 3 pp. https://www.bsh.de/DE/THEMEN/Wasserstand_und_Gezeiten/Sturmfluten/_Anlagen/Downloads/Nordsee_Sturmflut_20131206.pdf.

BSH, 2019: Draft Site Development Plan 2019 for the North and Baltic Sea. Bundesamt für Seeschiffahrt und Hydrographie, Accessed: 06 August 2019, https://www.bsh.de/EN/TOPICS/Offshore/Sectoral_planning/Site_development_plan/site_development_plan_node.html.

Buchana, P., and P. E. McSharry, 2019: Windstorm risk assessment for offshore wind farms in the North Sea. *Wind Energy*, **22 (9)**, 1219–1229, doi:10.1002/we.2351.

Cappelen, J., E. V. Laursen, and C. Kern-Hansen, 2019: DMI Report 19-02 Denmark - DMI Historical Climate Data Collection 1768-2018. Tech. Rep. tr19-02, Danish Meteorological Institute. https://www.dmi.dk/fileadmin/user_upload/Rapporter/TR/2019/DMIRep19-02.pdf.

Compo, G. P., and Coauthors, 2011: The Twentieth Century Reanalysis Project. *Quarterly Journal of the Royal Meteorological Society*, **137 (654)**, 1–28, doi:10.1002/qj.776.

Compo, G. P., and Coauthors, 2015: The International Surface Pressure Databank version 3. Research Data Archive at the National Center for Atmospheric Research, Computational and Information Systems Laboratory, Boulder, CO (United States), Accessed: 05 May 2018, doi:10.5065/D6D50K29.

CPC, 2020: Monthly tabulated Scandinavia teleconnection index dating back to 1950. Climate Prediction Center, Accessed: 2020-02-20, https://www.cpc.ncep.noaa.gov/data/teledoc/scand.shtml.

Cram, T. A., and Coauthors, 2015: The International Surface Pressure Databank version 2. *Geoscience Data Journal*, **2 (1)**, 31–46, doi:10.1002/gdj3.25.

Cusack, S., 2013: A 101 year record of windstorms in the Netherlands. *Climatic Change*, **116 (3-4)**, 693–704, doi:10.1007/s10584-012-0527-0.

Dangendorf, S., S. Müller-Navarra, J. Jensen, F. Schenk, T. Wahl, and R. Weisse, 2014: North Sea storminess from a novel storm surge record since AD 1843. *Journal of Climate*, **27 (10)**, 3582–3595, doi:10.1175/JCLI-D-13-00427.1.

de Haij, M., 2009: Automatische validatie van druk- en windwaarnemingen op het KNMI - een verkenning. Tech. Rep. IR 2009-03, Royal Netherlands Meteorological Institute (KNMI). http://bibliotheek.knmi.nl/knmipubIR/IR2009-03.pdf.

Dee, D. P., and Coauthors, 2011: The ERA-Interim reanalysis: Configuration and performance of the data assimilation system. *Quarterly Journal of the royal meteorological society*, **137 (656)**, 553–597, doi:10.1002/qj.828.

Dey, C. H., and L. L. Morone, 1985: Evolution of the National Meteorological Center Global Data Assimilation System: January 1982–December 1983. *Monthly Weather Review*, **113 (3)**, 304–318, doi:10.1175/1520-0493(1985)113<0304:EOTNMC>2.0.CO;2.

DiCiccio, T. J., and B. Efron, 1996: Bootstrap confidence intervals. *Statistical Science*, 189–212.

Donat, M. G., G. C. Leckebusch, J. G. Pinto, and U. Ulbrich, 2010: Examination of wind storms over Central Europe with respect to circulation weather types and NAO phases. *International Journal of Climatology*, **30 (9)**, 1289–1300, doi:10.1002/joc.1982.

DWD, 2002: Klimastatusbericht 2001. Tech. rep., Deutscher Wetterdienst, Offenbach am Main, Germany, 290 pp. https://www.dwd.de/DE/leistungen/klimastatusbericht/publikationen/ksb_2001.pdf.

DWD, 2015: Klimastatusbericht 2014. Tech. rep., Deutscher Wetterdienst, Offenbach am Main, Germany, 96 pp. https://www.dwd.de/DE/leistungen/klimastatusbericht/publikationen/ksb_2014.pdf.

DWD, 2017a: Klimastatusbericht 2016. Tech. rep., Deutscher Wetterdienst, Offenbach am Main, Germany, 116 pp. https://www.dwd.de/DE/leistungen/klimastatusbericht/publikationen/ksb_2016.pdf.

DWD, 2017b: Nationaler Klimareport. 3. korrigierte Auflage. Tech. rep., Deutscher Wetterdienst, Offenbach am Main, Germany, 46 pp. https://www.dwd.de/DE/leistungen/nationalerklimareport/download_report_auflage-3.pdf.

DWD, 2019: Climate Data Center. Deutscher Wetterdienst, Accessed: 11 March 2019, https://opendata.dwd.de/climate_environment/CDC/.

Efron, B., and R. Tibshirani, 1986: Bootstrap methods for standard errors, confidence intervals, and other measures of statistical accuracy. *Statistical Science*, 54–75.

Feser, F., M. Barcikowska, O. Krueger, F. Schenk, R. Weisse, and L. Xia, 2015: Storminess over the North Atlantic and northwestern Europe – A review. *Quarterly Journal of the Royal Meteorological Society*, **141 (687)**, 350–382, doi:10.1002/qj.2364.

Freeman, E., and Coauthors, 2017: ICOADS Release 3.0: a major update to the historical marine climate record. *International Journal of Climatology*, **37 (5)**, 2211–2232, doi:10.1002/joc.4775.

Ganske, A., N. Fery, L. Gaslikova, I. Grabemann, R. Weisse, and B. Tinz, 2018: Identification of extreme storm surges with high-impact potential along the German North Sea coastline. *Ocean Dynamics*, **68 (10)**, 1371–1382, doi:10.1007/s10236-018-1190-4.

Gelaro, R., and Coauthors, 2017: The modern-era retrospective analysis for research and applications, version 2 (MERRA-2). *Journal of Climate*, **30 (14)**, 5419–5454, doi:10.1175/JCLI-D-16-0758.1.

Hanna, E., J. Cappelen, R. Allan, T. Jónsson, F. Le Blancq, T. Lillington, and K. Hickey, 2008: New Insights into North European and North Atlantic Surface Pressure Variability, Storminess, and Related Climatic Change since 1830. *Journal of Climate*, **21 (24)**, 6739–6766, doi:10.1175/2008JCLI2296.1.

Hasse, L., 1974: Note on the surface-to-geostrophic wind relationship from observations in the German Bight. *Boundary-Layer Meteorology*, **6 (1)**, 197–201, doi:10.1007/BF00232484.

Heino, R., 1999: Homogeneity of the long-term urban data records. *Atmospheric Environment*, **33 (24)**, 3879 – 3883, doi:10.1016/S1352-2310(99)00130-2.

Hersbach, H., and Coauthors, 2018: Operational global reanalysis: progress, future directions and synergies with NWP. **(27)**, doi:10.21957/tkic6g3wm.

Hurrell, J. W., 1995: Decadal trends in the North Atlantic Oscillation: regional temperatures and precipitation. *Science*, **269 (5224)**, 676–679, doi:10.1126/science.269.5224.676.

Hurrell, J. W., Y. Kushnir, G. Ottersen, and M. Visbeck, 2013: An Overview of the North Atlantic Oscillation. *The North Atlantic Oscillation: Climatic Significance and Environmental Impact*, American Geophysical Union (AGU), 1–35, doi:10.1029/134GM01.

IPCC, 2014: *Climate Change 2014: Mitigation of Climate Change. Contribution of Working Group III to the Fifth Assessment Report of the Intergovernmental Panel on Climate Change*. Cambridge University Press, Cambridge, United Kingdom and New York, NY, USA.

Jones, P. D., T. Jonsson, and D. Wheeler, 1997: Extension to the North Atlantic oscillation using early instrumental pressure observations from Gibraltar and south-west Iceland. *International Journal of Climatology*, **17 (13)**, 1433–1450, doi:10.1002/(SICI)1097-0088(19971115)17:13<1433::AID-JOC203>3.0.CO;2-P.

Kalnay, E., and Coauthors, 1996: The NCEP/NCAR 40-Year Reanalysis Project. *Bulletin of the American Meteorological Society*, **77**, 437–472, doi:10.1175/1520-0477(1996)077<0437:TNYRP>2.0.CO;2.

KNMI, 2019: KNMI Data Centre. KNMI, Royal Netherlands Meteorological Institute, De Bilt, the Netherlands, Accessed: 20 August 2019.

Krueger, O., F. Feser, and R. Weisse, 2019: Northeast Atlantic Storm Activity and Its Uncertainty from the Late Nineteenth to the Twenty-First Century. *Journal of Climate*, **32 (6)**, 1919–1931, doi:10.1175/JCLI-D-18-0505.1.

Krueger, O., F. Schenk, F. Feser, and R. Weisse, 2013: Inconsistencies between Long-Term Trends in Storminess Derived from the 20CR Reanalysis and Observations. *Journal of Climate*, **26 (3)**, 868–874, doi:10.1175/JCLI-D-12-00309.1.

Krueger, O., and H. von Storch, 2011: Evaluation of an Air Pressure–Based Proxy for Storm Activity. *Journal of Climate*, **24 (10)**, 2612–2619, doi:10.1175/2011JCLI3913.1.

Krueger, O., and H. von Storch, 2012: The Informational Value of Pressure-Based Single-Station Proxies for Storm Activity. *Journal of Atmospheric and Oceanic Technology*, **29 (4)**, 569–580, doi:10.1175/JTECH-D-11-00163.1.

Lamb, H. H., 1991: *Historic storms of the North Sea, British Isles, and Northwest Europe*. Cambridge Univ Press.

Leiding, T., and Coauthors, 2016: Standardisierung und vergleichende Analyse der meteorologischen FINO-Messdaten (FINO123). Tech. Rep. Abschlussbericht, Deutscher Wetterdienst. https://www.dwd.de/DE/klimaumwelt/klimaforschung/klimaueberwachung/finowind/finodoku/abschlussbericht_pdf.pdf.

Liebmann, B., R. M. Dole, C. Jones, I. Bladé, and D. Allured, 2010: Influence of Choice of Time Period on Global Surface Temperature Trend Estimates. *Bulletin of the American Meteorological Society*, **91 (11)**, 1485–1492, doi:10.1175/2010BAMS3030.1.

Lindenberg, J., H. T. Mengelkamp, and G. Rosenhagen, 2012: Representativity of near surface wind measurements from coastal stations at the German Bight. *Meteorologische Zeitschrift*, **21 (1)**, 99–106, doi:10.1127/0941-2948/2012/0131.

Matulla, C., W. Schöner, H. Alexandersson, H. von Storch, and X. L. Wang, 2008: European storminess: late nineteenth century to present. *Climate Dynamics*, **31 (2)**, 125–130, doi:10.1007/s00382-007-0333-y.

NCAR, 2019: NAO Index Data provided by the Climate Analysis Section, NCAR, Boulder, CO (United States), Hurrell (2003). Updated regularly. Accessed: 2019-09-03, https://climatedataguide.ucar.edu/climate-data/hurrell-north-atlantic-oscillation-nao-index-station-based.

Paraskevopoulou, S. E., D. Y. Barsakcioglu, M. R. Saberi, A. Eftekhar, and T. G. Constandinou, 2013: Feature extraction using first and second derivative extrema (FSDE) for real-time and hardware-efficient spike sorting. *Journal of Neuroscience Methods*, **215 (1)**, 29 – 37, doi:10.1016/j.jneumeth.2013.01.012.

Pinto, J. G., and C. C. Raible, 2012: Past and recent changes in the North Atlantic oscillation. *Wiley Interdisciplinary Reviews: Climate Change*, **3 (1)**, 79–90, doi:10.1002/wcc.150.

Raible, C. C., F. Lehner, J. F. González-Rouco, and L. Fernández-Donado, 2014: Changing correlation structures of the Northern Hemisphere atmospheric circulation from 1000 to 2100 AD. *Climate of the Past*, **10 (2)**, 537–550, doi:10.5194/cp-10-537-2014.

Romanić, D., M. Ćurić, I. Jovičić, and M. Lompar, 2015: Long-term trends of the 'Koshava' wind during the period 1949–2010. *International Journal of Climatology*, **35 (2)**, 288–302, doi:10.1002/joc.3981.

Saha, S., and Coauthors, 2010: The NCEP Climate Forecast System Reanalysis. *Bulletin of the American Meteorological Society*, **91 (8)**, 1015–1058, doi:10.1175/2010BAMS3001.1.

Saha, S., and Coauthors, 2014: The NCEP Climate Forecast System Version 2. *Journal of Climate*, **27 (6)**, 2185–2208, doi:10.1175/JCLI-D-12-00823.1.

Schmidt, H., and H. von Storch, 1993: German Bight storms analysed. *Nature*, **365 (6449)**, 791–791, doi:10.1038/365791a0.

Sen, P. K., 1968: Estimates of the Regression Coefficient Based on Kendall's Tau. *Journal of the American Statistical Association*, **63 (324)**, 1379–1389.

Stendel, M., E. van den Besselaar, A. Hannachi, E. C. Kent, C. Lefebvre, F. Schenk, G. van der Schrier, and T. Woollings, 2016: Recent Change—Atmosphere. *North Sea Region Climate Change Assessment*, Springer International Publishing, 55–84, doi:10.1007/978-3-319-39745-0_2.

Thomas, B. R., E. C. Kent, and V. R. Swail, 2005: Methods to homogenize wind speeds from ships and buoys. *International Journal of Climatology*, **25 (7)**, 979–995, doi:10.1002/joc.1176.

Trenberth, K. E., and Coauthors, 2007: Climate Change 2007: The Physical Science Basis. *Contribution of Working Group I to the Fourth Assessment Report of the Intergovernmental Panel on Climate Change (Cambridge University Press, Cambridge, UK and New York, NY, USA, 2007), Chap. Observations: Surface and Atmospheric Climate Change*, 235.

Trigo, R. M., T. J. Osborn, and J. M. Corte-Real, 2002: The North Atlantic Oscillation influence on Europe: climate impacts and associated physical mechanisms. *Climate research*, **20 (1)**, 9–17, doi:10.3354/cr020009.

van der Schrier, G., A. van Ulden, and G. J. van Oldenborgh, 2011: The construction of a Central Netherlands temperature. *Climate of the Past*, **7 (2)**, 527–542, doi:10.5194/cp-7-527-2011.

Vose, R., R. Schmoyer, P. Steurer, T. Peterson, R. Heim, T. Karl, and J. Eischeid, 1992: The global historical climatology network: Long-term monthly temperature, precipitation, sea level pressure, and station pressure data. Tech. rep., Oak Ridge National Lab., TN (United States). Carbon Dioxide Information Analysis Center. doi:10.2172/10178730.

Wagner, D., 2016: Evaluation of Storminess by Early 20th Century Atmospheric Data from Signal Stations along the German Coastline. Ph.D. thesis, Universität Hamburg, Von-Melle-Park 3, 20146 Hamburg, http://ediss.sub.uni-hamburg.de/volltexte/2017/8854.

Wang, X. L., F. W. Zwiers, V. R. Swail, and Y. Feng, 2009: Trends and variability of storminess in the Northeast Atlantic region, 1874–2007. *Climate Dynamics*, **33 (7)**, 1179–1195, doi:10.1007/s00382-008-0504-5.

Wang, X. L., and Coauthors, 2011: Trends and low-frequency variability of storminess over western Europe, 1878–2007. *Climate Dynamics*, **37 (11)**, 2355–2371, doi:10.1007/s00382-011-1107-0.

Weisse, R., and H. von Storch, 2009: *Marine Climate and Climate Change. Storms, Wind Waves and Storm Surges*. Springer Praxis, 219 pp.

Wern, L., and L. Bärring, 2009: Sveriges vindklimat 1901-2008 - Analys av förändring i geostrofisk vind. Tech. Rep. METEOROLOGI Nr 138/2009, Swedish Meteorological and Hydrological Institute. http://www.smhi.se/polopoly_fs/1.8498!meteorologi_138v2.pdf.

Werner, P. C., and F.-W. Gerstengarbe, 2010: Katalog der Grosswetterlagen Europas (1881-2009). Tech. Rep. No. 119, Potsdam Institute for Climate Impact Research (PIK). https://www.pik-potsdam.de/research/publications/pikreports/.files/pr119.pdf.

Wilcox, R., 2001: *Fundamentals of Modern Statistical Methods: Substantially Improving Power and Accuracy*. Springer Nature Book Archives Millennium, Springer.

Wohland, J., N.-E. Omrani, D. Witthaut, and N. S. Keenlyside, 2019: Inconsistent Wind Speed Trends in Current Twentieth Century Reanalyses. *Journal of Geophysical Research: Atmospheres*, **124 (4)**, 1931–1940, doi:10.1029/2018JD030083.

Würtz, A., 2017: Wetterextreme in Deutschland und weltweit. Deutscher Wetterdienst, Accessed: 06 August 2019, https://www.dwd.de/DE/wetter/thema_des_tages/2017/2/16.html.

List of Figures

List of Tables

Appendix

Table A.1: List of all 56 possible triangles and their respective geometric properties. Red entries indicate that a triangle was discarded based on this property. Note that, for stations where relocations took place, these calculations are based on the coordinates of Vestervig, Nordby and Hamburg-Fuhlsbüttel given in Table 2.1.

Triangle	Smallest Angle (°)	Land only	Valid?
De Bilt-Groningen-Vestervig	6.4	No	No
De Bilt-Groningen-Nordby	5.3	No	No
De Bilt-Groningen-List	3.9	No	No
De Bilt-Groningen-Norderney	3.2	Yes	No
De Bilt-Groningen-Cuxhaven	9.3	Yes	No
De Bilt-Groningen-HH-Fuhlsbüttel	13.8	Yes	No
De Bilt-Vestervig-Nordby	8.2	No	No
De Bilt-Vestervig-List	12.0	No	No
De Bilt-Vestervig-Norderney	9.6	No	No
De Bilt-Vestervig-Cuxhaven	27.3	No	Yes
De Bilt-Vestervig-HH-Fuhlsbüttel	40.4	No	Yes
De Bilt-Nordby-List	3.8	No	No
De Bilt-Nordby-Norderney	6.9	No	No
De Bilt-Nordby-Cuxhaven	20.6	No	Yes
De Bilt-Nordby-HH-Fuhlsbüttel	32.6	No	Yes
De Bilt-List-Norderney	3.2	No	No
De Bilt-List-Cuxhaven	16.8	No	Yes
De Bilt-List-HH-Fuhlsbüttel	28.8	No	Yes
De Bilt-Norderney-Cuxhaven	13.8	Yes	No
De Bilt-Norderney-HH-Fuhlsbüttel	25.8	Yes	No
De Bilt-Cuxhaven-HH-Fuhlsbüttel	12.0	Yes	No
Groningen-Vestervig-Nordby	9.1	No	No
Groningen-Vestervig-List	14.2	No	No
Groningen-Vestervig-Norderney	3.1	No	No
Groningen-Vestervig-Cuxhaven	20.6	No	Yes
Groningen-Vestervig-HH-Fuhlsbüttel	33.7	No	Yes
Groningen-Nordby-List	5.1	No	No
Groningen-Nordby-Norderney	2.0	No	No

Triangle	Smallest Angle (°)	Land only	Valid?
Groningen-Nordby-Cuxhaven	31.9	No	Yes
Groningen-Nordby-HH-Fuhlsbüttel	51.4	No	Yes
Groningen-List-Norderney	0.0	No	No
Groningen-List-Cuxhaven	29.7	No	Yes
Groningen-List-HH-Fuhlsbüttel	46.3	No	Yes
Groningen-Norderney-Cuxhaven	20.8	Yes	No
Groningen-Norderney-HH-Fuhlsbüttel	16.8	Yes	No
Groningen-Cuxhaven-HH-Fuhlsbüttel	16.5	Yes	No
Vestervig-Nordby-List	0.0	Yes	No
Vestervig-Nordby-Norderney	9.9	No	No
Vestervig-Nordby-Cuxhaven	2.2	Yes	No
Vestervig-Nordby-HH-Fuhlsbüttel	9.6	Yes	No
Vestervig-List-Norderney	14.0	No	No
Vestervig-List-Cuxhaven	2.8	Yes	No
Vestervig-List-HH-Fuhlsbüttel	15.2	Yes	No
Vestervig-Norderney-Cuxhaven	16.7	No	Yes
Vestervig-Norderney-HH-Fuhlsbüttel	29.3	No	Yes
Vestervig-Cuxhaven-HH-Fuhlsbüttel	12.5	Yes	No
Nordby-List-Norderney	6.7	No	No
Nordby-List-Cuxhaven	2.1	Yes	No
Nordby-List-HH-Fuhlsbüttel	6.7	Yes	No
Nordby-Norderney-Cuxhaven	29.1	No	Yes
Nordby-Norderney-HH-Fuhlsbüttel	49.5	No	Yes
Nordby-Cuxhaven-HH-Fuhlsbüttel	20.4	Yes	No
List-Norderney-Cuxhaven	38.2	No	Yes
List-Norderney-HH-Fuhlsbüttel	53.5	No	Yes
List-Cuxhaven-HH-Fuhlsbüttel	25.0	Yes	No
Norderney-Cuxhaven-HH-Fuhlsbüttel	12.5	Yes	No

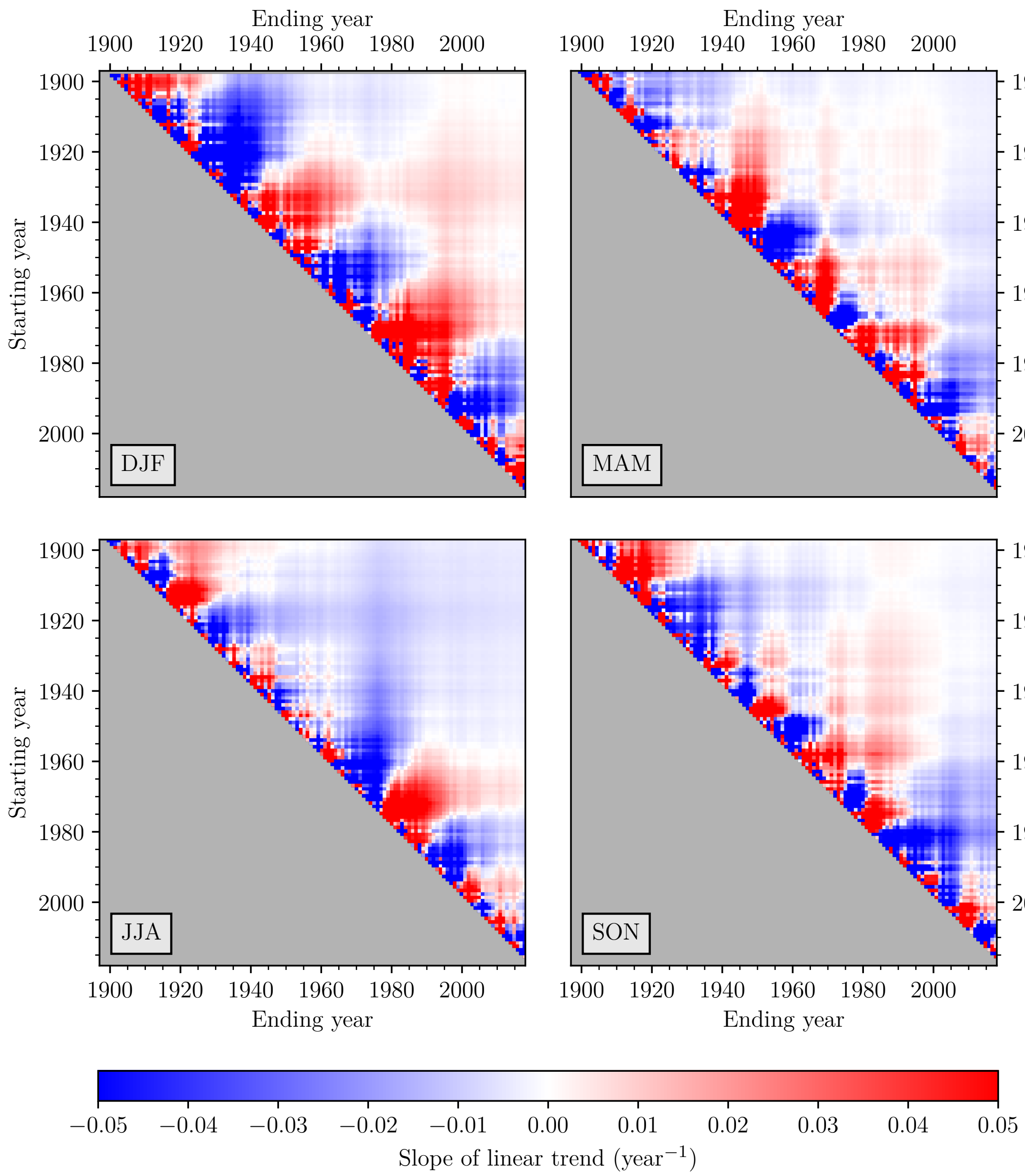

Figure A.1: Trends of 95th percentile-based seasonal German Bight storminess as a function of starting and ending years. The shortest periods are found near the diagonal, while the period length increases towards the top and right.

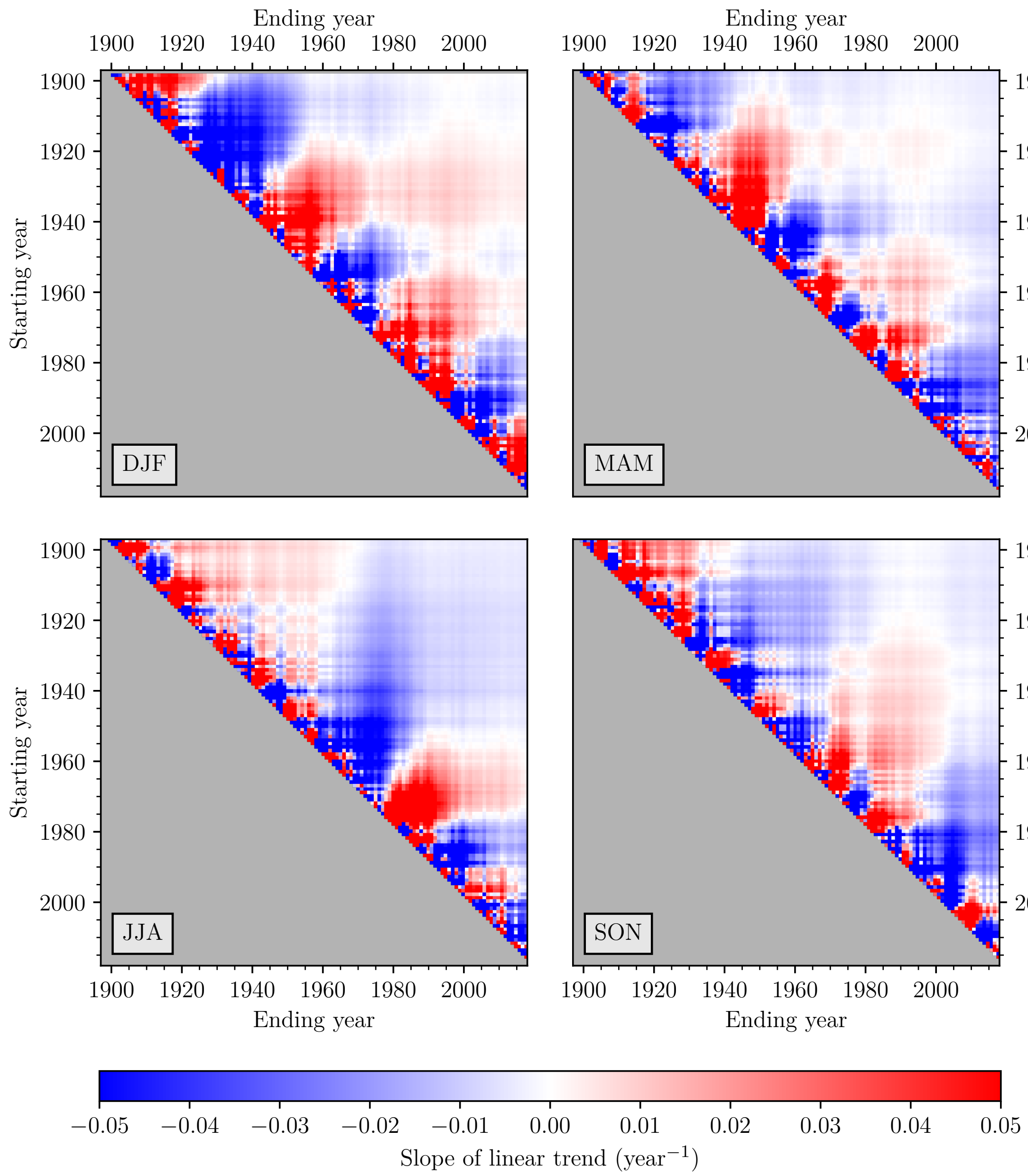

Figure A.2: Like Figure A.1, but for 99th percentiles.

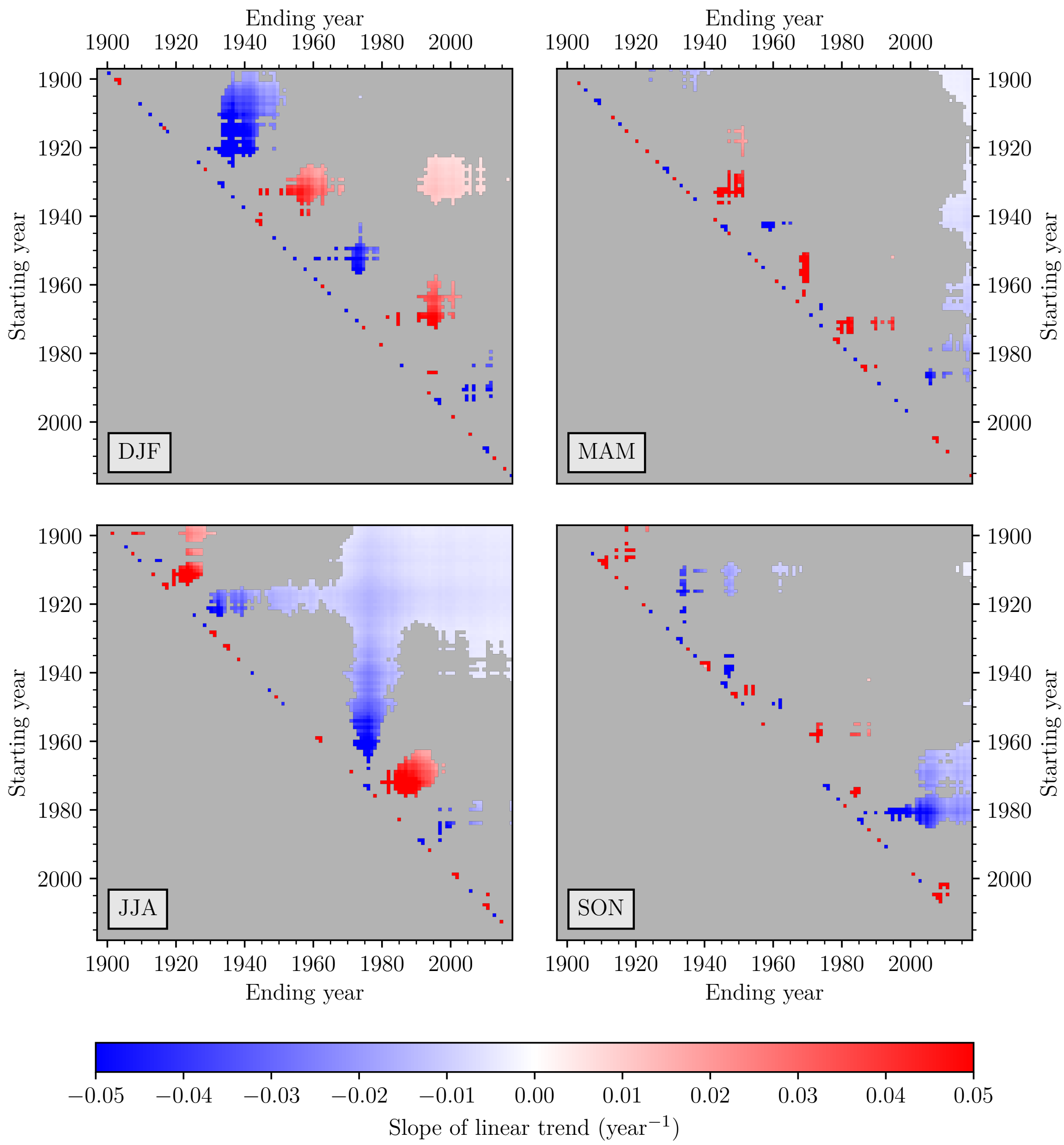

Figure A.3: Like Figure A.1, but only trends that reject the null hypothesis at the 0.05 significance level are shown.

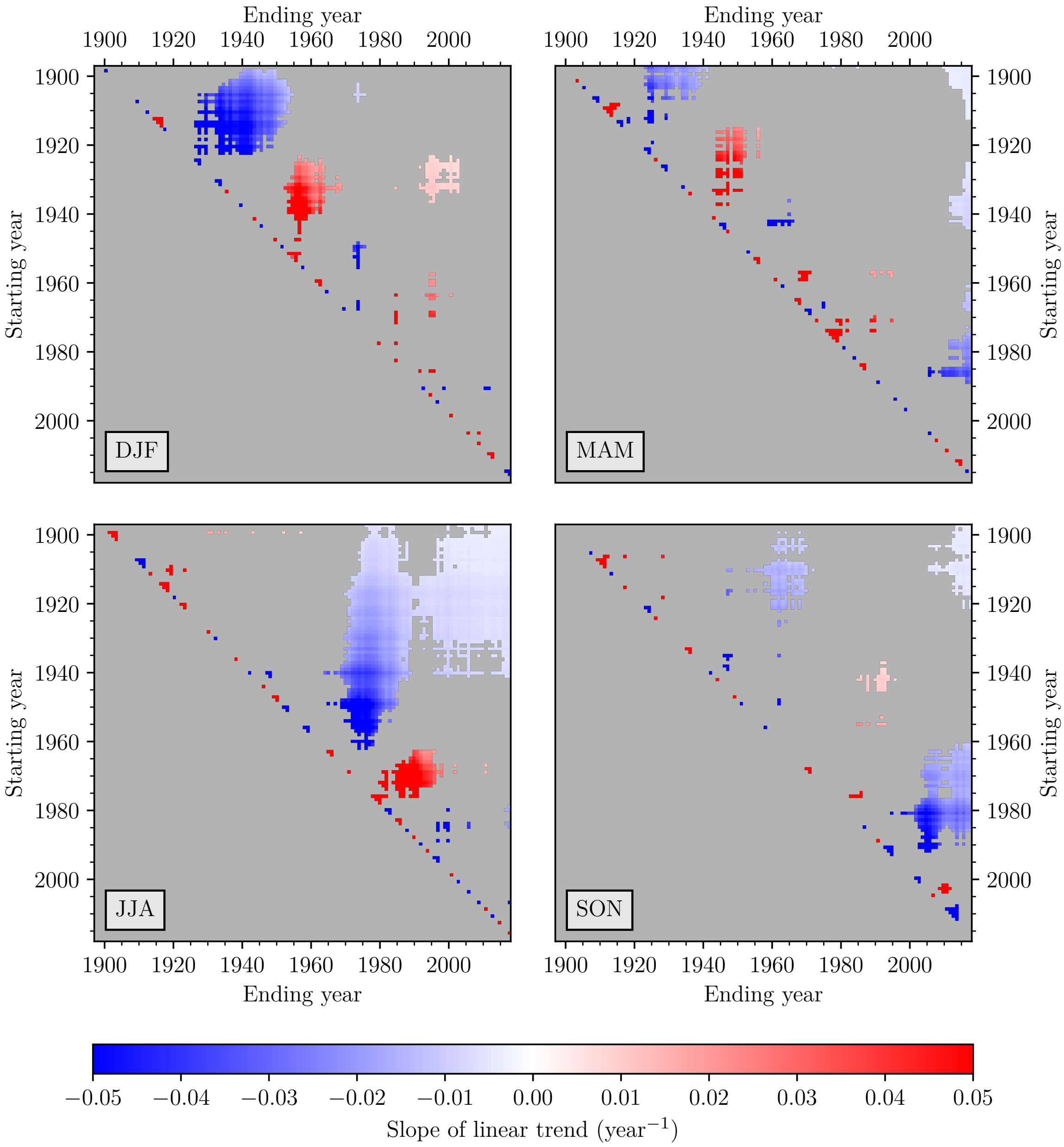

Figure A.4: Like Figure A.3, but for 99th percentiles.

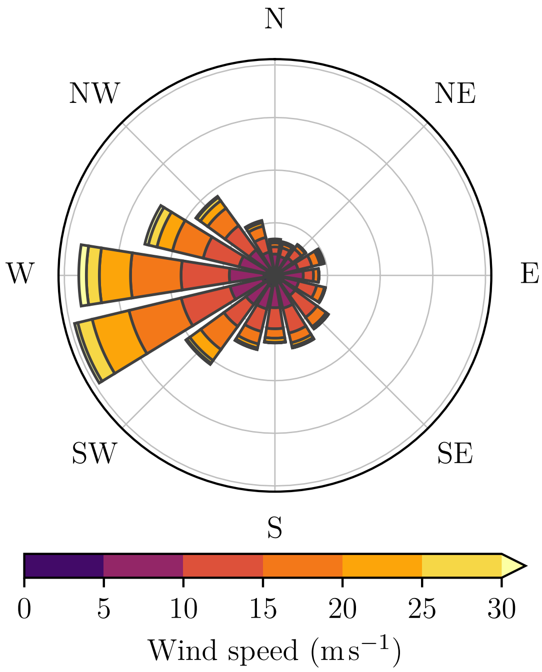

(a) DJF

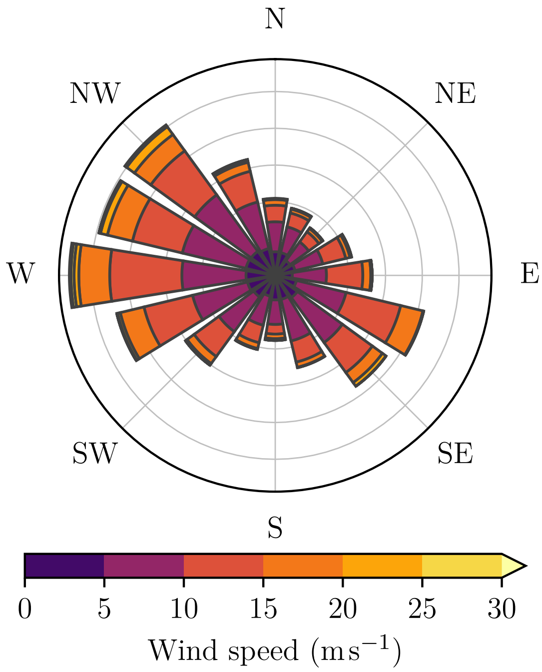

(b) MAM

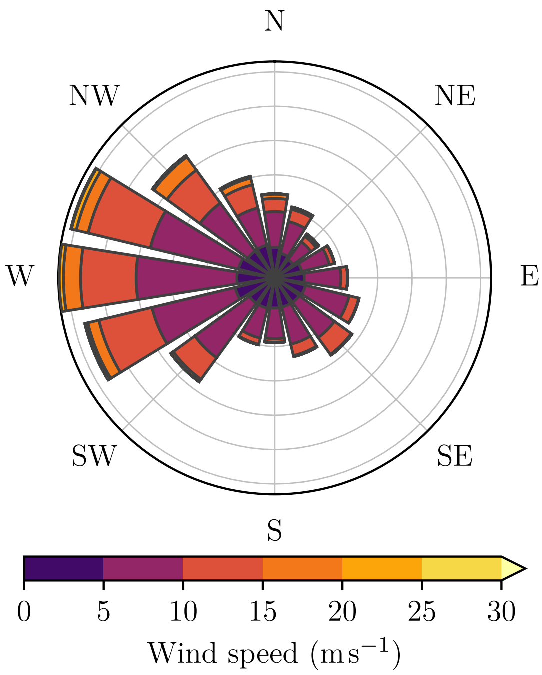

(c) JJA

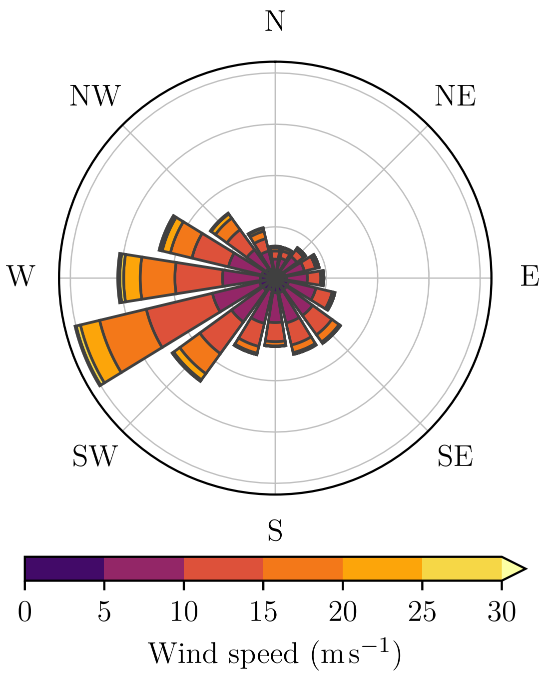

(d) SON

Figure A.5: Wind roses showing the seasonal distributions of wind directions and speeds, based on the reconstructed three-hourly geostrophic wind over the German Bight, 2004-2017.

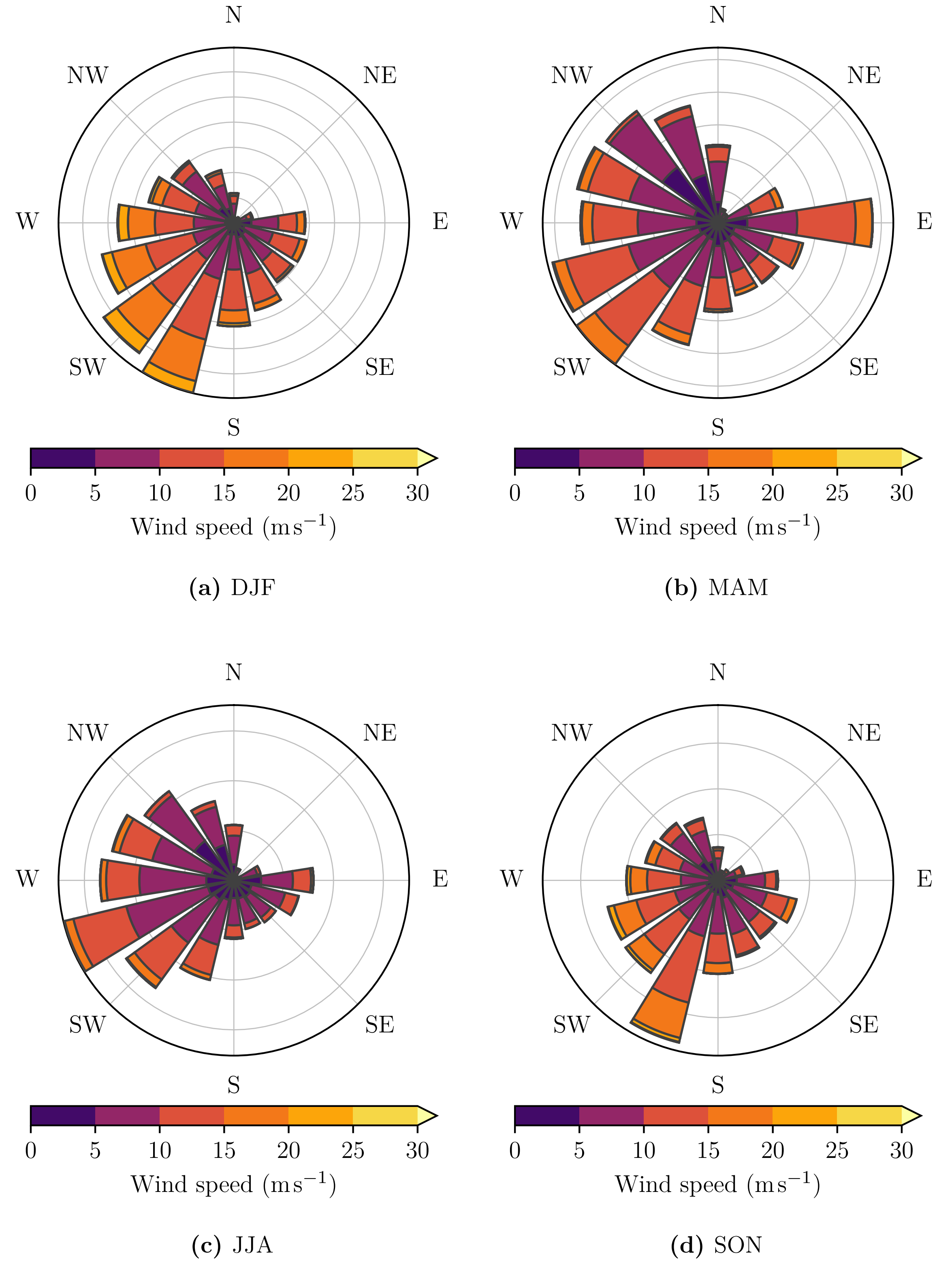

(a) DJF **(b)** MAM **(c)** JJA **(d)** SON

Figure A.6: Like Figure A.5, but based on three-hourly in-situ measurements from the FINO1 research platform, 71 m above sea level.

Acknowledgements

First of all, I would like to express my sincere gratitude to Dr. Oliver Krüger and Prof. Dr. Felix Ament for their excellent guidance, assistance and scientific input during the process of writing this Master's thesis.

I would like to thank Dr. Ralf Weisse, Dr. Frauke Feser, Dr. Birger Tinz and Prof. Dr. Hans von Storch for their valuable remarks which greatly improved the thesis.

Furthermore, I would also like to thank the Helmholtz-Zentrum Geesthacht for the support and cooperation over the past year which made this thesis possible.

I very much appreciate the Bundesministerium für Wirtschaft und Energie (BMWi), Projektträger Jülich (PtJ), and the Bundesamt für Seeschifffahrt und Hydrographie (BSH) for providing me with data from the FINO-WIND database which greatly helped to validate the results.

Last but not least, I would like to thank my very good friends Katharina Baier, Finn Burgemeister, Kai-Uwe Eiselt, Henning Franke, Lara Hellmich, Tobias Machnitzki, Julia Menken, Jule Radtke, Daniel Sorg, and Moritz Witt for their inspiration, advice, helpful comments, and, most importantly, countless unforgettable moments over the last two-and-a-half years.

Versicherung an Eides statt

Hiermit versichere ich an Eides statt, dass ich die vorliegende Arbeit im Studiengang M.Sc. Meteorologie selbstständig verfasst und keine anderen als die angegebenen Hilfsmittel – insbesondere keine im Quellenverzeichnis nicht benannten Internet-Quellen – benutzt habe. Alle Stellen, die wörtlich oder sinngemäß aus Veröffentlichungen entnommen wurden, sind als solche kenntlich gemacht. Ich versichere weiterhin, dass ich die Arbeit vorher nicht in einem anderen Prüfungsverfahren eingereicht habe und die eingereichte schriftliche Fassung der auf dem elektronischen Speichermedium entspricht.

Ich erkläre mich außerdem damit einverstanden, dass ein Exemplar dieser Arbeit in der Fachbibliothek veröffentlicht wird.

....

Ort, Datum Daniel Krieger